Development of Fluid-Curtain Sealing Technology to Improve the Efficiency and Operational Flexibility of Large Power Generation Turbines

JAMES ALEXANDER MACCALMAN

Development of Fluid-Curtain Sealing Technology to Improve the Efficiency and Operational Flexibility of Large Power Generation Turbines

James Alexander MacCalman

Durham University

Department of Engineering

A thesis submitted for the degree of Doctor of Philosophy

September 2020

Acknowledgements

This research would not have been possible without the knowledge, assistance, and patience of the supervisory team as well as colleagues in the thermofluids laboratory.

I would like to thank Prof. Simon Hogg and Dr. Grant Ingram for their technical advice, advice on the direction of the project, as well as their constant encouragement. I would like to thank Dr. Richard Williams for his limitless patience in assisting with the experimental campaigns carried out and for offering valuable technical knowledge whenever it was needed. I am very grateful for the assistance rendered by the entire workshop staff, who always had time to offer their advice on designing parts and manufactured the most delicate components used in my test rig.

I would also like to thank General Electric for funding the research and making this thesis possible.

Finally I would like to thank my family, in particular my wife Sarah, who have all been immensely supportive and encouraging during the course of my research.

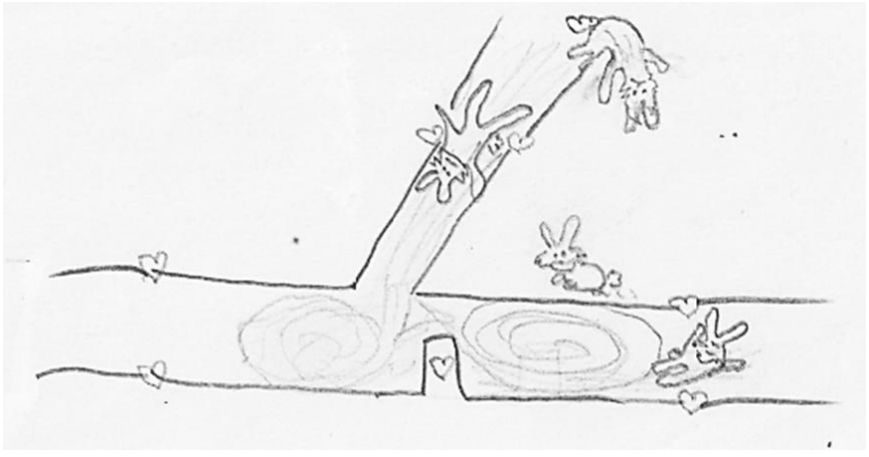

The fluidic seal depicted with rabbits (sketch by Sarah MacCalman, 2016)

Abstract

Fluidic curtain sealing has recently been shown to offer significantly reduced leakage in rotating turbomachinery seals. The seal type uses an additional flow injected into the leakage path to reduce some existing leakage flow. Shrouded steam turbine tip seals were the focus of research in this thesis, but the seal has potential applications in blade tip seals, stator root seals, shaft seals, and end gland seals in steam turbines as well as in gas turbines. The implementation of such a seal may be simplified in the case of gas turbines since secondary flows of air are already built into the machine to provide cooling flows to high temperature components. The fluidic curtain seal is especially effective when a combination of fluidic curtain and a conventional labyrinth seal is used, and the research presented will generally feature a fluidic curtain placed upstream of a labyrinth fin type restriction. The new addition to knowledge on fluidic curtain sealing described in this work is in characterising seal performance in terms of its design parameters. Better characterisation of the seal allows the development of a set of realistic design rules to specify how fluidic curtains may be applied to the design of new, high performance turbomachinery seals.

Two main advances in characterising fluidic curtain seals resulted from the research. The first advance was to numerically and experimentally test basic geometric parameters and their influence on performance to identify design rules which maximize the performance gain of incorporating a fluidic curtain. A series of fundamental dimensionless geometric ratios were proposed and the design space created by these parameters was explored and validated experimentally using a simple annular test rig. CFD was then used to demonstrate that it is possible to incorporate a high performance design into a labyrinth seal independent of the existing labyrinth seal geometry. The second advance is to explore the effect of swirl velocity at the leakage channel inlet on overall seal performance. This was first achieved using CFD to model the selected realistic tip seal design with different levels of inlet swirl. This CFD study was then validated by building the design in a rotating annular test rig where the inlet swirl velocity was controlled. The research findings resulted in a proposed design process for new fluidic curtain seals (Section 8.2) which considers; the geometry of an existing seal, fluid conditions in the leakage path and elsewhere in the turbine stage, rotational speed, and minimum allowable physical clearances.

Contents

List of Figures

List of Tables

Nomenclature

a	Fluidic curtain width	(mm)
b	Leakage channel height	(mm)
c	Labyrinth seal clearance height	(mm)
d	Spacing between curtain inlet and labyrinth seal	(mm)
p	Axial distance between increase in channel height and first restriction	(m)
A_c	Fluid curtain annular frontal area	(m^2)
A	Ratio of b to a	(-)
C	Ratio of b to c	(-)
D	Ratio of d to b	(-)
C_d	Discharge coefficient	(-)
L	Percentage reduction in leakage flow rate	(-)
M	Mach number	(-)
$\dot{m}$	Mass flow rate	(kg/s)
P_0	Total pressure	(bar)
P	Static pressure	(bar)
P_n	Pressure at location n	(bar)
ΔP	Change in pressure	(bar)
PR	Pressure ratio	(-)
$PR_{optimum}$	Optimum pressure ratio above which fluidic seal overblows	(-)
R_v	Velocity ratio	(-)
t	Fluid curtain thickness	(m)
v	Velocity	(m/s)
ρ	Density	(kg/m^3)
μ	Dynamic Viscosity	($kg/m.s$)
W	Swirl velocity	(m/s)
ω	Angular velocity	(rad/s)
$\tau_{r\theta}$	Angular velocity flux	($kg.m^2/s^2$)

1. Introduction

The concept of the fluidic curtain seal is introduced in this chapter. First, the need for sealing in turbomachinery is outlined. A brief overview of different classes of turbomachinery rotating seals, including the potential advantages of fluid curtain seals, is then discussed. The fundamental physical principles behind the operation of seals that incorporate fluid curtains are explained in the next sub-section. A summary of what the body of research described in the thesis adds to the current state of knowledge on this type of turbomachinery seal is provided next. Finally, the Introduction concludes with an overview of the content of each chapter in the thesis.

1.1.Turbine Seals

Turbine seals are used to prevent working fluid from leaving the turbine or to maintain an internal pressure difference between two turbine cavities, while minimising any leakage mass flow between them [**1**]. Where no relative motion occurs between leakage path surfaces, zero mass flow is accomplished easily by devices such as gaskets or o-rings. However, the solution becomes more complex when a leakage pathway is formed between parts which must move relative to each other during service. Turbomachinery contains leakage pathways between surfaces which often see particularly high speed relative rotational movement and usually also high and low frequency relative motion due to vibrations and thermal differential expansion etc. Figure 1 shows the main leakage pathways between stationary and rotating parts in a large power generation steam turbine. For example, across a turbine rotor there is a leakage path through the clearance between the blade tips and the casing. The working fluid can expand through this clearance without exerting aerodynamic forces on the turbine blades, and therefore without contributing significantly to the useful work output of the turbine. By reducing this type of leakage flow, less of the working fluid is expanded through the turbine stages without contributing to work output, therefore increasing efficiency.

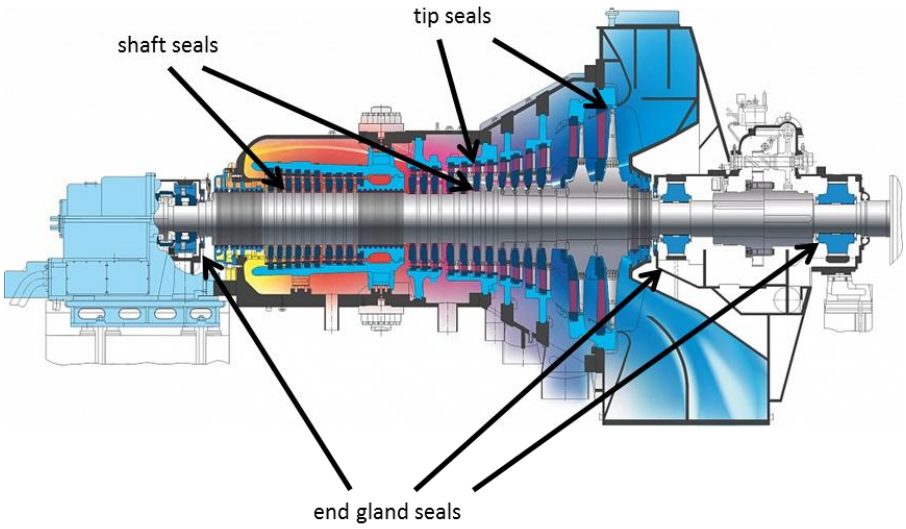

Figure 1: Cross section view of an example of a power generation steam turbine [**2**]

Sealing turbine blade tip leakage flow presents a greater challenge than sealing leakage flow on the shaft due to the greater radius from the axis of rotation. This increases the relative velocity between stationary and rotating parts linearly with the increase in radius. Greater relative speed increases the damage caused by contact and increases rotordynamic forces [**3**] which can destabilise the rotor. Increased radius also increases radial stress on the turbine blades proportionally to the square of the increase in radius, which limits the weight of tip sealing devices placed on the rotor. In the case of high pressure gas turbine stages the seal is exposed to flows which can reach temperatures in the range 1500-2000 K for the first turbine stage downstream of the combustor. These conditions often demand the use of specialised cooling methods which use air bled from the compressor to cool turbine blades and the seal segments on the stationary wall [**4**]. Secondary air flows used to cool blades and prevent hot gas ingestion into the internal core of the engine from the blade roots are shown in Figure 2. The figure depicts a three stage high pressure turbine; the combustor flame tube is visible immediately upstream of the first nozzle guide vane.

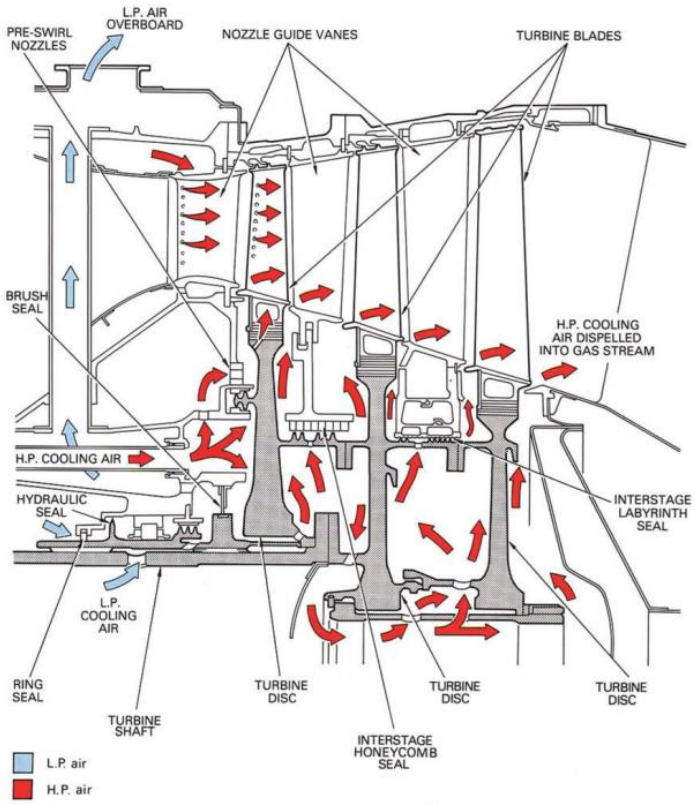

Figure 2: Example of high pressure turbine secondary air flows.
L.P. – low pressure compressor, H.P. – high pressure compressor [**4**]

Although some types of rotating seal, such as the brush seal, allow physical contact during operation, most turbomachinery seals are designed to avoid contact between stationary and rotating parts, as this would damage the seal. During normal operation in many power generation turbines, light contact may be caused by rotor excursion in transient operation during start up and shut down. Over time this contact will predictably lower performance, resulting in a known service life for a given seal. Geometry may be rigid, or compliant. Compliant seal geometry is variable to some degree, and adjusts in order to accommodate rotor movement while minimising clearance. Brush seals and hydrostatic floating seals are examples of compliant seals. In labyrinth seals, which are rigid, increasing clearance between stationary and rotating parts will increase leakage flow but also increase the robustness of the seal to rotor excursions. This means that life is traded against leakage performance when designing labyrinth sealing systems.

1.2.Turbine Seal Types

Sealing has been the subject of a large amount of research since the first power generation turbines were developed, although the most commonly used type of turbomachinery seal, the labyrinth seal, has changed little in that time. Current turbine designs employ a variety of seals

to create barriers to fluid motion through clearances between rotating and stationary parts of the turbine. Seals which restrict flow by forming a narrow channel for leaking fluid to pass through without physical contact between stationary and rotating parts are referred to as non-contacting seals. Seals which present a blockage to leakage flow with physical contact between stationary and rotating parts are referred to as contacting seals. The most common types of contacting and non-contacting seal are described briefly in this section. Fluid curtain seals are then put into context in relation to these basic types of turbine seal technology in the next sub-section of this Chapter. A more thorough review of different seal types is provided in Chapter 2.

1.2.1. Non-Contacting Seals

Non-contacting seals operate by forcing leakage to pass through narrow clearances at one or more locations in a leakage pathway. Labyrinth seals (see Figure 3) are the earliest and still the most commonly used type of turbomachinery seal used to reduce turbine leakage flows. Labyrinth seals force the leakage flow through a series of restrictions which are created by circumferential fins projecting from either the rotor or stator [**5**].

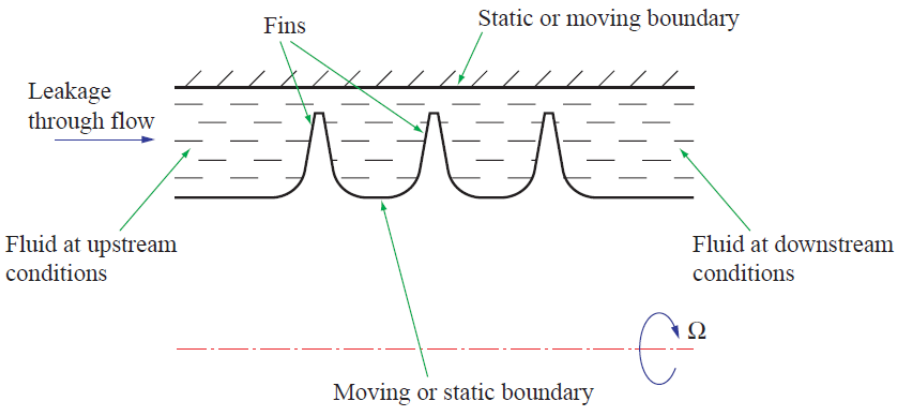

Figure 3: Cross section diagram of a labyrinth seal containing three restrictions [**3**]

The losses generated by rapidly accelerating and then decelerating the flow in an uncontrolled expansion into the space between adjacent restrictions, means that large static pressure drops are needed to drive flow through the seal . As the fluid enters the restriction the total dynamic pressure increases and static pressure drops, but as the high velocity stream expands freely into the downstream cavity the dynamic pressure is not recovered back into static pressure giving rise to a drop in both static and total pressure through the seal. Decreasing the cross sectional area of the restriction will cause a greater resistance to leakage flow. Therefore by decreasing the clearance between labyrinth fins and the opposite wall, the same pressure difference can be maintained at a lower leakage flow rate. In reality, the clearance of the rigid geometry is limited by the need to avoid fouling caused by factors such as: any eccentricity in

the rotor, surface height variation in blade or shroud tips, thermal expansion, creep, vibration, etc. Therefore, a labyrinth seal is limited to operation at the smallest clearance that avoids contact as the static and rotating parts undergo the relative radial motion expected during normal service. Dynamic floating seals, such as the aerostatic seal developed by Messenger [**6**] utilise hydrostatic forces acting on individual segments of a labyrinth type seal arrangement to position each segment as close as possible to the rotor without contacting. If the rotor surface moves radially then the seal segment 'rides' with this motion and maintains the desired clearance. This type of compliant seal can allow the rotor to move by a distance greater than the clearance height of the seal without causing fouling.

1.2.2. Contacting Seals

Contacting seals restrict leakage flow by using a physical blockage which spans the full width of the leakage channel. Contacting seals can give up to 80 % less leakage compared to labyrinth seals. However, their application is currently much more limited in turbomachinery applications compared to non-contacting seals. This is due to the design challenges associated with maintaining contact in hostile turbomachinery environments with relative surface speeds of often more than 100 m/s. Brush seals (see Figure 4) work by blocking the clearance between the stationary and rotating parts using a ring of densely packed radial bristles. They are an attractive alternative to labyrinths because leakage flow rates are significantly lower. The flexibility of the bristles makes the seal compliant, tolerating a degree of rotor excursion without degrading the sealing capability [**7**]. However, contact between bristles and the shaft causes wear and shaft heating which can damage the shaft and seal over time.

Figure 4: A brush seal shown in section view [**8**]

Ideally a turbomachinery seal would give the advantages of both of seal types, i.e. the barrier to flow offered by a contacting seal combined with the physical clearance of a non-contacting seal. If only solid features are considered in the seal design then these requirements are clearly

contradictory; a full blockage in the leakage channel cannot be achieved without reducing the clearance to zero at which point physical contact must occur at all times. However if the blockage were to be provided by a body of fluid injected into the leakage path then blockage against leakage flow could be improved, without the need to reduce the operating clearance between the solid rotor and stator.

1.3.Fundamentals of Fluid Curtain Sealing

New types of non-contacting turbomachinery seals using fluidic jets or curtains to act against leakage flows have been the subject of some recent research (see Section 2.6 in Chapter 2). They hold the key advantage that they are aerodynamic devices that allow leakage to be reduced, without increasing the risk of solid stationary and rotating surfaces coming into contact. Previous work [**9**] [**10**] [**11**] has started to demonstrate the potential of this type of technology, and Hilfer [**5**] demonstrated a possible 30 % reduction in rotor tip leakage flow on a small pre-commercial Rankine cycle impulse turbine.

The use of fluid curtains could combine the advantages of labyrinth and brush seals i.e. allow seal designs to be developed which, similar to brush seals, have an effective clearance much lower than that from the physical clearance between the fixed non-conformable parts of the seal, whilst avoiding the bristle damage, wear and shaft heating challenges that are often encountered with brush seals.

Fluid curtains employ a moving body of fluid, which interacts with the leakage flow in such a way that the overall flow is reduced. The curtain is injected at an angle so that it adds momentum opposing that of the main channel leakage flow. Figure 5 shows an idealised seal geometry where a fluid curtain is injected into a leakage channel upstream of a generic labyrinth seal. In the absence of any curtain flow, the labyrinth seal will experience the full channel pressure drop across it (as illustrated in the upper diagram in Figure 5), assuming that viscous effects are neglected. When a curtain flow is added, a pressure drop is needed in the leakage channel across the curtain flow, in order to turn the curtain flow to the same direction as the main channel leakage flow. This acts to reduce the static pressure in the leakage channel downstream of the curtain, causing a reduction in the pressure difference across the labyrinth seal and therefore a reduction in the total mass flow through it [**10**] (as illustrated in the lower diagram in Figure 5). It is important to note that this must achieve an overall reduction in leakage flow through the seal compared to the case without a curtain. As long as the curtain injection pressure is less than that required to cause reverse flow at the leakage channel inlet, the flow which exits from the labyrinth seal in Figure 5 will be the sum of the curtain flow and

the leakage channel inlet flow. This must always be less than the leakage flow for the no-curtain case, because the static pressure drop that is driving the flow through the labyrinth seal is reduced when the curtain is applied.

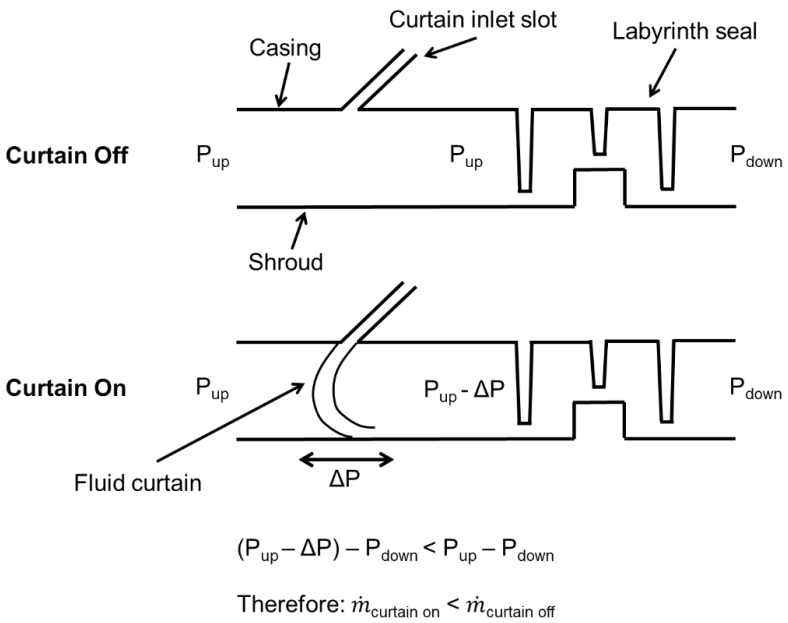

Figure 5: The operating principle of the fluid curtain seal.

The requirement to inject additional fluid poses an obvious question: how is the fluid supplied? It will be shown in the following chapters that a fluidic curtain can potentially be operated at a low enough feed pressure that it can be supplied by fluid extracted upstream within the same turbine stage, and therefore not remove energy from the working fluid which may be better spent elsewhere in the cycle. Additionally, in gas turbines, the air system includes a number of secondary flows that are used for cooling purposes, as shown in Figure 2. This means that gas turbines have a ready source of fluid which may be used to supply a fluidic seal whilst also still providing a cooling function. This might potentially simplify the implementation of fluid curtains in gas turbines seals compared to those in steam turbines.

The benefit from combining fluid curtains with conventional labyrinth, or other turbomachinery seal types, can be exploited to two ways. Firstly, for a given seal physical clearance, the addition of a fluidic curtain upstream of the seal will reduce the overall leakage through it and improving aerodynamic efficiency. Alternatively, for a given target leakage mass flow rate, the addition of a fluidic curtain will allow the physical seal clearance to be increased, allowing greater relative movement between stationary and rotating turbomachinery components, without an aerodynamic performance penalty. This would increase the service life of a given seal since the

increased physical clearance will make contact less frequent, reducing the rate at which damage and therefore seal degradation occurs. The fluidic seal can be seen as a means of improving aerodynamic performance for a given design of static and rotating turbomachinery, or improving the operational flexibility, or some combination of these.

1.4.Research Objectives

This body of research adds to the current knowledge on fluid curtain seals and their application to turbomachinery. The use of fluidic curtain seal designs in power generation turbines is examined. Research is focused specifically on shrouded turbine tip seals in steam turbines, although the findings can be applied generally to other applications in turbomachines. The new knowledge will be useful to engineers in the design of fluid curtain seals in turbine tip seal applications, and will also serve as a starting point for further research and development of the fluid curtain sealing concept. Three main research objectives were identified:

1. Investigate the effect of systematically varying important dimensions on the operating characteristics of the seal. A wide range of seal geometries will be tested and the effect of varying different aspects of their geometric design on seal performance explored.
2. The understanding of the effect of geometric design which is gained by satisfying the first objective will be used to create a set of design rules for fluidic seals in turbine tip seal applications. This will provide engineers with a generic set of guidelines when designing a new fluid curtain seal for use in a given turbine tip cavity with known flow conditions.
3. Apply the design rules to design a fluid curtain seal for use in the turbine tip seal of a steam turbine test rig. Build and test the design and demonstrate an improvement over the baseline seal design which the fluid curtain seal replaces.

In short, the research aims to quantify the potential performance of a fluidic curtain seal in terms of its geometric design. As new knowledge was gathered over the course of the project this was expanded to include the effect of flow conditions in the turbine seal application.

1.5. Publications

During the project, two conference papers were produced and presented: MacCalman et al, "Using Fluidic Curtains to Reduce Turbine Leakage," 23rd ISABE Conference, Manchester, 2017, (ISABE-2017-22588) [**12**]; MacCalman et al, "Application of Fluidic Curtains to Turbine Rotor Tip Seal Geometries," ASME Turbo Expo, Lillestrøm, 2018, (GT2018-75835) [**13**].

1.6.Structure of Thesis

The chapters contained in this thesis aim to satisfy these research objectives. Earlier chapters investigate the effect of geometry on seal performance, propose design rules, and then validate these findings experimentally. The later chapters apply the design rules to a seal design for a turbine test rig, but the effect of swirl on the fluid curtain is found to be important during the design of this seal. The third research objective was therefore adjusted and the investigation is focused on understanding the effect of swirl on the fluidic curtain.

Chapter 2 – Literature Review

Turbine sealing and the history of fluidic sealing is explored. The different types of seal found commonly in turbomachinery are described in detail and previous research on fluid curtain seals is described. The chapter concludes by evaluating the current state of knowledge on fluid curtain seals, and shows how the research objectives described above fit into the context of fluid curtain seal research.

Chapter 3 – Fundamental Study to Understand Geometric Parameters

This is the first systematic investigation of a wide design space for fluidic seal geometry. The chapter establishes the effects of key seal dimensions on performance. It leads to the first set of design rules for this type of seal. This first examination of fluidic seal geometries is performed using computational fluid dynamics (CFD).

Chapter 4 – Experimental Validation of Geometric Characterisation

The computational findings in Chapter 3 are validated through experiment. A subset of the seal geometries tested computationally is recreated in a small fluidic seal test rig and their performance is compared to the predictions made by CFD. The experiments successfully show that the performance predicted by CFD is accurate and therefore the design rules proposed in Chapter 3 can be used with confidence in designing fluid curtain seals.

Chapter 5 – Adapting a Turbine Stage Shrouded Rotor Tip Seal to Incorporate a Fluid Curtain

This chapter examines how a fluidic seal might be incorporated into an existing high pressure steam turbine tip seal. A design incorporating a fluid curtain seal into a shrouded turbine tip labyrinth seal on a steam turbine test rig is created by applying the design rules from Chapter 3. The research carried out in this chapter reveal the first evidence of the effect of swirl in the incoming leakage flow on fluidic curtain performance. It is found that the expected swirl velocity which is encountered by the seal in the test turbine would be sufficient to eliminate any performance benefit of the fluid curtain.

Chapter 6 – Investigation of the Effects of Swirl on Fluidic Curtain

The effect of gradually increasing swirl velocity from zero up to those found under service conditions is investigated using CFD. The design created in Chapter 5 is used for this study. The simulations model the conditions found in the scale steam turbine test rig as well as typical high pressure steam turbine conditions. A relationship is demonstrated between the swirl velocity of the flow entering the leakage channel and the maximum leakage reduction the fluid curtain can generate compared to the baseline seal design.

Chapter 7 – Experimental validation of findings on the effect of swirl

The effect of inlet swirl on fluid curtain seal performance investigated in Chapter 6 is demonstrated experimentally. A rotating turbine seal test rig is modified to include a fluid curtain seal and to produce a range of seal inlet swirl velocities. The shearing effect of the swirling leakage flow is measured and its effect on the leakage reduction caused by the fluid curtain is studied.

Chapter 8 – Conclusions and Recommendations for Further Work

The final chapter describes how each of the research objectives were satisfied, giving the main research outcomes and how these have expanded the current state of knowledge on fluid curtain sealing. A design process is proposed which uses the new design rules as well as the findings on swirl to guide an engineer through the preliminary design of a fluid curtain seal for some given turbomachinery application. The chapter ends with recommendations on the direction of future research.

2. Literature Review

2.1.Overview

Seals in various forms have been developed over many decades as a means of reducing leakage losses in turbomachinery. These vary in mechanical and aerodynamic complexity from simple gaskets between static components to more complex seals between stationary and rotating components.

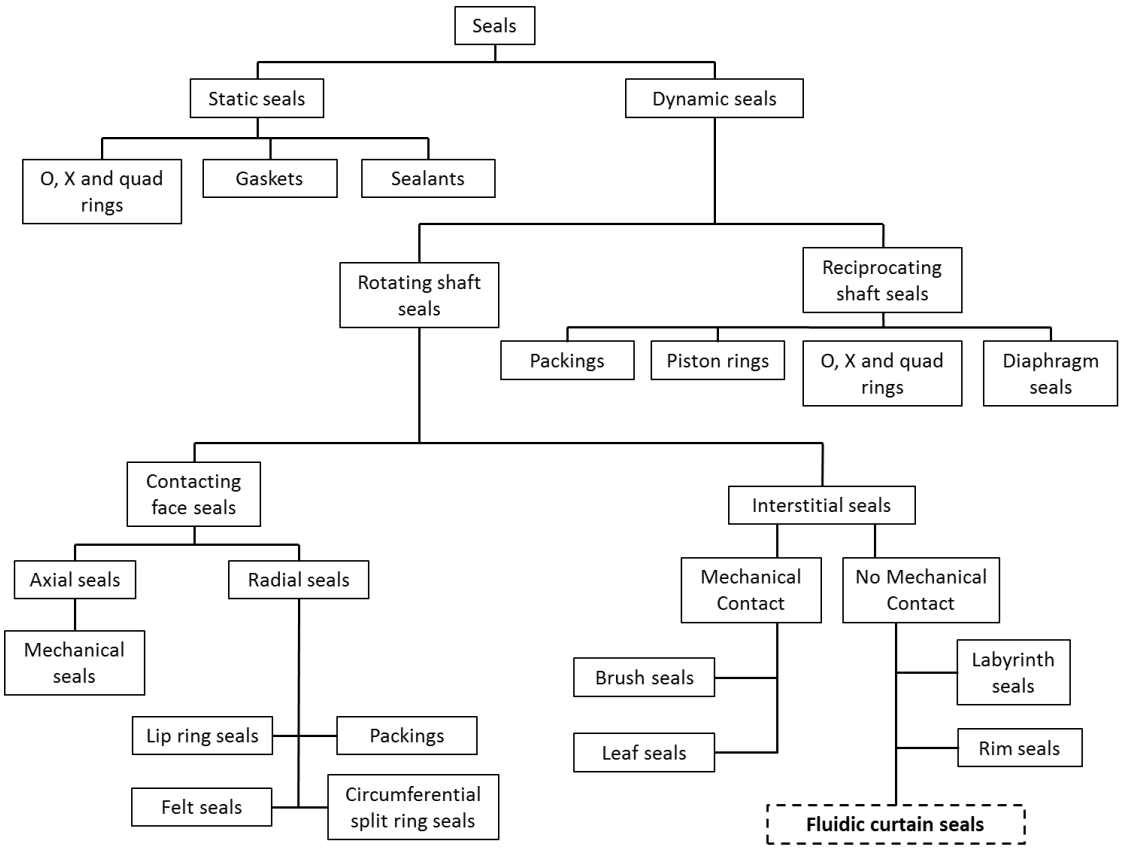

Figure 6: Seal taxonomy (adapted from [3]).

The conceptual family tree of different seals used in turbomachinery applications is shown in Figure 6. The fluidic seal falls under the category of dynamic seals since they allow movement, while sealing between stationary and rotating parts. They can be categorised as interstitial seals alongside labyrinth seals, brush seals and leaf seals because they do not allow 'hard-on-hard' contact between components. They therefore allow rotation to occur at high speed and relative movement to occur between stationary and rotating parts with minimal risk of rubbing.

In this section, the main types of interstitial seals used in modern turbomachinery are described, followed by a discussion of the history of fluidic sealing.

2.2.Labyrinth Seals

For many years, labyrinth seals have been the most common form of seal used in turbomachinery. They are found at the blade tip on shrouded turbine blades, around turbine and compressor discs where it is necessary to control the movement of pressurised fluid, at the hub on gland seals, as well as other locations where rotation occurs between stationary and rotating components, e.g. the ends of the shaft. They are mechanically very simple and consist of a series of tight annular restrictions in a given leakage channel [**14**]. The restrictions are formed by a set of fence-like bodies projecting radially from either the stator or rotor, and oriented normal to the axis of the turbine. The leakage flow is accelerated through each restriction and the raised kinetic energy is then dissipated in the following cavity, while a small amount is carried over through the following restriction [**15**]. The seal geometry is designed so as to maximise the kinetic energy that is dissipated in each cavity rather than being carried over.

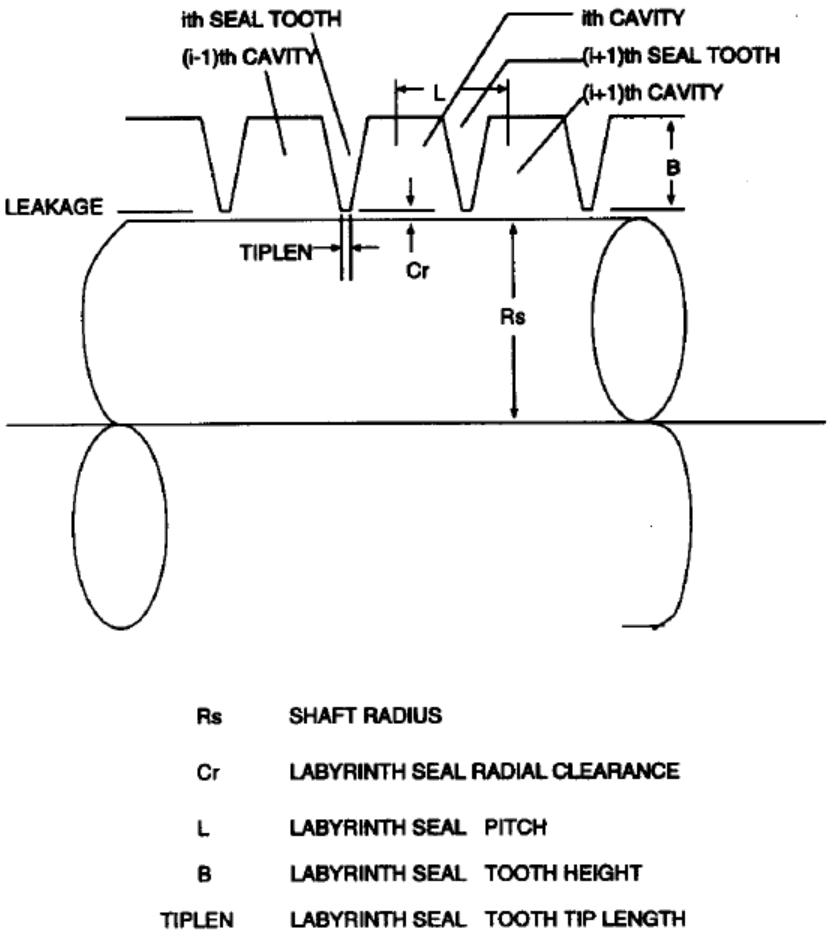

Figure 7: Geometry of a straight through labyrinth seal [**14**]

Figure 7 shows a straight through labyrinth seal. The important parameters that affect the leakage flow rate are [**3**]:

- Radial clearance between the labyrinth fin (or 'tooth') tip and the sealing surface.
- Axial pitch between labyrinth fins.
- Number of fins.
- Fin height.
- Fin tip width.

As radial clearances are reduced, the cross sectional area that the flow must pass through decreases, increasing the velocity with which the leakage flow enters the next cavity. This increases the amount of kinetic energy that can be dissipated in the cavity and results in a greater loss in total pressure through each restriction/cavity pair.

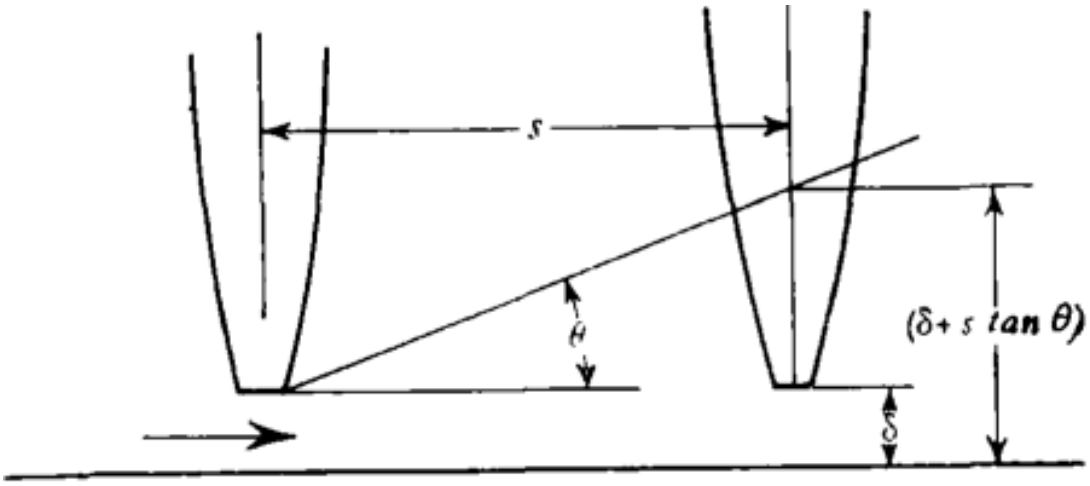

Figure 8: The kinetic energy carry over factor from Hodkinson [**16**]**.**

Similarly increasing the axial pitch between fins increases the distance over which the high velocity jet issuing into the next cavity can dissipate. The more dissipated this jet becomes the less kinetic energy is carried over into the next cavity. This idea is shown in Figure 8. Hodkinson [**16**] proposed that if the high velocity stream expands in a cone shape across the cavity between two restrictions then the fraction of the kinetic energy carried over will be, in the case shown above, $\delta/(\delta + s \tan \theta)$. Therefore, because s will generally be much greater than δ, kinetic energy carried over is approximately inversely proportional to axial pitch.

As the number of labyrinth fins in the seal increases, the number of times the leakage flow is accelerated and decelerated increases, so this has a strong influence on leakage flow rate.

Hendricks and Stetz [**17**] showed that for a generic series of sufficiently spaced orifices, the flow rate followed a power law relation with the number of orifices.

$$\frac{\dot{m}_{N\ restrictions}}{\dot{m}_{Single\ restriction}} = N^{-0.4} \tag{2.1}$$

Equation 2.1 shows the leakage mass flow rate through a series of restrictions such as a labyrinth seal will vary inversely proportionally to approximately the square root of the number of restrictions. The fin height and tip width have less direct effect on leakage flow, provided the fin height is much greater than the fin clearance and that axial pitch is much greater than the tip width.

Some other labyrinth seal arrangements are shown in Figure 9. By adding steps, castellations or locating labyrinth fins on both the inner and outer wall, the path taken by the leakage flow is made more convoluted and less kinetic energy is allowed to be carried over into the next cavity, which increases overall pressure drop. In addition to the parameters listed for a straight through labyrinth seal, the additional parameter of step height must be considered in a stepped or castellated labyrinth seal.

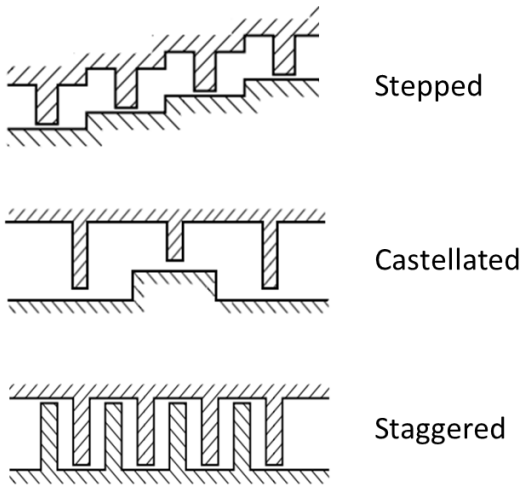

Figure 9: Sketches of basic labyrinth seal configurations which are used reduce kinetic energy carry over [**3**]

The ratio between the labyrinth fin pitch and the radial step height for each restriction affects leakage flow rate. Figure 10 is from Zimmermann and Wolff [**18**] and shows the relationship between leakage discharge through a labyrinth restriction and the ratio between step height and fin pitch.

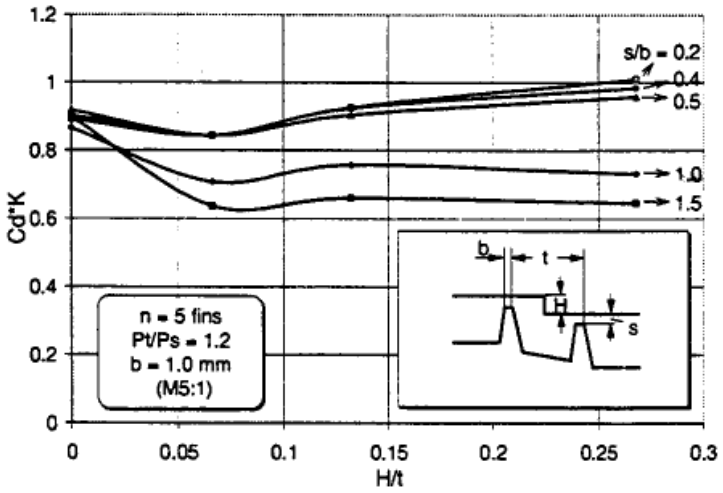

Figure 10: Cd*K vs *H/t*, minimum at *H/t* = 0.075 [18]

(C_d = discharge coefficient, *K* = K.E. carry over factor, *H* = step height, *t* = pitch)

The minimum discharge across the seal occurs where *H/t* = 0.075; showing this is the ideal proportion for a stepped labyrinth seal design.

In 1908, Martin [**19**] published a leakage calculation method for labyrinth seals. This formula is still used extensively to predict labyrinth seal leakage flow rates.

$$\dot{m} = \mathrm{C}_d A \frac{\mathrm{P}_0}{(RT_0)^{\frac{1}{2}}} \left[\frac{1-(P_n/P_0)^2}{N-\ln(P_n/P_0)} \right]^{\frac{1}{2}} \tag{2.2}$$

Where:

$\dot{m}$ = Leakage mass flow rate (kg/s)

C_d = Annulus discharge coefficient (-)

A = Annular area (m^2)

P_0 = Upstream total pressure (Pa)

T_0 = Upstream total temperature (K)

R = Gas constant (J/Kg.K)

N = Total number of restrictions (-)

P_n = Static pressure downstream of N restrictions (Pa)

Equation 2.2 assumes that the seal is isothermal and that the velocity drops to approximately zero between restrictions, so that all kinetic energy is dissipated as heat. It is useful for estimating leakage flows quickly, using only basic seal dimensions and fluid properties. Martin's equation forms the basis of other more refined methods for calculating leakage flows.

Vermes [**15**] improved on the leakage analysis developed by Martin by considering the annular clearance factor of the labyrinth restrictions. The improved method takes into account the flow structure and consequent kinetic energy carry over that will occur in different combinations of stepped and straight through labyrinths.

$$\dot{m} = KC_d A \frac{P_0}{(RT_0)^{\frac{1}{2}}} \left[\frac{1-(P_n/P_0)^2}{N-\ln(P_n/P_0)}\right]^{\frac{1}{2}} \tag{2.3}$$

Equation 2.3 is essentially the same as equation 2.2 with the addition of a dimensionless clearance factor, K. This factor is a function of the ratio of labyrinth fin tip width to clearance height, as well as Reynolds number and can be obtained from Figure 11. Equation 2.3 does not account for the effect on leakage of using a stepped labyrinth seal; accounting for the effect of steps is a more involved process detailed in the same paper by Vermes.

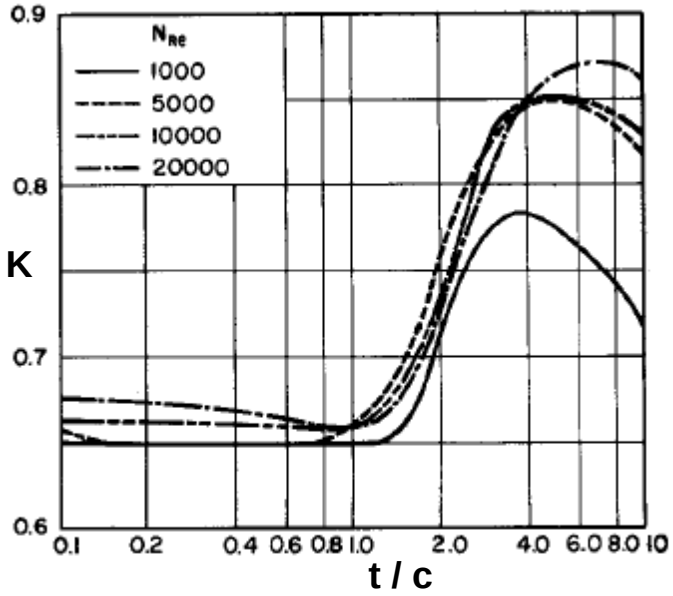

Figure 11: Clearance factor, K

Where t = fin tip width, c = fin clearance height, N_{Re} = Reynolds number

2.3.Brush Seals

Brush seals are a type of rotating contacting shaft seal in which bristles cross the leakage channel in the radial direction from the stationary wall to the rotating wall, to provide a restriction to the leakage flow. The flexibility of the bristles means that contact between bristles and the rotating surface does not damage the seal during normal service. This allows the build clearance between the bristle tips and the rotating components to be reduced to below zero, i.e. an interference fit between the seal and the rotor if desired. The flexibility of the bristles also means that the seal can withstand small radial movements of the rotor, for

example during turbine start up, without damage. Effective clearance can be used to directly compare brush seals and labyrinth seals and represents the clearance size of the equivalent single stage labyrinth seal [**20**]. Typical labyrinth fin clearance heights are on the order of tenths of millimetres in steam turbine tip seal applications; whereas brush seals give effective clearances on the order of hundredths of millimetres. The much smaller effective clearance means that brush seals can reduce leakage flow rates by ~80 % or more compared to labyrinth seals in the same application [**21**], this is the main advantage of the brush seal [**7**] [**22**]. Figure 12 shows the layout of a typical brush seal, the main components are given in Table 1. This type of seal was first developed for and used on aero gas turbine engines, and since the 1990s they have also been applied in steam turbine applications [**22**].

Brush seals work by the bristle pack presenting a physical barrier to flow through the clearance between the rotor and the inner radius of the backing ring. The axial force from the high upstream pressure also compresses the bristle pack so that the bristles are closely packed, which requires a high pressure drop for any leakage passing through the bristle pack [**22**]. The main disadvantages of brush seals stem from the dynamic contact between the bristles and the rotor. Surface speed of the rotor is limited to prevent excessive wear of the bristles or heating of the rotor. This generally excludes brush seals from use in tip seals where the surface speed at the higher radius would be much higher than for a shaft at the same rpm. The flexibility of the bristles also means the seal cannot operate beyond a certain pressure difference. In addition the brush seal can be damaged if the bristle pack is flexed the wrong way by rotating in reverse. The initial level of force pressing the bristles against the surface of the shaft may be increased to increase the initial sealing capability. However this will also increase the effects on the shaft, causing greater heating and wear for the same surface speed.

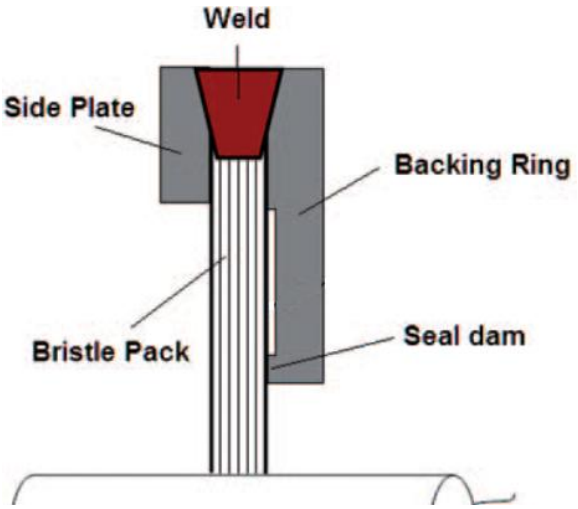

Figure 12: Sketch of a typical brush seal - side view, leakage flow left to right [**22**]**.**

Bristle pack	Provides the restriction to the flow.
Side plate	Provides structural rigidity and restrains the bristles.
Weld	Attaches the bristles to the seal. Machined to form sealing surface with seal housing.
Backing ring	Provides structural rigidity and restrains the bristles. Extends to smaller inner diameter than the side plate to control flexing of the bristles due to high upstream pressure
Seal dam	Reduces the area of the backing ring in contact with the bristle pack, which reduces friction on the bristles allowing easier movement.

Table 1: Main components of a typical brush seal [**22**]

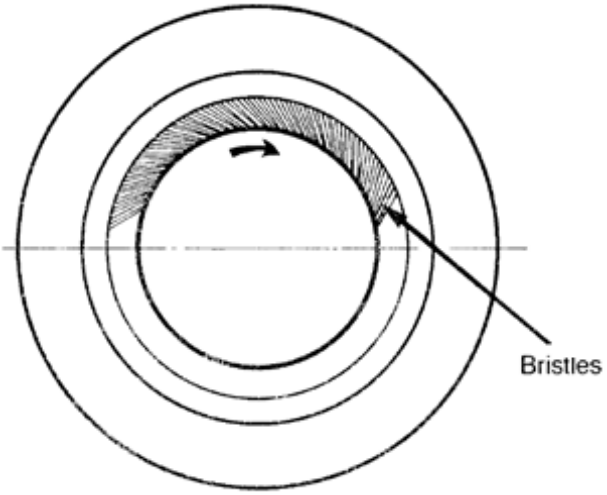

Figure 13: Schematic of a typical brush seal – front view [**7**]**.**

The bristles are generally inclined to the radial direction with an angle of 45 - 55 degrees [**22**] to reduce bristle bending; this is shown in Figure 13. This means that if the rotor were to turn in the reverse direction the individual bristles would come under compressive loading along their long axis, resulting in them buckling or breaking. The performance of a brush seal is greatly reduced by bristle damage [**7**]. This means that each application must be carefully considered to avoid causing bristle damage and harming performance.

Improvements have been suggested to the design of brush seals as they have become better understood and further developed. Shoed brush seals add a set of pads, or "shoes" to the free ends of the bristles. Each shoe covers a short circumferential section across the axial length of the seal. This addition reduces leakage flow rate while also allowing for rotation in either direction [**22**]. A shoed brush seal design is shown in Figure 14.

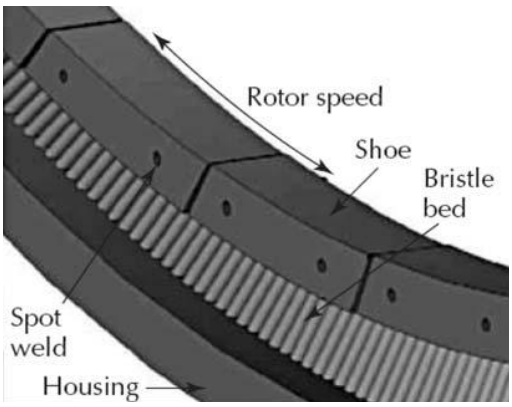

Figure 14: Shoed brush seal [**22**]

The weld which bonds bristles in the bristle pack to each other and to the side plate and backing plate (see Figure 12) is a point of weakness in the structural design of the seal. Heating during welding can cause embrittlement in the bristles at the location of the weld, causing a loss of bristles and damaged seal performance during service [**22**]. To completely remove this design issue, MTU created a new fabrication process resulting in a design which fixes the bristles mechanically [**23**].

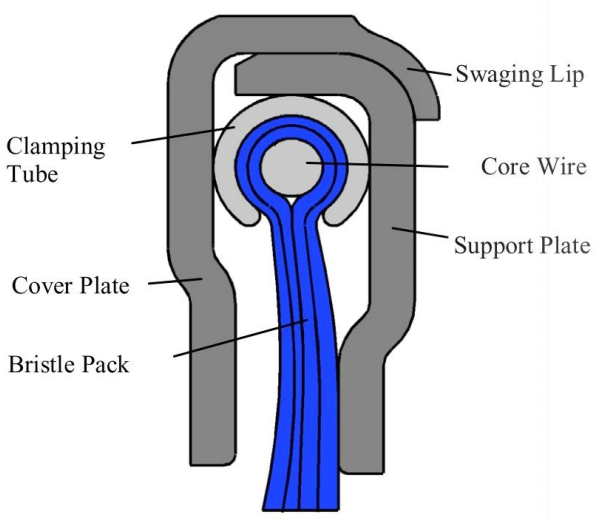

Figure 15: MTU Brush seal design [**23**]

In the MTU design, the bristles are wrapped around a core wire and restrained by the clamping tube to form the core element. The core element is then placed inside the support plate and cover plate, and the unit is crimped together, deforming the swaging lip to join the two plates.

2.4.Leaf Seals

Leaf seals reduce leakage by forming a physical blockage across the leakage channel to the surface of the rotor in a similar manner to the brush seal. They consist of a set of flat plates, or "leaves" which stack together to fill the whole circumference of the seal [**24**]. The leaves may be inclined to the radial direction in the same way as in brush seals, allowing some degree of rotor movement. Figure 16 shows this arrangement. Alternatively the leaves may be rotated 90 degrees about the radial axis and be inclined forward. In this arrangement the high upstream pressure causes each leaf to bend toward the rotor, this presses hydrodynamic runners down on to the rotor which then 'ride' on a thin film of leakage flow at very small clearances of less than half a millimetre [**25**].

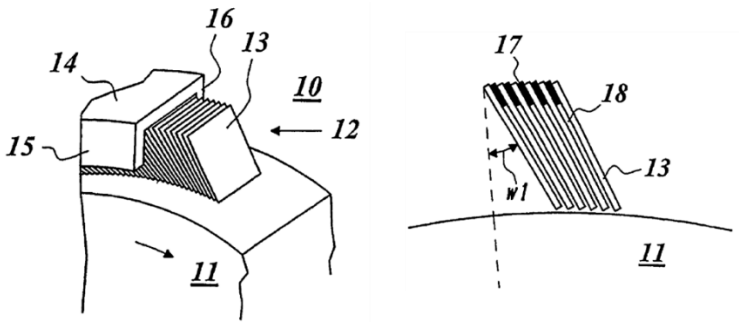

Figure 16: Sketch of the leaf seal from the original patent [**24**]

Leaf seals have the advantage over brush seals that axial force due to the pressure difference across the seal will not bend the leaves downstream. Brush seal bristles can bend downstream which opens up the seal clearance, but the geometry of each leaf means that this cannot occur in either design. However the leaf seal is a relatively new concept that has not yet been implemented in production turbomachinery [**24**].

2.5.Rim Seals

In modern gas turbines, the working fluid in the main gas path can reach extreme temperatures of the order of 1800 - 2000 K at the inlet to the turbine. The first stage of the high pressure turbine in most modern gas turbines therefore tends to use some combination of advanced materials, coatings, and film cooling on the nozzle guide vanes (NGVs) and turbine blades. There is a clearance and therefore a possible leakage path between the stationary NGV row and the rotor. This leakage path leads from the main gas path through a non-contacting seal, and into a cavity between the stator and the rotating turbine disc. This is called the rim cavity and is shown in Figure 17. While the NGVs and turbine blades are protected from the high temperature by internal and surface film cooling, the turbine disc is not. It is therefore important to prevent hot gas ingestion from the main gas path into the rim cavity where the high temperature gas would cause damage. Purge jets are used to maintain a positive pressure in the rim cavity and ensure net flow out of this zone through the rim seal rather than into it.

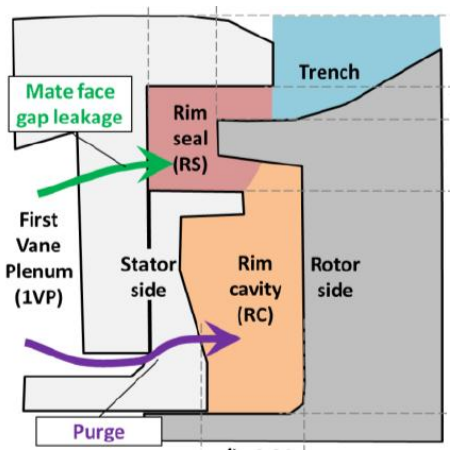

Figure 17: Turbine rim real showing position purge flow is injected into rim cavity [**26**]

Clark et al [**26**] studies the effect of purge jet configuration on rim seal effectiveness. The research shows that the smaller the number of purge jet holes, and therefore the higher the purge jet momentum flux, the greater the sealing effectiveness for a given mass flow rate of purge gas. While the configuration of this seal is very different to the fluidic curtain seals studied in this body of research, this result is in agreement with the findings of Auld et al (Section 2.6.6): Using a smaller number of purge jet holes is physically equivalent to using a thinner fluid curtain, which will also give a higher momentum flux in the curtain for a given curtain mass flow rate [**10**].

2.6.Fluidic Curtain Seals

The first patent for a fluidic curtain seal was filed in 1954, and several more have been filed since. These patents cover a range of ways that a fluidic seal may be implemented; some describe seals which apply the operating principles discussed in Section 1.3 by utilising either fully circumferential fluidic curtains or discreet jets. However, most of the patents describe technologies which remain undeveloped, so the exact effects on leakage and on turbine stage efficiency are not well known. In 2009 the first paper was published on a fluidic curtain seal design [**9**], which had successfully increased turbine efficiency in a test rig. Since then, others have successfully designed and tested other fluidic curtain seal designs. At the time of writing fluidic curtain seals have never been used in production turbomachinery applications.

2.4.1 Auyer, 1954

Auyer [**27**] registered a patent in 1954 in which a circumferential slot provides a fluid curtain to be used to redirect tip leakage radially inward so that it passes through the blade row for an unshrouded turbine rotor.

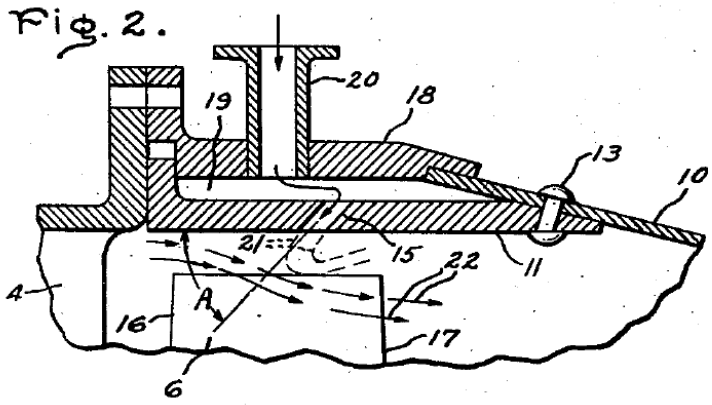

Figure 18: Auyer patent [27].

Figure 18 shows the turbine casing and the tip of one of the blades. A cavity in the casing is pressurised from some external source, and the pressurised fluid in the cavity exits through the slot labelled item 15. The slot is angled to direct the fluidic curtain both radially inward and against the direction of the leakage flow (i.e. upstream). The fluid issuing from the cavity is depicted turning to the downstream direction. By reversing the direction of this fluid jet to flow downstream as well as radially outwards, there is a reaction on the turbine working fluid entering the tip gap, directing it radially inward. This causes more of the incoming working fluid to be directed over the turbine blades and to do useful work.

2.6.1. Smile et al, 1960

Smile et al [**28**] proposed in 1960 a fluidic seal in which a circumferential chamber around a shrouded turbine rotor is pressurised by fluid injected from the casing, to reduce tip leakage and allow a more lightweight tip shroud design.

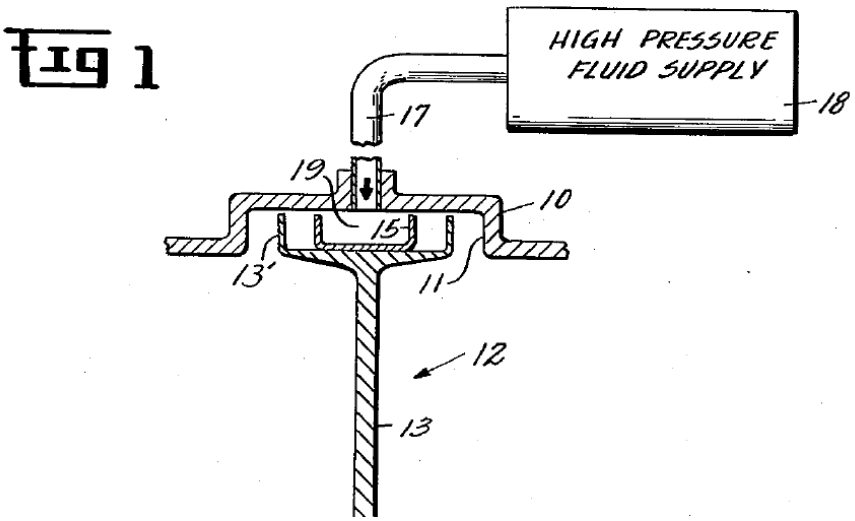

Figure 19: Smile patent [28].

The concept of this design is slightly different to other fluidic sealing concepts. The main purpose of the design is not in itself to reduce the leakage flow rate but to counter the centrifugal forces exerted on the rotating portion of the tip seal. By applying pressure force inward on the rotating seal from an external fluid supply, the outward forces on the seal due to its rotation can be counteracted. This means that a lower strength shroud structure can be used without ill effect, reducing the physical dimensions of the seal as well as its mass [**28**]. Since the rotational forces exerted on the shroud increases linearly with the radius of the rotor, the effectiveness of the concept will increase as seal radius increases. It is for this reason that the patent depicts a turbine tip seal.

2.6.2. Unsworth and Burton, 1971

A patent by Unsworth and Burton [**29**] describes the fluidic seal design shown in Figure 20. Fluid issuing from a circumferential slot in the casing forms a continuous fluidic curtain between the casing and the turbine rotor shroud, which opposes the tip leakage flow.

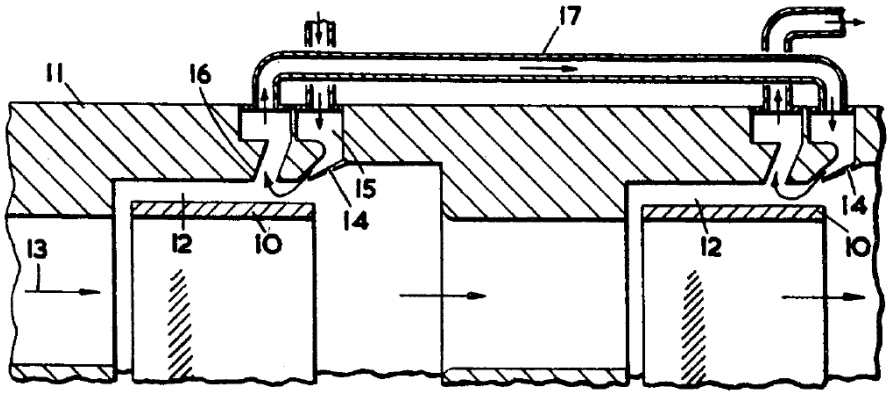

Figure 20: Unsworth and Burton patent [**29**]

Unsworth and Burton do not specify the initial source of fluid to their seal design, but depending on the required supply pressure a passive source may be sufficient to supply the seal with fluid. Multiple configurations are discussed. The simplest configuration consists of a single externally supplied fluid curtain. This patent also discussed a curtain that is re-ingested slightly upstream and reused in a second curtain in a turbine stage downstream of the first. The most complex configuration specifies that the fluid curtain injected is to be re-ingested in the same shroud cavity and fed into another fluidic curtain in the following turbine stage; and then the following stage and so on, facilitated by the duct labelled ‘17’ in Figure 20. This could allow the same source of high pressure fluid to operate fluidic seals in multiple turbine stages.

2.6.3. Turnquist, 2009

The source of the fluid used in the fluidic curtain is considered by Turnquist et al [**30**]. If the fluidic seal is not passively supplied from upstream in the same turbine stage, then it must be ensured that the energy expended pressurising the fluid used in the seal does not exceed the energy recovered by the overall increase in efficiency that the fluidic curtain causes.

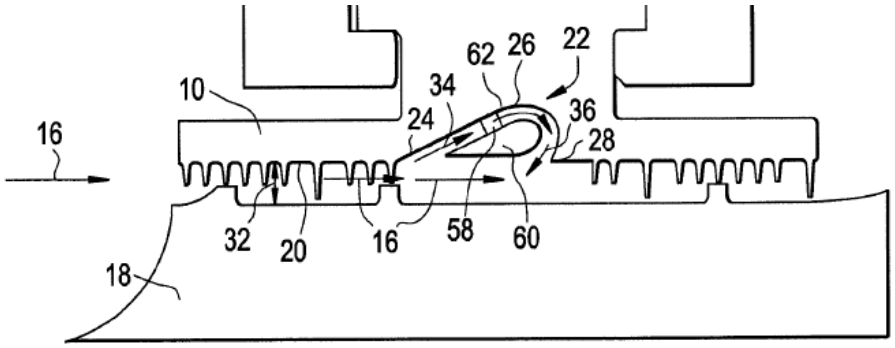

Figure 21: Turnquist patent

In one of the concepts described in Turnquist's patent, a fluidic curtain seal is incorporated into a shaft gland seal and is fed by a slot in the gland, upstream of the slot from which the fluidic curtain issues but still within the same shroud cavity. The first slot is inclined at a smaller angle to the axial direction than the second slot. This means that a greater component of the dynamic pressure in the leakage flow is directed into the first slot than the second slot. Therefore some amount of the leakage flow must pass into the first slot and then exit back into the leakage cavity through the second slot. Upon exiting from the second slot the flow forms a fluidic curtain, where it causes a pressure drop in the bulk of the leakage flow as in the Unsworth and Burton design.

2.6.4. Curtis et al, 2009

Curtis et al [**9**] designed and tested a fluidic curtain in a shroud cavity on an intermediate pressure turbine stage test rig. The design is shown in Figure 22.

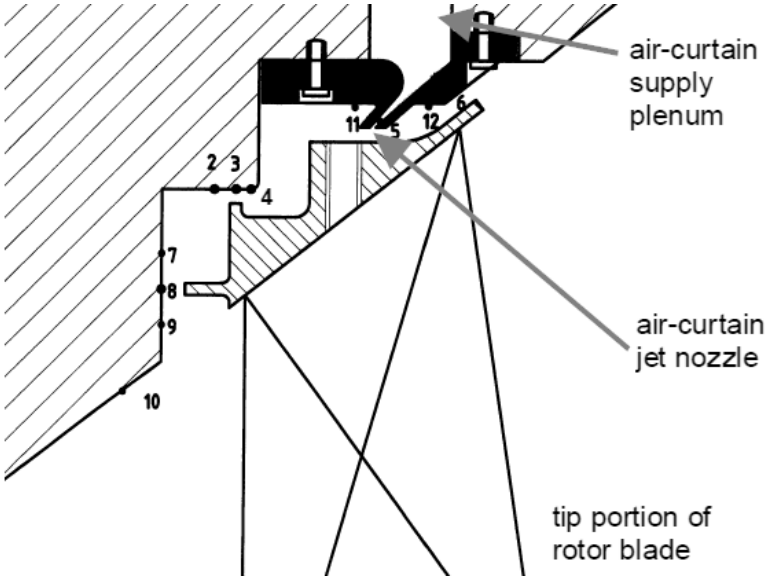

Figure 22: Tip seal design tested by Curtis et al [**9**]

The test rig used air supplied at low pressure from fans to produce the main gas path flow and the fluidic curtain flow. Turbine efficiency was measured and the variation in efficiency shown across a range of fluid curtain flow rates for a fixed turbine shaft speed was investigated.

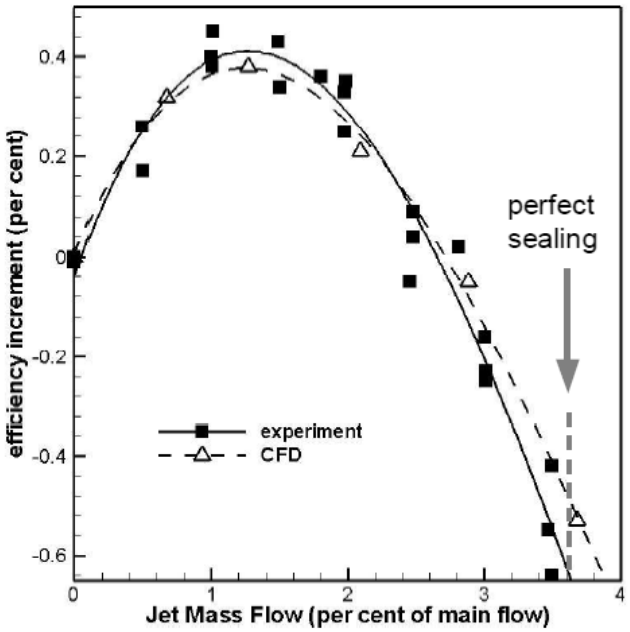

Figure 23: Efficiency change vs fluidic curtain flow [**9**]**.**

The research examined the overall effect on turbine efficiency, taking into account the performance cost of supplying the fluidic curtain. Supplying the fluid curtain at the optimum rate allowed the overall turbine stage efficiency to be increased by a maximum of ~0.5 % as seen in Figure 23. It was also shown that at a certain supply pressure, the fluidic curtain was

able to completely stop the flow at the inlet to the shroud cavity, indicated by the 'perfect sealing' point in the Figure above.

In Figure 23 the overall stage efficiency improved by 0.4 % at a curtain flow rate of ~1.5 % of the main flow. It can be seen in Figure 24, that at this curtain flow rate the inlet leakage flow dropped by ~30 % while the net mass flow at the shroud cavity exit varied by only a few percent.

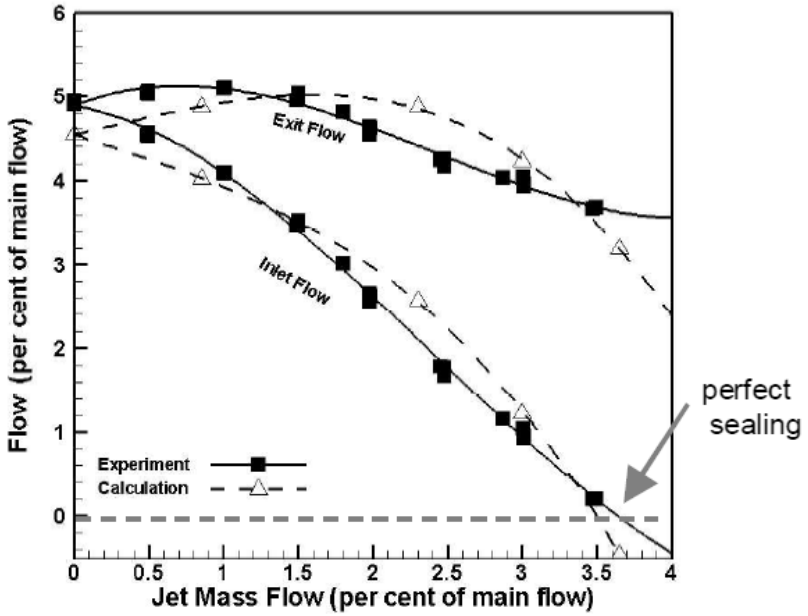

Figure 24: Shroud inlet and outlet flow rates vs fluidic curtain mass flow [**9**]**.**

2.6.5. Hogg and Ruiz, 2011

Hogg and Ruiz [**31**] showed a fluidic curtain seal is effective when incorporated into a labyrinth type restriction, where it acts to reduce the 'effective clearance' of this restriction and therefore decrease overall mass flow rate. A range of operating conditions and fluid curtain configurations were explored.

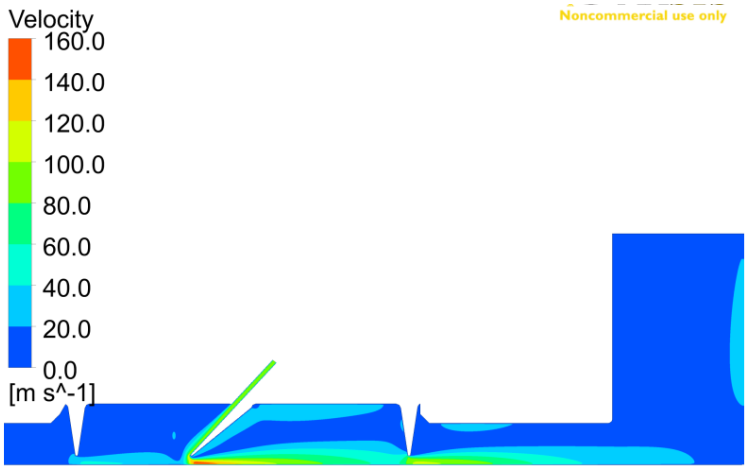

Figure 25: Velocity contour plot from Hogg and Ruiz seal design [**31**]

Figure 25 shows a seal design in which a fluid curtain is injected immediately upstream of an inclined labyrinth fin. The curtain flow remains attached to the front face of the fin until it reaches the tip, at which point it acts to reduce the cross section of the vena contracta for the flow that is discharged through the labyrinth restriction [**31**]. By reducing the size of the vena contracta the fluid curtain reduces the effective area of the existing labyrinth seal, and therefore leakage mass flow rate. The seal design using a curtain injected on the front face of a labyrinth fin were explored further [**32**] [**33**] and it was found that the leakage reduction is greatest when the curtain is positioned toward the front of the leakage channel.

2.6.6. Auld et al, 2013

Auld et al [**10**] describe a CFD study to design a fluid curtain seal to reduce rotor tip leakage on a shrouded turbine rotor of a single stage axial flow Organic Rankine Cycle turbo-expander unit. The study explored the effects of changing three features in the fluid curtain; fluid curtain thickness, fluid curtain axial position, and fluid curtain angle. The results of this study showed that to increase sealing effectiveness the thickness of the curtain should be minimised, the curtain angle should be made as acute as possible with respect to the turbine axis, and that the axial position of the curtain should be as far downstream as possible while still allowing the curtain to impinge on the shroud surface. These design rules must be traded off against ease of manufacture. The research also explored the effect on the power contribution by shroud shear. As leakage flow enters the shroud cavity from the main stage through-flow, it retains a high degree of swirl from the upstream nozzles and therefore exerts a tangential force component on the surface of the shroud. This tangential force contributes to the rotor torque and therefore turbine output power. It was found that one of the effects of the fluid curtain (if it is introduced without pre-swirling the curtain flow), is to reduce the swirl in the shroud leakage

flow which reduces the turbine output power. This effect reduces the overall power available to the turbine and could cause a net windage loss in the shroud cavity.

2.6.7. Hilfer et al, 2015

Hilfer et al [**34**] carried out experimental tests on the turbo-expander unit and fluid curtain seal design from Auld et al [3]. Turboexpanders are small waste heat recovery turbines used on large diesel engines.

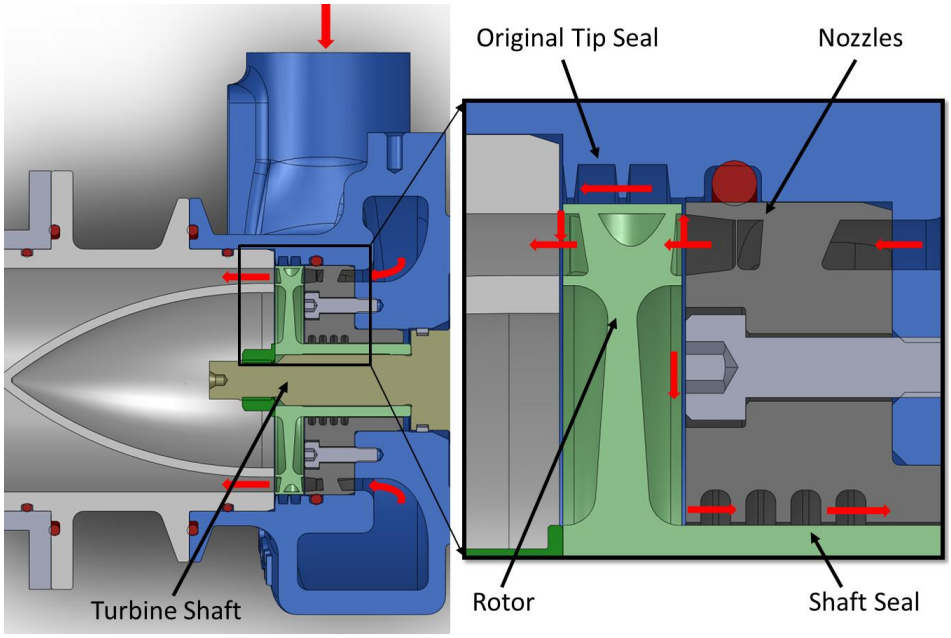

Figure 26: The turbo expander original design [**34**]

.

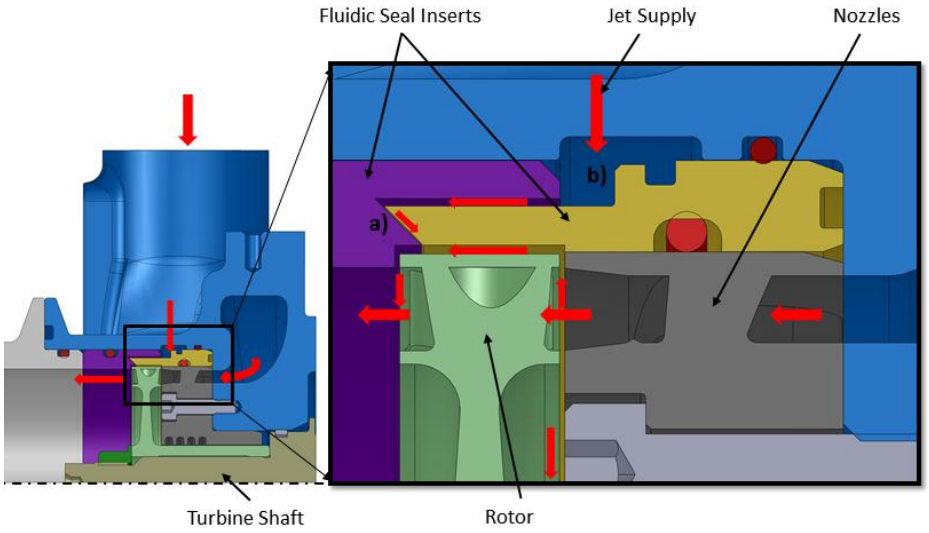

Figure 27: The turbo expander modified design [**34**]

The turbo expander unit is shown in Figure 26 and the hardware modifications needed to incorporate the fluid curtain into the rotor tip seal are shown in Figure 27. The tests confirmed that the fluid curtain produced the expected reduction in shroud leakage flow predicted by the CFD calculations. However, the expected benefit of increased turbine efficiency due to the fluid curtain reducing shroud leakage flow was not measured successfully in the tests.

Hilfer developed and validated an analytical expression for the pressure drop across a fluid curtain. The formula can be found in Hilfer's PhD thesis [**5**]:

$$P_{in} - P_{out} = \frac{\rho {v_{jet}}^2}{2} \cdot \left[\frac{R^2}{(R-th)^2} - 1\right] \quad (2.4)$$

Where:

P_{in}= Upstream pressure (Pa)
P_{out} = Downstream pressure (Pa)
R = Radius of curve traced by curtain as it is turned downstream (m)
th = Curtain thickness (m)

2.6.8. Ghaffari and Willinger, 2016

Whilst a fluidic curtain can reduce leakage mass flow rate through a shrouded turbine tip seal, it will also have an effect on the tangential velocity of the leakage flow, which is highly swirled by the upstream stators. As the swirling leakage flow leaves the shroud cavity it mixes with the turned flow leaving the turbine blades. This causes mixing losses and interferes with the incidence of the flow entering the downstream stator row; both of these effects contribute to overall tip leakage loss [**35**]. Ghaffari and Willinger [**36**] showed that it is possible to use a fluid injected into the tip seal of a shrouded low pressure turbine to alter the flow structure in the shroud cavity, in such a way that the downstream mixing losses are reduced and the incidence of the flow on the downstream stators improved.

2.6.9. Rai et al, 2016

Rai et al [**37**] describe a study using fluid curtains within one or more pockets in a labyrinth seal in order to reduce leakage flow rate. The designs investigated were representative of a gas turbine compressor shaft seal. The leakage was modelled using CFD for a baseline seal design both with and without a honeycomb stator, and then with fluid curtains added. The fluid curtains used were injected from the stationary wall at right angles to the incoming leakage flow. Figure 28 shows one of the simulated seal designs, featuring a honeycomb stator and a fluid curtain being injected into the centre of the first labyrinth seal pocket.

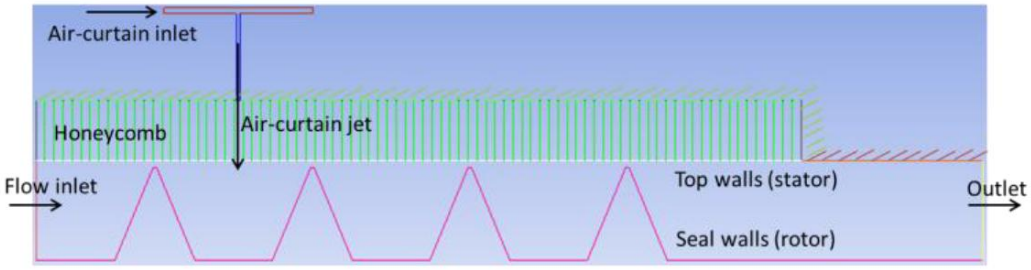

Figure 28: A seal design tested in CFD by Rai et al [37]

Three fluid curtain configurations were explored; a single curtain in the first pocket, single curtains in the first three pockets, or three curtains in the first pocket. These designs achieved leakage reductions over the baseline design of ~30 %, ~40 % and ~50 % respectively. The improvement did not differ between a smooth stator and honeycomb stator. The mechanism of leakage reduction was to detach the high speed jet issuing from each labyrinth restriction from the top wall. This is shown in Figure 29 Once it has been diverted radially inward, the flow must turn to pass through the next labyrinth restriction. The more that the flow has to turn to pass through each labyrinth restriction, the smaller the 'effective clearance' of the restriction becomes.

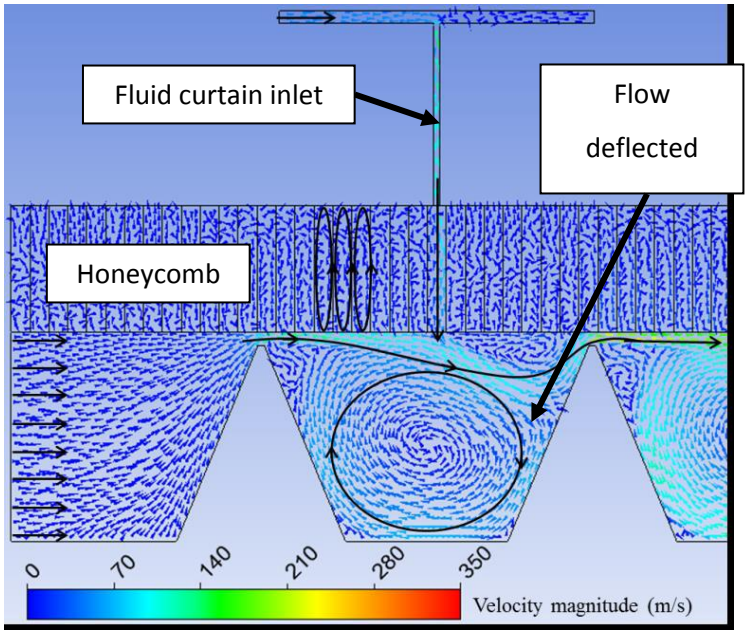

Figure 29: Velocity vectors from Rai et al – design case 4 [37].

2.7.Conclusion

The literature describing a variety of methods of interstitial sealing in turbomachinery has been discussed in this chapter. Labyrinth seals are the most common type of turbomachinery seal currently in use and have been well understood for over 100 years. Brush seals are a less mature technology than labyrinth seals and are currently much more limited in their application. However, there are brush seals in service and they generally give leakage flow rates approximately an order of magnitude lower than the labyrinth seals used in similar applications. Fluidic curtain seals have been considered in a wide variety of application types. Many patents have been registered going back to the 1950's, but until recently the technology has not been developed and incorporated into any production turbomachinery applications. Following a paper in 2009 describing work which demonstrated a performance benefit from incorporating a fluid curtain into a shrouded rotor blade tip seal, fluidic curtain seals have begun to receive more attention. Seal leakage flow reductions of more than 40 % have been found in some studies due to the presence of a fluid curtain. However the current state of knowledge on fluid curtains is not complete enough to repeatably create new high performance fluid curtain designs:

- A wide range of fluidic seal architectures and design concepts have been proposed. No standard design or set of design rules has been established so far for fluidic curtain seals.
- Only Auld et al examined the effect of systematically varying critical dimensions of the seal geometry; curtain thickness, curtain angle, and the axial position of the seal.

The aim of the research described in this thesis is to start to address the above points, through a systematic study to investigate and establish some fundamental design rules and parameters for developing effective fluid curtain type seals for turbomachinery applications.

3. Fundamental Study to Understand Geometric Parameters

This chapter examines a wide design space of generic fluidic seal designs in order to understand the effect of seal geometry on its performance characteristics. The most important dimensions of the seal were varied to produce a range of designs, and then CFD was used to calculate their performance. This allows the performance of a generic fluidic curtain seal to be mapped against its physical dimensions, which provided a useful tool to assist in designing seals in following chapters.

3.1.Overview of the Study and its Aims

A computational investigation into the effect of geometry on the performance of a fluidic curtain seal is described in this chapter. This was identified as a research objective in Section 1.4. The intent was to explore how the performance of a fluidic curtain is affected by various fundamental seal parameters such as leakage channel height and fluid curtain thickness etc. The results have been used to create a performance map for quickly estimating the performance of new seal designs based on seal geometry and operating conditions.

First, a standard geometry for the fluidic curtain seal was defined; a fluid curtain inclined at 45 degrees to the incoming leakage flow, followed by a single labyrinth fin type restriction in a leakage channel of constant height. This geometry was selected because:

- Hilfer [**5**] showed that the best leakage reduction due to a fluidic curtain is achieved when the curtain is used to decrease the pressure drop across a downstream conventional seal.
- This is the simplest arrangement of a fluidic curtain followed by a labyrinth seal, with the smallest number of dimensions to be defined. This makes the geometry as generic as possible. The leakage performance (relationship between pressure drop across and leakage flow through) of any type of turbomachinery seal operating under given flow conditions can be reduced to a single fin restriction with a clearance set to the effective clearance of the multi-fin labyrinth seal or brush seal etc that is being represented.

The important dimensions in the seal geometry were identified and a set of geometric ratios were proposed to non-dimensionally characterise each seal design. The fluidic curtain inlet pressure was also non-dimensionalised. Ranges of values were selected for these non-dimensional parameters, giving a range of seal designs and operating pressures. Test cases were created and run using CFD for every combination of geometric ratios and operating

pressures. This allowed the effect of changes in these parameters on seal performance to be examined and some design guidelines to be established for fluid curtain seals.

3.2.Idealised Parametric Seal

The generic seal design used in the study is shown in Figure 30. The geometry consists of a constant height leakage channel with a fluidic jet issuing from the outer wall and a labyrinth fin placed downstream, with a kinetic energy blocker placed axially half way between these features. The kinetic energy blocker prevents the high velocity flow in the curtain from travelling along the inner wall after impinging on it, and passing straight through the downstream restriction. This feature was first added by Hilfer [**5**] and diverts this stream back toward the outer wall instead. The only function of the blocker is to detach the flow from the inner wall, so it should not be large enough to create a restriction that causes a signficant pressure drop in the channel. In this study the blocker height was 20% of the channel height.

For many axisymmetric leakage channels in turbomachinery applications the radius ratio of the outer to inner channel walls is close to unity. This is definitely the case for the rotor tip seal applications that are investigated later in the present study. Some preliminary CFD calculations were conducted to compare the performance of the generic seal geometry in Figure 30 with planar and axisymmetric leakage channels. A radius ratio of 1.1 was selected for the axisymmetric channel. This value is considered to be an extreme case of typical leakage channel radius ratios for fixed and moving blade rotor clearances in turbomachinery stages. The results for leakage reduction were within 1% for the planar and axisymmetric cases and so a planar leakage channel has been used to develop the generic fluid curtain seal performance map described in this chapter.

The four most important geometric dimensions are indicated in Figure 30. These are:

- Fluidic curtain width (*a*)
- Leakage channel height (*b*)
- Single labyrinth fin clearance height (*c*)
- Distance between the point at which the fluid curtain enters the leakage channel and the labyrinth fin (*d*)

Note that *c* is the clearance height of the equivalent single fin labyrinth seal, this decreases with the square root of the number of labyrinth fins of a given clearance in a full multi-fin labyrinth seal. This way, a single fin can be used to represent a multi-fin seal.

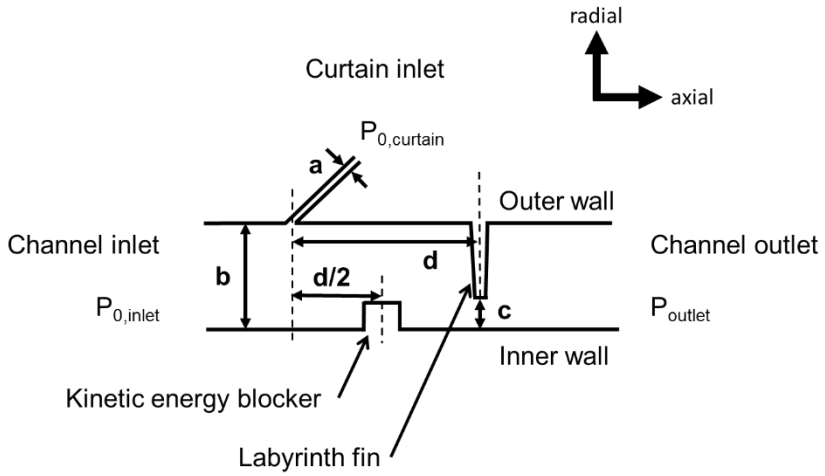

Figure 30: Generic seal layout

The channel height is combined with the other dimensions to form three dimensionless geometry parameters that are used in this study: *A*; *C*; *D*.

- *A* = *b*/*a*, ratio of channel height to fluidic curtain width.
  High value means thinner fluidic curtain.

- *C* = *b*/*c*, ratio of channel height to effective single labyrinth fin clearance height.
  High value means tighter labyrinth restriction.

- *D* = *d*/*b*, ratio of the axial distance between fluidic curtain inlet slot and the labyrinth fin compared to the channel height.
  High value means greater axial spacing.

In this way each geometry to be tested could be fully defined by the three parameters, *A*, *C*, and *D*. The dimension *b*, leakage channel height, governs the annular area of the leakage channel and so was used to non-dimensionalise the others. By considering equation 2.2, it can be seen that the dimension b therefore sets the flow rate through the leakage passage if there is no fluidic curtain or labyrinth seal present. Parameters *A*, *C*, and *D* then control the change in the flow rate through the leakage channel due to the addition of the fluid cutain and the labyrinth fin seal. In parameter *A* and *C* the channel height is used as the numerator while in parameter *D* it is used as the denominator. The ratios are defined this way for convenience, so that their numerical values are greater than unity.

Previous work [**10**] [**11**] [**5**] [**38**] shows that the thickness of the fluidic jet is an important factor governing sealing effectiveness, and clearly the size of labyrinth fin clearance will also have a

powerful effect on seal effectiveness. The values of *A* and *C* were therefore varied widely. The distance between the fluidic curtain and the labyrinth fin however was expected to have less impact on the flow through the seal. The seal shown in Figure 30 essentially consists of two components. These are the fluid curtain and the labyrinth fin. It was anticipated that the seal flow would be a weak function of *D*, provided there was sufficient distance between the location of the fluid curtain injection and the labyrinth fin, for the curtain flow to be unaffected by the acceleration through the labyrinth restriction. For this reason, just two values of *D* were examined.

Each design was investigated using CFD over a range of fluidic seal inlet total pressures for a fixed leakage channel inlet total to outlet static pressure. Pressure ratio (*PR*), as defined in equation 3.1, was used to define the non-dimensional fluidic seal inlet total pressure with respect to channel inlet total and outlet static pressure.

$$PR = \frac{P_{0,jet} - P_{outlet}}{P_{0,inlet} - P_{outlet}} \tag{3.1}$$

For each design, there is an inherent maximum useable value for *PR*. When this *PR* value is reached, the strength of the fluidic curtain is such that it completely eliminates any inlet flow into the leakage channel. Increasing *PR* further will cause the flow across the leakage channel inlet to reverse. This corresponds to some of the fluid curtain flow being forced back out of the leakage channel through its inlet. This situation would have a detrimental impact on the turbine aerodynamics and must be avoided when designing this type of seal. The condition is referred to as 'overblowing' the seal. The maximum useable *PR* will vary depending upon the seal geometry and its operating conditions. It represents the limiting operating condition for each configuration and will yield the greatest reduction in overall leakage mass flow rate.

3.3. CFD Study

The idealised seal designs were investigated using CFD by constructing 2D, mainly unstructured, axisymmetric meshes using Pointwise Version 17.3 Release 5. Calculations were carried out with ANSYS Fluent version 15.0.7.

Figure 31 shows the dimensions of the idealised seal geometry used in the parametric study for one of the selected combinations of *A*, *C* & *D*. Table 2 shows the ranges of values of parameters *A*, *C* and *D* that were investigated. The geometries for combinations of *A*, *C* & *D* all used a channel height of 10 mm, a curtain channel length of 12 mm, a square section kinetic energy blocker of side 2 mm and labyrinth fin root and tip thicknesses of 2 mm and 0.5 mm

respectively. All other dimensions were defined by the selected values of *A*, *C* and *D*. The kinetic energy blocker was positioned mid-way between the curtain injection cross-channel plane and the labyrinth seal tip, for both *D* = 1 and *D* = 2.

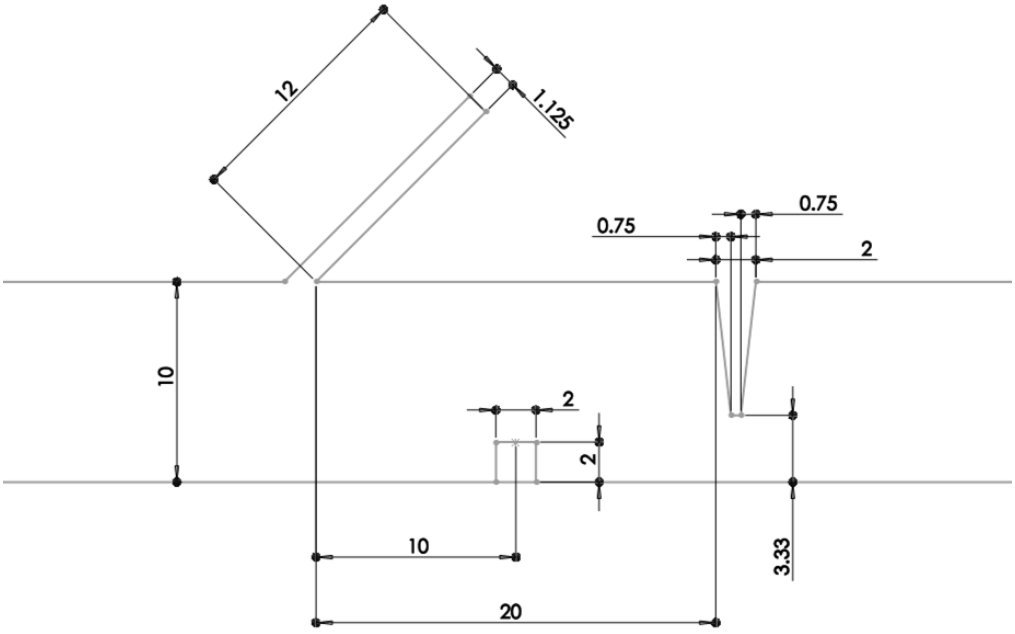

Figure 31: Geometry in case where *A* = 8, *C* = 3, *D* = 2 (all dimensions in mm)

Parameter	Levels
A	6, 8, 10, 12, 14, 16, 18, 20
C	1, 1.25, 1.5, 2, 2.5, 3, 4, 6, 8
D	1, 2

Table 2: Test points run in full factorial experiment.

CFD parameters	
Cell count	~780 000
Minimum orthogonal quality	~0.52
Simulation type	RANS steady state, pressure based
Format	2D, axisymmetric

Viscosity model	k-epsilon realisable		
Wall functions	Fluent enhanced wall treatment		
Boundary conditions	Channel inlet	Pressure inlet	Total pressure = 1.5 bara Flow direction normal to inlet planes
	Channel outlet	Pressure outlet	Static pressure = 1.0 bara Flow direction normal to inlet planes
	Curtain inlet	Pressure inlet	Total pressure varied to give PR range to just beyond the overblown condition
	Walls	Stationary wall	-

Table 3: Parameters used in CFD study, all meshes used have similar values.

Since a large proportion of the effect of the fluidic seal is generated through the addition of momentum opposed to the channel flow [**39**], near-wall viscous effects were considered less important for the study and so a 2 equation turbulence model was adopted using wall functions. The k-epsilon realisable turbulence model has been shown to be the most appropriate for modelling fluidic curtain seals in previous research [**40**]. The movement of the wall representing the rotor shroud was likewise disregarded. Fluent gives an option for 'enhanced wall treatment,' where the first cells in the laminar sublayer use the linear law of the wall where $y+ < 10$, a blending function in the buffer layer where $10 < y+ < 30$, and the log law of the wall where $y+ > 30$ [**41**]. This meant that using an unstructured mesh with a variation in wall y+ values was expected to produce an accurate prediction of the seal flow, despite the near-wall flow behaviour not being captured in fine detail.

Mesh dependency was checked by calculating results for coarser and finer meshes. Boundary lines were placed 50 mm upstream of the fluidic jet inlet and 40 mm downstream of the labyrinth seal, and the cell count in this 'working section' was varied.

	Mesh		
	Coarse	**Nominal**	**Fine**
Cell count in working section	35253	67272	78570
Outlet mass flow max reduction	46%	48%	49%
Max operating pressure ratio	2.64	2.69	2.54

Table 4: Mesh independence study.

If working section cell count is reduced by ~50 % or increased by ~15 % there are small enough changes in the results that they can be considered independent of changes in the mesh.

3.4. Analysis Method

CFD simulations were carried out for each design point. A first run was carried out with no fluid curtain, followed by a series of further simulations with the fluid curtain present and increasing values of curtain pressure ratio *PR* (see equation 3.1). The channel inlet total pressure and channel outlet static pressure were both kept constant at 1.5 bar and 1.0 bar respectively, as given in Table 2. CFD simulations with the fluid curtain were carried out starting from *PR* = 1.0, with PR increasing in increments of 0.5 until the over blown condition (seal inlet mass flow reversed) was exceeded.

For each of the CFD runs the seal performance was characterised by a leakage reduction factor (L) defined in equation 3.2.

$$L = \frac{\dot{m}_{out,no\ curtain} - \dot{m}_{out,with\ curtain}}{\dot{m}_{out,no\ curtain}} \tag{3.2}$$

L is the proportional reduction of outlet mass flow rate compared to the corresponding no jet case.

3.5. Results and Discussion

As discussed in the previous section, each design point was tested using CFD over a range of pressure ratios. As an example, the CFD prediction of the mass flow rates at the channel inlet, channel outlet and curtain inlet boundaries for the design point where *A* = 8, *C* = 2 & *D* = 2 is shown in Figure 32. The mass flow rates shown are the mass flow rates per metre in the planar 2D fluid domain.

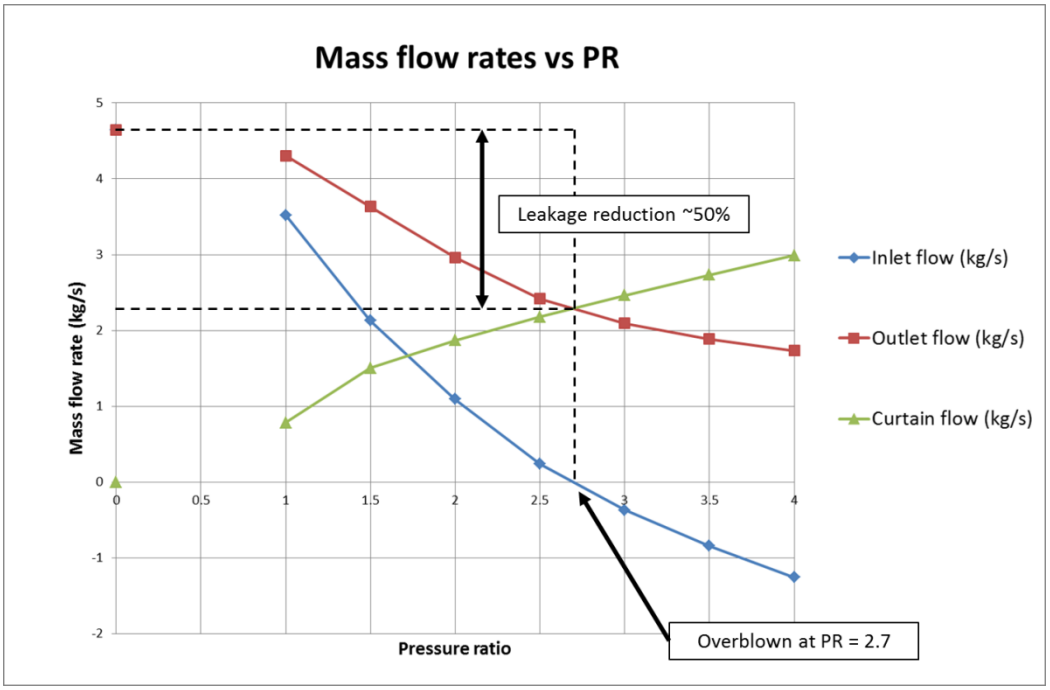

Figure 32: Changes in mass flow across each boundary as PR increases – Example shows the case where *A* = 8, *C* = 2, and *D* = 2.

Figure 32 shows how as *PR* is increased and the curtain mass flow rises, the seal inlet mass flow decreases and the overall leakage flow leaving from the outlet (channel inlet flow plus jet inlet flow) is also reduced. The curve of inlet mass flow rate crosses the x-axis at an interpolated optimum pressure ratio of 2.7, this is the point the flow is reversed at the inlet and the system became over blown. The maximum achievable reduction in overall leakage (Leakage Reduction Factor, *L*) is from 4.8 kg/s to 2.2 kg/s, a reduction of just over 50 % at a $PR_{optimum}$ of 2.7 for the example shown.

3.5.1. Response Surface for L and PR

The values of *L* at the point at which the seal becomes over blown, obtained for all combinations of *A* and *C* (for *D* = 2) are shown as a performance map in Figure 33. The black contour lines superimposed on the figure indicate the value of *PR* needed to deliver the leakage reduction shown, for any particular value of parameters *A* and *C*. The CFD calculation points used to generate the contours are shown by black diamonds in the Figure.

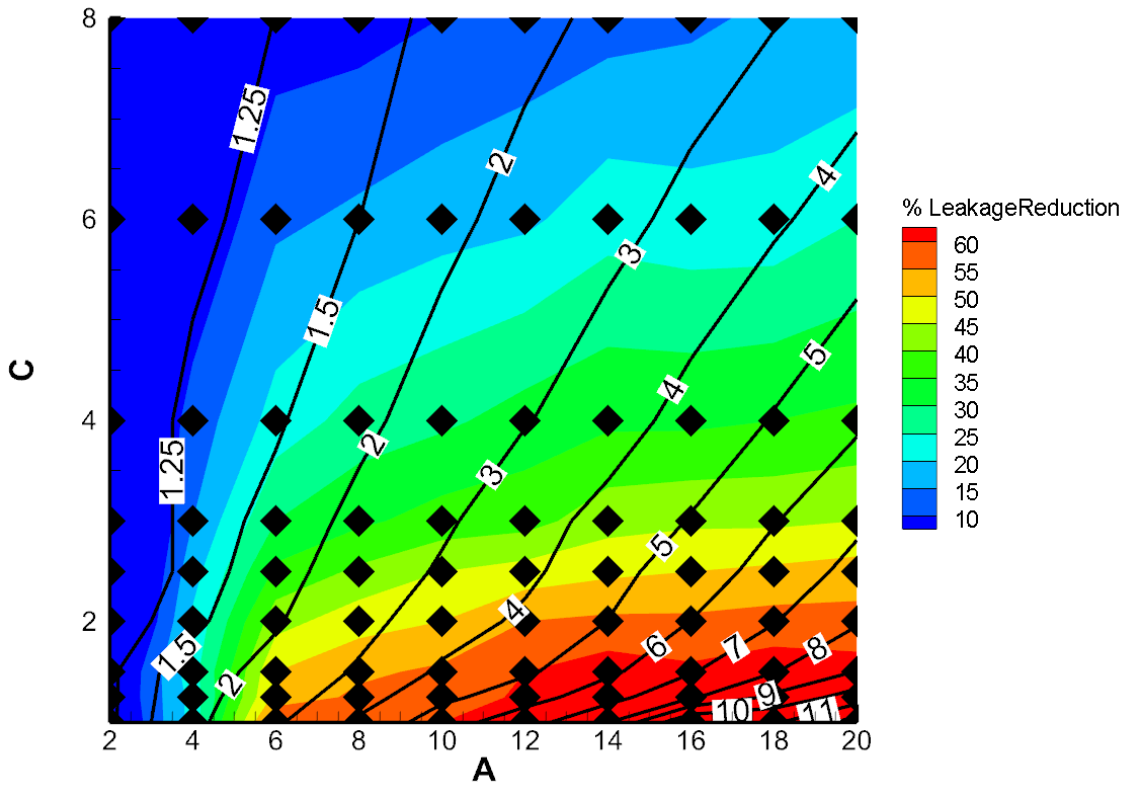

Figure 33: Max % Leakage Reduction L_{max} – Generic seal. Bold lines show $PR_{optimum}$

Figure 33 shows that the maximum possible reduction in leakage flow with the fluid curtain for this geometry increases as the thickness of the fluidic curtain is reduced (increased *A*) and the labyrinth seal clearance is increased (reduced *C*). It is also shown that as the maximum attainable leakage flow reduction increases with changes to geometry, so does the value of *PR* needed to achieve this flow reduction. These results are consistent with results in Hilfer [**34**]. This is the first time that generic fluidic seal performance has been mapped out in this way and contributes to knowledge in this field by providing a starting point for a working fluidic seal design based on some fundamental seal dimensions. The most promising region for developing a fluidic seal/labyrinth seal combination is with the following parameters:

- *A* in the range 10 to 16
- *C* in the range 1.5 to 2.5
- *D* approximately 2

In this region the achievable leakage reduction is ~50 % over the baseline and the predicted leakage reduction is relatively insensitive to variations in both *A* and *C*.

Results were also obtained for cases with D = 1. These results are discussed later in Section 3.5.4. It was found that with D = 1 the fluid curtain and the labyrinth fin were close enough that there was significant interaction between the curtain flow and the flow structure in the region of the labyrinth fin. As a result of the interaction effects, where D = 1 it was not possible to generate a consistent response surface map for L and PR similar to the one shown in Figure 33.

3.5.2. Effect of Fluid Curtain Width

For a given jet velocity, thinner jets have a lower mass flow rate, and therefore lower momentum flux. Therefore thinner jets must require higher values of PR to over blow the system. For example, Figure 33 shows that a pressure ratio of 6.0 is needed where A = 16, C = 2 compared to a pressure ratio of 2.7 where A = 8, C = 2. This higher maximum pressure ratio permits a higher jet velocity, and therefore greater pressure drop across the jet according to equation 2.4. In practice this improvement using a thinner jet may not be worth the increase in inlet pressure demanded by the fluidic seal system, or the practical issue of physical jet blockage by debris, which would be worse for smaller curtain slots. Blockage is a risk in narrow channels in steam or gas turbines where small amounts of solid material in the working fluid can be deposited over time. The benefits of thinner curtains must be traded off against possible design issues such as these.

3.5.3. Effect of Labyrinth Restriction Size

Two designs with equal curtain width (A = 8) and different labyrinth fin restriction sizes (C = 2 and C = 8) produce significantly different improvements in sealing while using the fluidic curtain, L = 45 % and L < 10 % respectively, according to Figure 33. The flow physics that causes the difference in seal performance improvement caused by the curtain for these two geometries can be seen by examining the static pressure plots for the two cases shown in Figure 34. The drop in static pressure across the fluidic jet is smaller where the labyrinth restriction is tighter.

Equation 2.4 explains this difference in behaviour well, although it carries assumptions on the development of the jet as it enters the cross flow in terms of both jet thickness and turning path [**5**]. The equation can be used to predict the difference in pressure drop across the fluid curtain expected for the two cases, by taking the curtain injection velocity from the relevant CFD predictions and by assuming that the jet width remains constant as the curtain flow crosses the leakage channel and aligns with the leakage flow direction. The jet velocities obtained from the CFD predictions were 260m/s for the C = 2 case and 180m/s for C = 8. Using these velocities in equation 2.4 yields a ~0.3 bar predicted pressure drop across the curtain for C = 2 and a

~0.15 bar for *C* = 8. This analysis gives pressure drops that are in good agreement with the drop in static pressure across the curtain predicted by the CFD and shown in Figure 34a and Figure 34b.

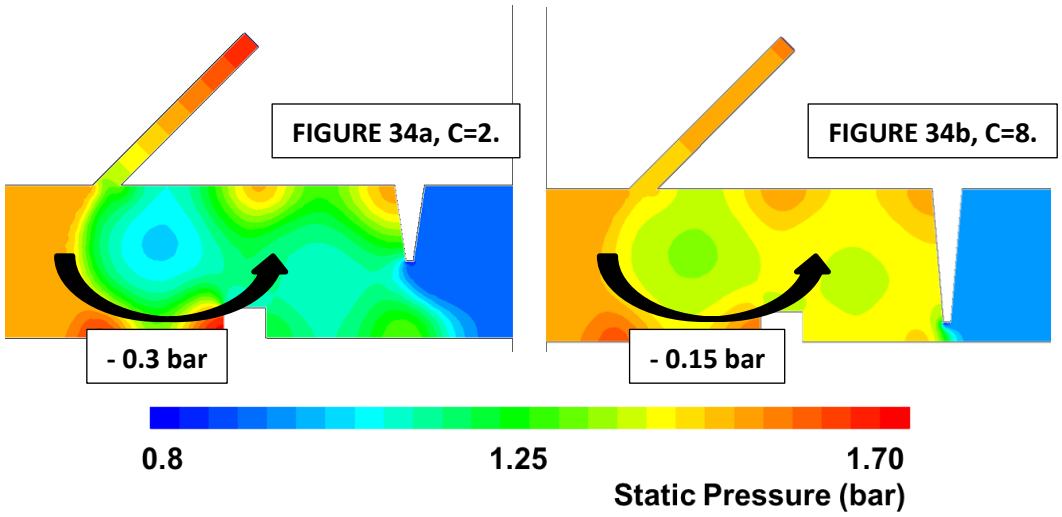

Figure 34: Static pressure contours for two geometries both with *A* = 8 & *D* = 2. The curtain pressures shown are the closest tested pressure to the overblow pressure for each geometry, Figure 34a shows a PR of 2.5, Figure 34b shows a *PR* of 1.5

It is clear that a reduction in *PR* causes a decrease in curtain velocity. This decrease in velocity reduces the pressure drop that occurs across the fluid curtain. By reducing the effective single fin clearance size, the leakage flow with no fluid curtain operating will decrease. This means that the momentum required of the fluid curtain to stop the incoming leakage flow will be lower and the change in static pressure when the flow crosses the fluid curtain will therefore also be lower.

3.5.4. Effect of Axial Spacing, *D*

The results for the seal designs presented so far have all been for *D* = 2. Calculations were also carried out for geometries with *D* = 1. The performance of the sealing system with *D* = 1 was influenced much more by fluid curtain and labyrinth fin flow structure interaction effects, compared to the results obtained with *D* = 2.

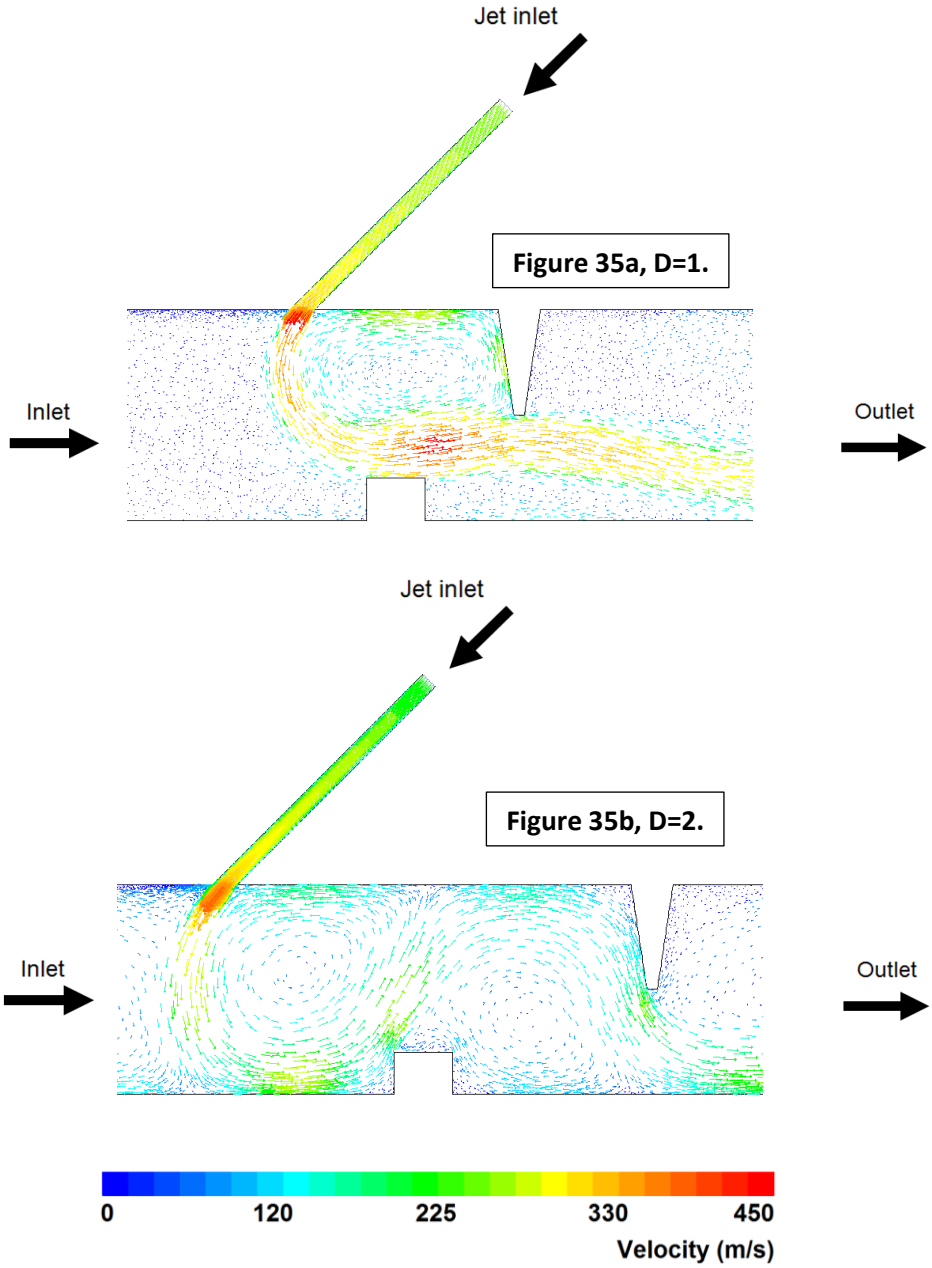

Figure 35: Velocity vectors for *A* = 12, *C* = 2, *PR* = 6.0 with *D* = 1 and *D* = 2.

The flow structure in the vicinity of the working section calculated for *D* = 1 and *D* = 2 with both calculations using *A* = 12, *C* = 2 and *PR* = 6.0, are compared in Figure 35. In the case of *D* = 1 (Figure 35a), *PR* = 6.0 is insufficient to allow the fluid curtain to fully traverse the leakage channel and impinge on the lower wall. This is because the relatively short axial distance between the fluid curtain and the kinetic energy blocker causes the high kinetic energy curtain flow stream to be deflected over the top of the blocker and through the clearance under the labyrinth fin. This results in high kinetic energy carry-over from the fluid curtain flow through the labyrinth seal resulting in a poor sealing performance. Figure 35b, on the other hand, shows the impact of switching to *D* = 2 with all other parameters unaltered. In this case, the increased

distance between the fluid curtain injection slot and the kinetic energy blocker allows the fluid curtain to touch down on the opposite side of the leakage channel. The kinetic energy blocker is now able to deflect the curtain flow back across the leakage channel, eliminating any opportunity for the high kinetic energy curtain flow to impinge directly onto the clearance underneath the labyrinth fin. The curtain flow can be seen in Figure 35b to flow down the upstream face of the labyrinth restriction giving the flow a large vertical component of velocity on the upstream side of the labyrinth fin. The leakage flow has to turn ~80^{o} in order to pass through the clearance underneath the fin, which results in a more pronounced vena contracta, and significant acceleration. This results in greatly increased pressure loss in the leakage flow and therefore better performance for the geometry in Figure 35b than the geometry in Figure 35a. Figure 36 shows the effect of increasing *PR* to 7.0 for the same *D* = 1 geometry as in Figure 35a. At the higher pressure ratio the momentum of the fluidic curtain is sufficient to cause the curtain flow to impinge on the opposite side of the leakage channel upstream of the kinetic energy blocker. The blocker successfully deflects the curtain flow back across the leakage channel. However, the increase in *PR* causes the seal to become over blown, such that a large proportion of the curtain flow is directed upstream and eventually out through the seal system inlet plane. The result shown in Figure 36 demonstrates the sensitivity of the flow structure to what is a relatively small change in *PR* value. It is a good illustration of why it was found not to be possible to develop a consistent performance map similar to Figure 33, when the distance between the curtain and the labyrinth fin was reduced to *D* = 1.

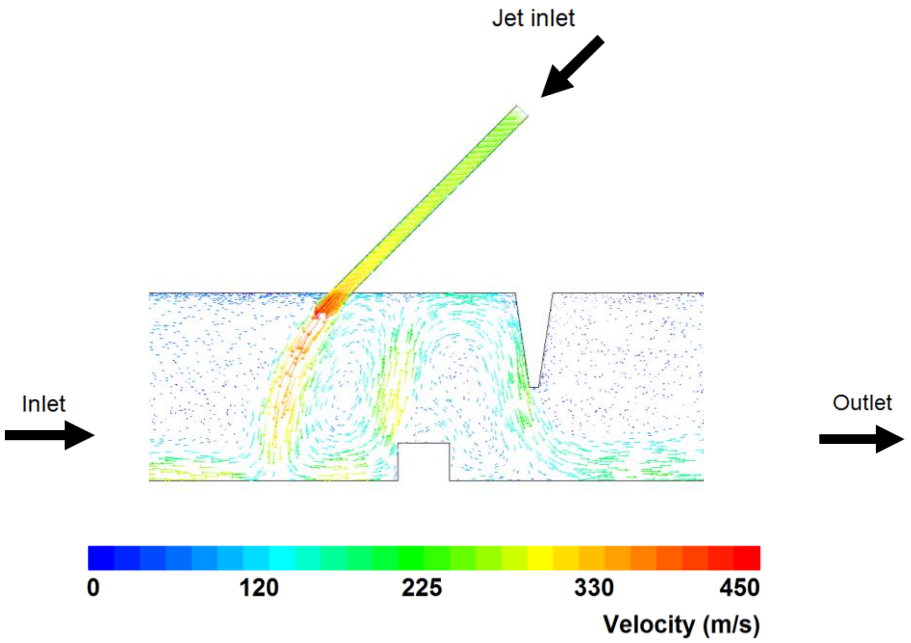

Figure 36: Velocity vector plot *A* = 12, *C* = 2, *D* = 1, *PR* = 7.0

Designs where *D* = 1 were discounted because:

- Prior to overblowing, inlet mass flow is reduced less for the same pressure ratio compared to *D* = 2. At a *PR* of 6.0, optimum sealing is achieved where *D* = 2, but where *D* = 1 the inlet mass flow is still positive. Where *D* = 2 there is a higher radial velocity component of the flow passing through the labyrinth restriction. This will give a tighter vena contracta and therefore smaller effective restriction area, explaining the difference seen in seal performance.

- When nearing the *PR* required to overblow the seal, the system rapidly switches between two discreet flow structures for a small increase of *PR*, as was seen from comparing Figure 35a and Figure 36.

The seal must always be designed such that the fluidic curtain is allowed to freely cross the leakage channel and impinge on the opposing wall upstream of the kinetic energy blocker. This leads immediately to the design rule that the fluidic curtain must be allowed sufficient axial space upstream of the kinetic energy blocker to turn smoothly across the leakage channel and impinge on the opposite wall before it interacts with the kinetic energy blocker. Also, the axial spacing between the blocker and the labyrinth fin should be the same as that between the curtain inlet slot and the blocker. This allows the high velocity stream to impinge on the front face of the labyrinth fin close to the outer wall and stay attached to this face until flowing underneath the fin. This high vertical component of velocity ensures a tight vena contracta,

maximizing the effectiveness of the labyrinth seal. For these reasons, a recommended design rule is that $D \geq 2$.

3.5.5. Comparison with Previous Work

The sealing behaviour predicted by the results of the CFD study are consistent with previous work by Hilfer [**5**]. Hilfer describes experimental work using a fluidic jet followed by a kinetic energy blocker and two labyrinth fins. The equivalent geometric ratios to the work described in this thesis are A=7.14, C=2.83, D=2. The leakage reduction achieved in Hilfer [**5**] for this design point is ~40 %, which is in agreement with the response surface shown in Figure 33.

3.6.Conclusion

In this chapter, the effect of fluidic curtain seal geometry on sealing capability has been explored. A set of simulations were carried out on the generic seal design described in Section 3.2 for a range of values of dimensionless parameters A, C, and D. For each design, CFD was used to calculate solutions with no fluidic curtain present. Further predictions were then made with the curtain turned on and for successively increasing values of PR. This allowed the maximum value of leakage reduction and PR before the system became over blown to be determined. This yielded values for the maximum leakage reduction, L, and the PR required for each design. These results have been used to generate a response surface showing the variation in maximum leakage reduction factor (L) and the value of PR needed to achieve this, with the dimensionless geometric design parameters. The response surface shown in Figure 33 is essentially a design tool that is a central part of the fluid curtain seal design methodology that is developed in the work described in this thesis. The CFD results have also shown that it is important to have sufficient distance between the fluid curtain injection and the downstream seal, to prevent significant flow interaction effects between the two. This has led to the design rule that the distance between these two components of the sealing system is a minimum of two leakage channel heights (D = 2) with a kinetic energy blocker positioned mid-way between these two components.

The experimental validation of the CFD used to develop these design rules is described in the next chapter of this thesis.

4. Experimental Validation of Geometric Characterisation

This chapter describes the experimental validation of the CFD study in Chapter 3. Demonstrating that the results used to create the surface plot in Figure 33 can be repeated experimentally, will allow the surface plot to be trusted as a design tool for predicting the performance characteristics of a generic seal design. This will be useful in the early stages of designing a new fluidic curtain seal. The experiments were carried out using a modified version of the annular static seal test facility described by Hilfer [**34**]. This test rig consists of an annular channel of constant height connecting inlet and outlet plenum chambers. A pressure difference between these plenum chambers causes axial flow through the annulus, creating the same simulated shrouded tip seal leakage flow as was studied in Chapter 3. An axisymmetric slot in the outer wall provides an inlet for a fluidic curtain. The working section of the static test rig was modified to change the test seal geometry to Generic Seal Geometry shown in Figure 30. The channel height (b) was fixed for all tests and the dimensionless geometric parameters A (= b/a) and C (= $b/$c) were varied by changing the fluid curtain thickness (a) and labyrinth fin clearance (c) in the tests. The axial length (d) from plane of the fluid curtain injection to the labyrinth fin was two channel heights ($D = d/b = 2$) in all tests. A kinetic energy blocker was positioned around the static test rotor axially equidistant between the curtain inlet plane and the labyrinth fin, as also shown in Figure 30.

The range of fluidic curtain seal geometries which were selected for validation is described first. The Durham University Blowdown Facility is then described, followed by the design modifications needed to the Static Seal Test Rig to create the range of generic seal geometries for the tests. The experimental test programme is discussed next. Finally, the results from the tests are presented and used to validate the CFD data that forms the basis of the fluid curtain seal performance map in Figure 33 which was presented in Chapter 3.

4.1. Test Points

In order to validate the study in Chapter 3, a range of design points were tested and compared with the corresponding CFD results. The CFD study covered a wide design space and validating the entire range of geometries would require a long experimental campaign. For this reason the experimental validation will focus on the region of the design space which the CFD study showed to be the most promising. Figure 33 shows that the best leakage reduction for the generic seal design occurs for low values of the geometric ratio C: when the labyrinth fin clearance height is a large proportion of the leakage channel height. Where $C \sim 2$ the leakage reduction factor is in the range of 40 - 60 %, depending on the value of A. Previous work on

fluidic curtain seals has achieved leakage reductions in this range, and leakage reduction in the order of half the baseline would make the technology extremely attractive to turbomachinery designers. The experimental validation will therefore be carried out for values of *C* close to 2. The points which were selected for testing are indicated by the red crosses in Figure 37. The range of test pressure ratios and corresponding expected performance for each of these geometries is summarised in Table 5. Test geometries were produced for *C* values of 2 and 2.5. For these values of *C*: where the ratio *A* drops much below a value of 6, the maximum leakage reduction drops to below 25 %, and where *A* is greater than 18 the leakage reduction does not vary with further increases in *A*. These limits were used to guide the selected values for *A* for the tests. As discussed in Section 3.5.4, the ratio *D* is not expected to have much effect on performance as long as it is greater than or equal to 2. In all the geometries tested, the value of *D* was 2. The leakage channel inlet pressure was set to 1.5 bara and the leakage channel outlet pressure to 1 bara, for all test points. These are the same boundary conditions for the seal inlet and exhaust, as was used in the CFD study.

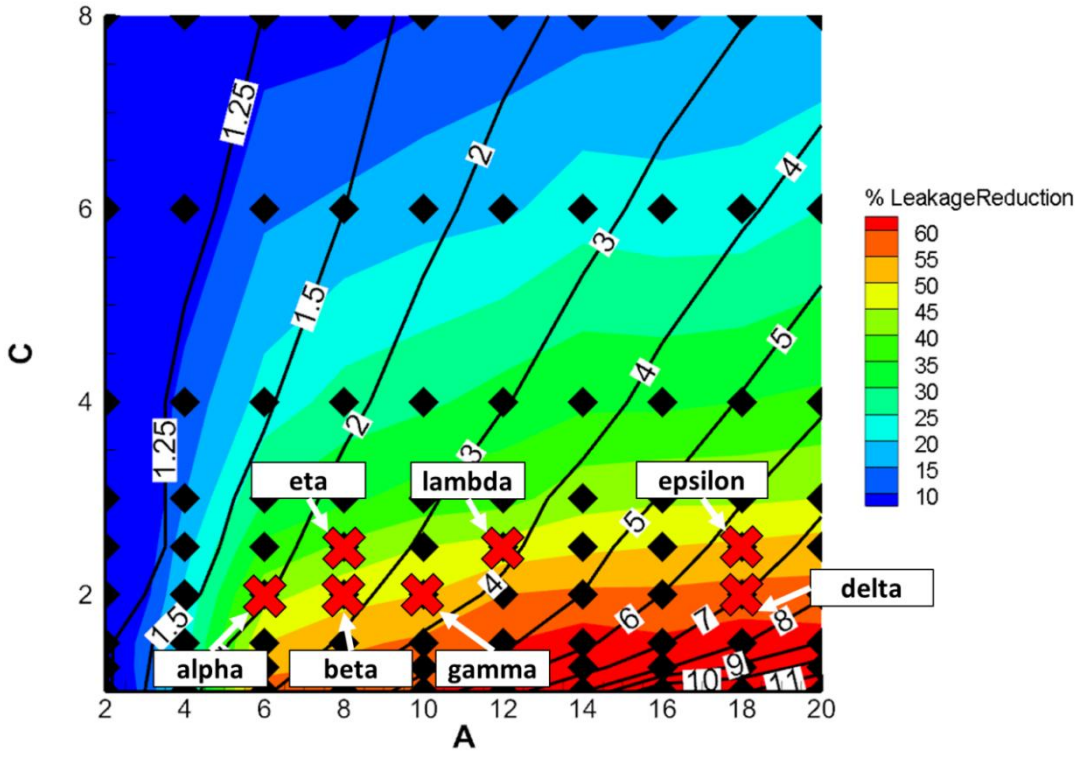

Figure 37: Response surface from Chapter 3 – Red crosses indicate the set of geometries included in the experimental validation

Table 5: Summarised experimental test matrix

Geometry	*A*	*C*	*D*	*PR* test range	~$L_{expected}$	~Max $PR_{expected}$
Alpha	6	2	2	1 – 3	40 %	2.0
Beta	8	2	2	1 – 3	45 %	2.5
Gamma	10	2	2	1 – 4	50 %	3.5
Delta	18	2	2	1 – 8	55 %	7.0
Epsilon	18	2.5	2	1 – 7	50 %	6.5
Lambda	12	2.5	2	1 – 5	45 %	4.0
Eta	8	2.5	2	1 – 3	40 %	2.5

4.2.The Durham Blowdown Test Facility

The Durham Blowdown Facility was used to supply the test rig with fluid to test the seal designs. This facility consists of a large refillable tank of compressed air connected to a system of pipework. The tank can be pressurised to a maximum of 30bar, and can supply air to several test rigs. For additional safety, most test rigs which use the blow down facility are situated in an under floor test cell for containment. This is located close to the blowdown tank with a roof of concrete floor beams forming the ceiling over the test cell.

The Durham University Static Seal Test Rig is described in Section 4.3. The test rig is connected to the Blowdown Facility as shown in Figure 38.

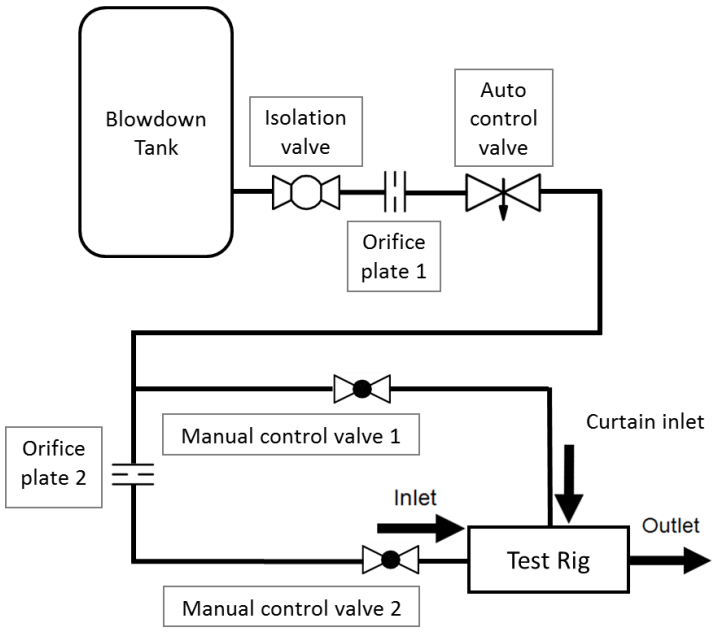

Figure 38: Experimental facility setup.

Blowdown Tank:

The tank was pressurised using a commercial electric compressor and dryer, capable of pressurising the tank to a maximum of 15 bar with dry air. The tank has a volume of 10 m^3, so at 15 bar it contains a total of 178 kg of air. For the typical total mass flow rates required during

this experimental campaign, this capacity restricted the run time of each blow down test to the order of a few minutes. The loss through the pipework and orifice plate to the point where the curtain supply line branches off from the inlet flow line in Figure 35, was estimated to be approximately 2 bar at the maximum expected mass flow in the tests of 0.24 kg/s, based on the CFD results. The maximum fluid curtain supply pressure for the highest *PR* value needed in the tests was 7 bar. Therefore, the highest pressure at which the blowdown tank would not be able to supply the Static Seal Test Rig during the tests was 9 bar. At the highest expected mass flow rate, the time taken to lower the pressure in the blowdown tank from 15 bar to 9 bar was calculated to be 295 seconds at 20 °C i.e. just under 5 minutes.

Pipework:

The blowdown tank is connected to the test facility by a system of 2 inch galvanised steel pipes. The pipework is connected by threaded pipe fittings and flanged connections in accordance with British Standard BS EN 10226:2005 [**42**].

Stop (Isolation) Valve:

A SpiraxSarco 2 inch ball valve fitted with a pneumatic quarter turn actuator, connected to the blowdown facility control system, was used as an emergency stop valve. If the emergency stop button is pushed or the shop air supplying the valve actuator loses pressure, then the valve will turn to the closed position, making this valve the facility's main safety isolation feature.

Governing (Auto Control) Valve:

A SpiraxSarco LE33 control valve chasis was used to regulate the pressure of the air being supplied to the test rig inlets. A DN20 valve with a throat diameter of ¾" was fitted to the control valve chasis. The bore of orifice plate 1 (Figure 35), was sized so that as the ratio of the pressure in the blowdown tank to the rig supply pressure at the exit from the governing valve increases, choking occurs first in the throat of the governing valve. With this arrangement, the maximum mass flow rate that can be supplied to the test rig for a test period of order 1 minute was limited to 0.3 kg/s.

Manual Control Valves:

Manually controlled 2 inch globe valves were installed in the pipes supplying the fluid curtain and the seal inlet flow to the test rig. These two valves allowed independent control of the two flows supplying the test rig.

Instrumentation and Data Acquisition

The instrumentation used in the tests is described in detail later in Section 4.4.3. Pressure transducers were used to measure pressure at various locations in the test rig and orifice plates were used to measure mass flow rates. The signals were logged on a desktop computer using National Instruments data acquisition cards. The University's proprietary Durham Software for Wind Tunnels suite of software was used to monitor, control and apply calibration coefficients to the data being logged.

4.3.Static Seal Test Rig

The Static Seal Test Rig has been developed to investigate the effect on leakage flow rate of various fluidic curtain seal geometries. The facility was originally designed by Messenger [**39**], for studying the blockage effects of pure fluid curtains (i.e. in isolation with no other sealing component present) in a constant height annular leakage channel. The test rig is made up of a concentric stack of steel rings held together by a concentric ring of threaded steel tie bars, with a central stationary cylindrical shaft. The stacked rings form the outer surface of an annular channel while the central shaft forms the inner surface of the channel. This arrangement is shown in section view in Figure 39.

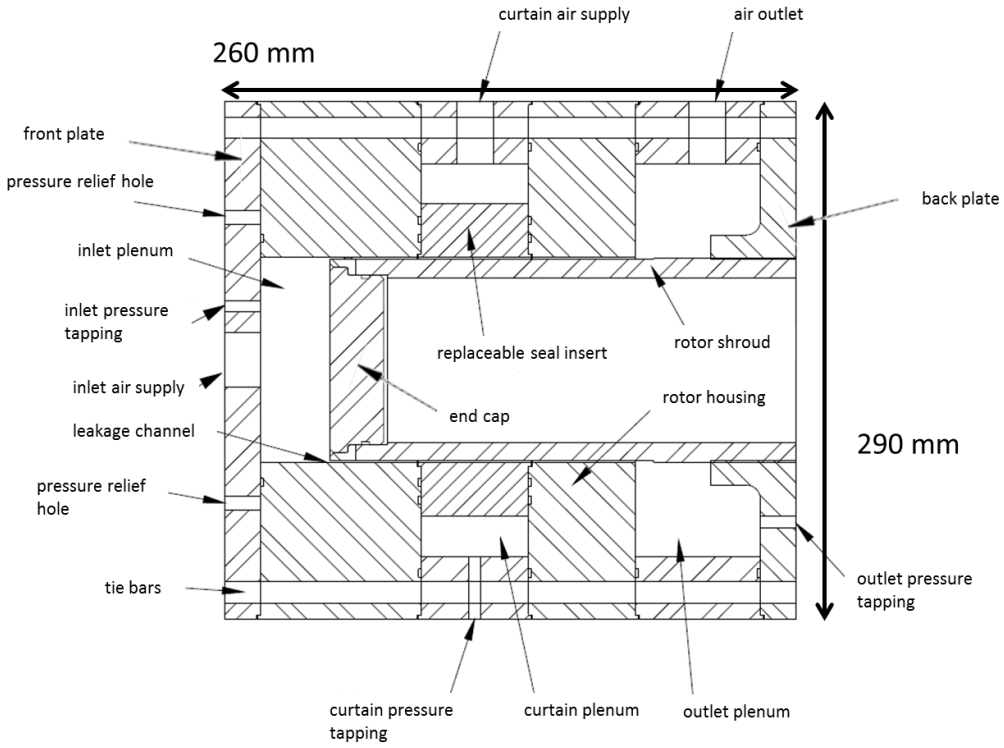

Figure 39: Sectional view of the Static Seal Test Rig [**39**]

Air is supplied from the blowdown tank (see Section 4.2) to the inlet plenum on the left hand side of the diagram, from where it passes into the leakage channel. It flows along the channel and exhausts into the outlet plenum chamber, from where it exits through the outlet port. A third plenum chamber is placed axially about half way along the leakage channel and is available to supply fluid curtains of different geometries (curtain thickness and angle) using a replaceable fluid seal insert. The insert shown in Figure 39 is an insert for a baseline constant height leakage channel test with no fluid curtain included.

4.3.1. Hilfer Experiment

Messenger's test rig design was modified by Hilfer [**5**], who used it to test a seal design which was close to the generic fluid curtain seal geometry from Chapter 3. It included a kinetic energy blocker and a downstream labyrinth seal.

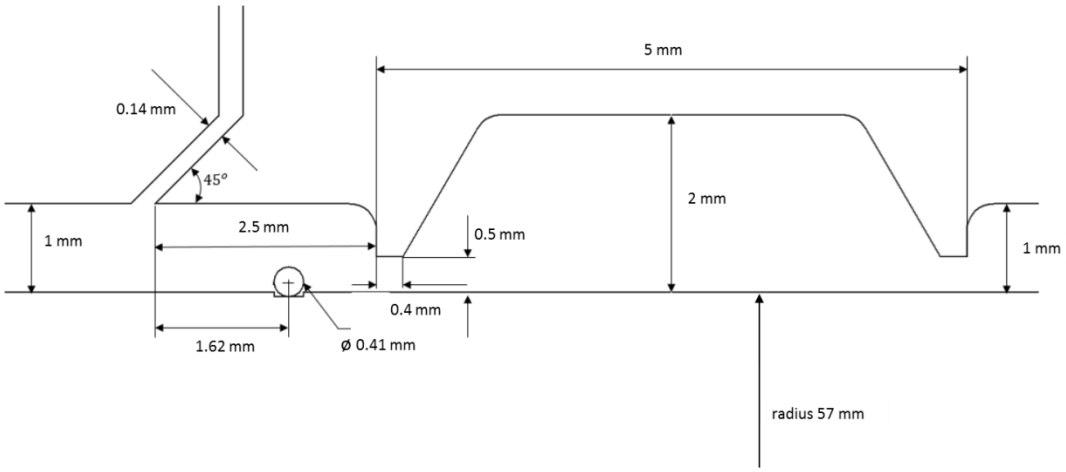

Figure 40: Hilfer geometry tested using non rotating fluidic seal rig [**5**]

The fluid curtain seal geometry tested by Hilfer is shown in Figure 40. It consists of two labyrinth type restrictions, each of 0.5 mm clearance in a 1mm high leakage channel. The restrictions were positioned downstream of a 45^{o} fluid curtain of thickness 0.14 mm. The two labyrinth restrictions can be modelled as a single restriction with an effective clearance, $c = 0.5/\sqrt{2} = 0.354$ mm, which represents the combined effect of the two physical restrictions. Using this value together with $b = 1.0$ mm and $a = 0.14$ mm gives values for the geometric ratios defined in Section 3.2 of $A = b/a = 7.14$ and $C = b/c = 2.82$. The performance map in Figure 33 shows a leakage reduction of around 40 % due to the presence of the fluid curtain for these values of A and C and that a curtain pressure ratio of approximately $PR = 2$ (Equation 3.1) will be needed to deliver this reduction. It should also be noted that $D = 2.5$ for the geometry in Figure 40 and so it is appropriate to use Figure 33, as the complications for low values of D of

around *D* = 1 noted in Section 3.5.4 will not apply in this case. The results obtained by Hilfer for the three mass flow rates as PR was varied are shown in Figure 41.

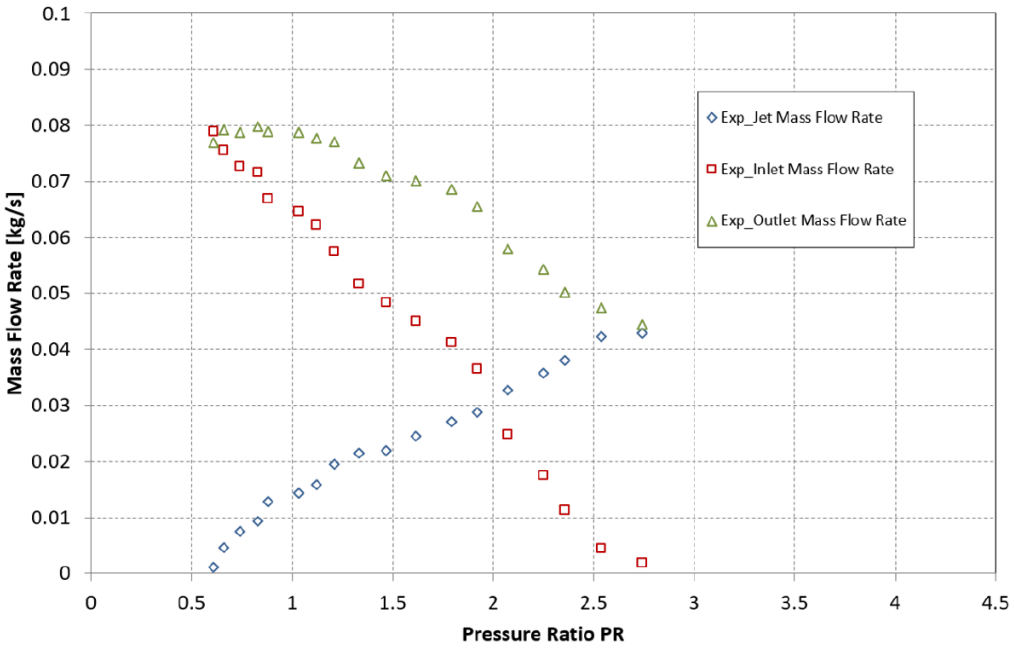

Figure 41: Experimental results for the fluidic curtain seal tested by Hilfer [**5**]

In the Hilfer experiment it was found that the flow rate with no curtain present was 0.079 kg/s, which was reduced by 43 % to 0.045 kg/s by operating the curtain at a *PR* of 2.65. This means that the performance map in Figure 33 could have been used in this case to predict the approximate operating conditions and leakage reduction potential of this seal geometry.

4.4.Test Rig Modification

The working section of the Static Seal Test Rig was modified to reproduce the generic seal architecture from Chapter 3. The fluidic curtain slot width and the labyrinth restriction height were designed so that they could be altered between tests in order to create the multiple test geometries described in Table 5 in Section 4.1. The working section was modified in a number of areas. The leakage channel height was increased to 5 mm (in order to make tolerancing easier to reduce the manufacturing uncertainty around achieving specific values for the parameter *C* in tests) and was 140 mm long, and a square section kinetic energy blocker with a height of of 1 mm was added. This gives a new radius ratio of 45mm/40mm, or 1.125. Section 3.2 explained that a radius ratio of 1.1 gives results within 1 % of those for a planar channel. Therefore experimental results obtained using a channel height of 5 mm were not expected to differ from results to the planar CFD results from chapter 3 due to radius ratio effects. The rig components either side of the 'Replaceable Seal Insert' shown in Figure 39 were modified to

allow a longer seal insert to be mounted between them (this was needed because the test geometry includes a labyrinth fin and fluid cutain slot with *D* = 2, whereas the test rig was originally designed just to test fluid curtains in isolation) . The 'Replaceable Seal Insert' had an axial length of 60 mm. The modifications allowed this to be replaced by the 'New Working Section' shown in Figure 42, which has an axial length of 115 mm. The 'New Working Section' incorporated an interchangeable single labyrinth fin restriction and a redesigned 45^{o} fluid curtain slot with the ability to change the width of the curtain by placing spacers of shims behind the Labyrinth seal (see Figure 43). The leakage flow rates in these tests are higher than they were in earlier tests by Messenger and Hilfer. In order to accommodate the increased mass flows, the inlet to the channel inlet plenum chamber was increased in size from a 1 ½ inch pipe to a 2 inch pipe and the number of outlets from the outlet plenum chamber was increased from one to four.

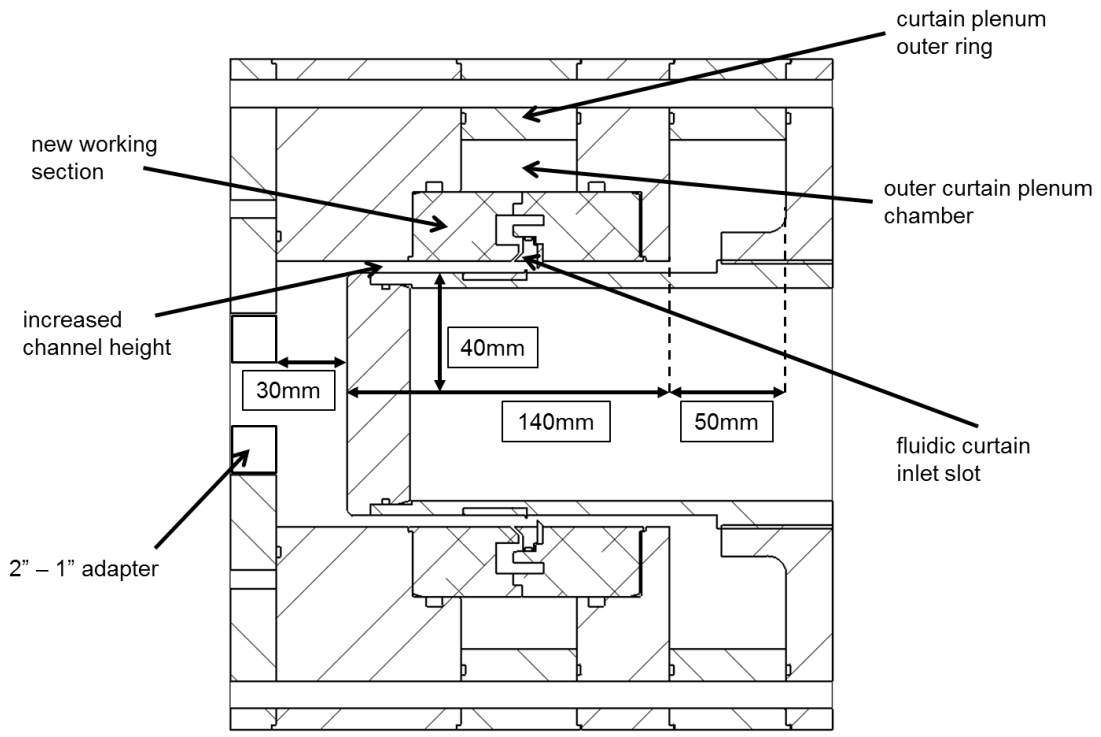

Figure 42: Section view of the modified non-rotating fluidic seal test rig

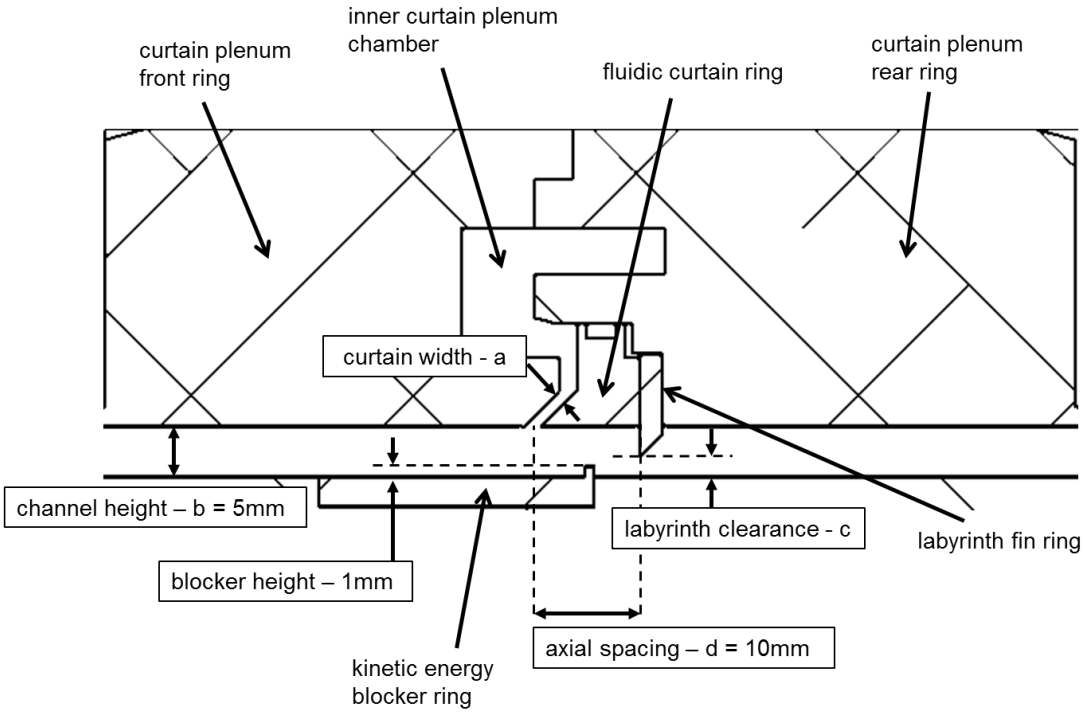

Figure 43: Section view of modified test rig working section

The labyrinth fin clearance, *c*, and hence geometric parameter *C* (channel height *b* was constant in the tests) was adjusted by changing labyrinth fin ring in Figure 43 for a replacement component with a different labyrinth fin tip diameter. Tests were carried out using curtain widths ranging from 0.29 mm to 0.84 mm, while the labyrinth fin clearance was set to 2 mm or 2.5 mm, in order to achieve the range of values for dimensionless geometric parameters *A* and *C* listed in Table 5 in Section 4.1.

4.4.1. Component Design

Some test rig components were modified from existing parts of the Static Seal Test Rig, whilst others were newly design parts. This section describes the component designs for the new and modified parts of the test rig. Most new rig components are not under any significant loading and were therefore all manufactured from aluminium 6063 alloy. However the cantilever inner shaft and the 2 ” to 1 ” adapter used mild steel to ensure rigidity in the case of the inner shaft and a long lasting screw thread in the case of the adapter.

Curtain Plenum Front Ring

The space between the two plenum rings formed the inner curtain plenum chamber (see Figure 43). This was fed by 24x 12 mm diameter feed holes leading from the outer curtain plenum chamber, which was in turn fed by a set of four 1 inch pipes through holes drilled through the curtain plenum outer ring. This number of inlets ensured that under maximum flow rate

conditions the dynamic pressure in either set of feed holes would not exceed 5 kPa. This is less than 2.5 % of the pressure in the curtain inner plenum chamber. Pressure loss was therefore minimal, and satisfactory measurement of curtain feed pressure could be made in the outer plenum chamber, simplifying the mechanical design of the rig. The front ring contains 12 of the 24 feed holes to the inner curtain plenum chamber. As well as forming half of the inner curtain plenum chamber the front ring forms one of the two conical faces which make up the fluidic curtain inlet slot.

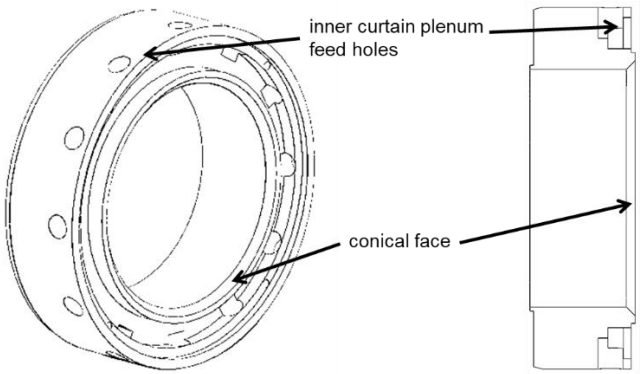

Figure 44: Curtain plenum front ring

Curtain Plenum Rear Ring

The curtain plenum rear ring forms the second half of the curtain inlet plenum chamber. Like the front ring it has 12 feed holes leading from the outer plenum chamber to the inner plenum chamber. This component also incorporates the locating face for the labyrinth fin ring (see Figure 43.

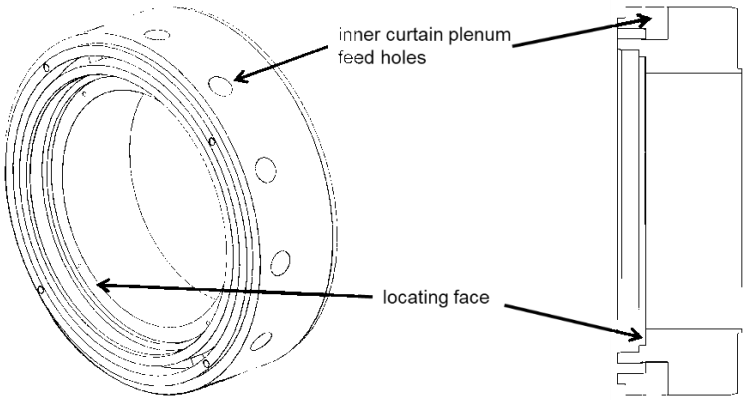

Figure 45: Curtain plenum rear ring

Since the locating face was downstream of the labyrinth fin, a small gap between this component and the rear face of the labyrinth fin would not affect the flow in the working section. Therefore, shims placed between the locating face and the downstream side of the labyrinth seal ring could be used to control the fluid curtain width. As the fluid curtain ring and the labyrinth fin ring were both displaced by the same axial distance when shims were added, the axial spacing, d, between the labyrinth fin tip and the downstream side of the fluid curtain where it enters the leakage channel, remains unchanged. Like the front plenum ring, this part was made from aluminium.

Fluidic Curtain Ring

The conical face on the fluidic curtain ring forms the fluidic curtain inlet slot together with the conical face on the plenum front ring. It was secured to the plenum rear ring using four M2 screws, which first passed through clearance holes in the labyrinth seal ring. An o-ring seal was used to prevent leakage through the clearance fit between the fluidic curtain ring and the plenum rear ring (see Figure 43).

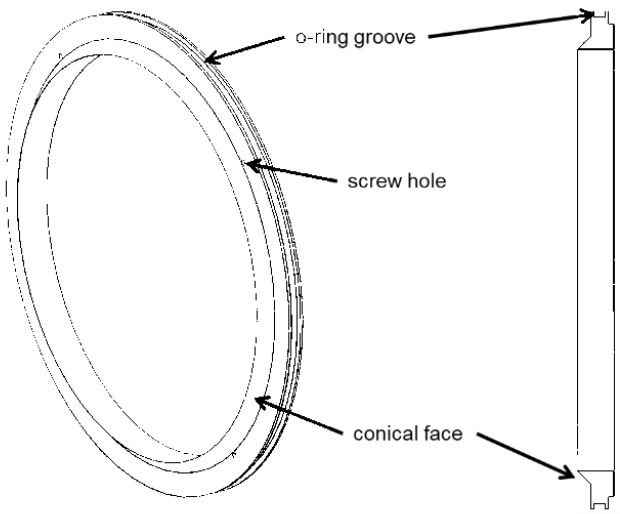

Figure 46: Fluidic curtain ring

Labyrinth Fin Ring

A single labyrinth fin type restriction was provided by a ring on which the inside circumference was profiled to a 45 degree point. The sharp edge was located at the same axial position as the front face of the ring, with the 45 degree face on the downstream side of the restriction. The component was made from mild steel.

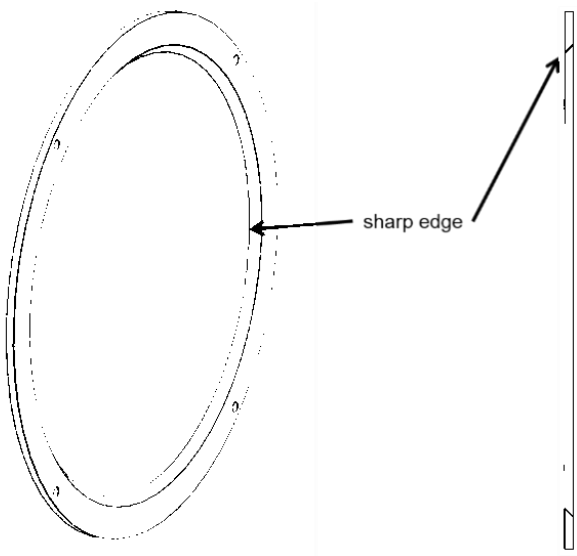

Figure 47: Labyrinth fin ring

Inner Shaft and Cap

The inner shaft provided a non-rotating inner wall of the annular leakage channel. The shaft was manufactured from a section of pipe. A threaded section on the end of the pipe was used to secure the shaft to the back plate of the test rig (see Figure 42). The other end of the pipe section was plugged by a metal cap, which was sealed by an o-ring. When the rig was assembled the cap was contained with the test rig and was held in place at the end of the shaft by the pressure difference between the seal inlet total pressure and ambient pressure. The front face of the cap contained a 5mm hole which led to a ½" threaded hole on the reverse face for a ½" pressure tap fitting. This hole was used to measure the total pressure of the channel inlet air, which entered the rig and immediately impinged on the front face of the cap. The inlet plenum was sized to ensure that the dynamic pressure in the chamber was negligible even at the highest test flow rates, however by placing the tapping on this face any dynamic pressure component will have been detected using this port.

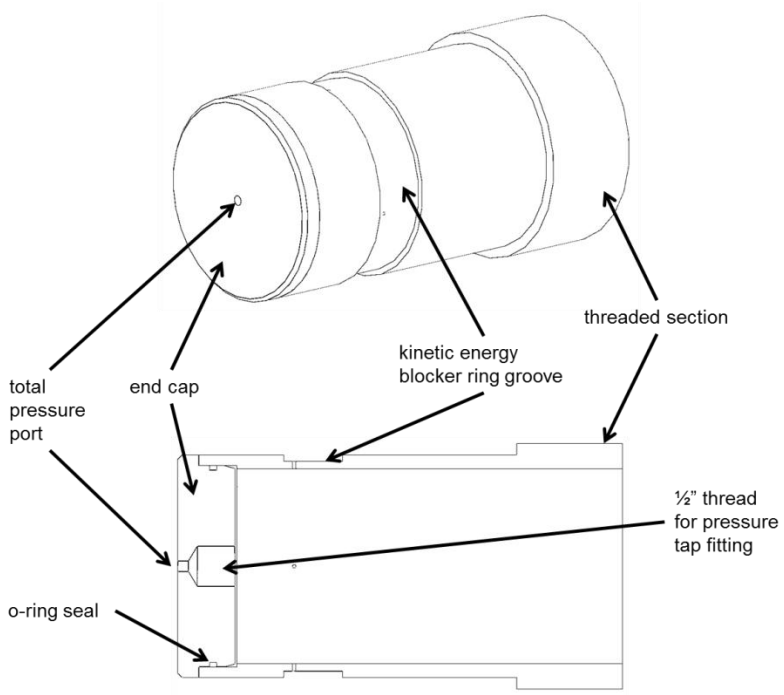

Figure 48: Inner shaft and end cap

A 3 mm deep and 28 mm long groove or recess was machined into the shaft to locate a two-piece split ring containing the kinetic energy blocker (see below).

Kinetic Energy Blocker Half Ring

The kinetic energy blocker ring was split into two 180 degree segments to allow assembly. Each half was attached to the kinetic energy blocker groove using two M2 screws. The kinetic energy blocker feature was located at the rear end of the ring.

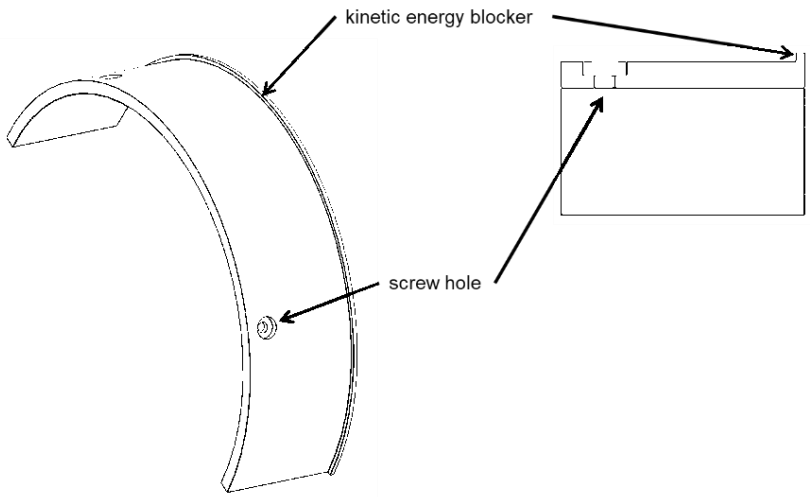

Figure 49: Kinetic energy blocker half ring

2 Inch Inlet Adapter

To accommodate the higher mass flow rate through the modified rig, the diameter of the pipe supplying air to the inlet plenum chamber was increased from 1.5 ” to 2 ” (almost doubling the inlet pipe flow area). The diameter of the threaded axial supply hole through the test rig front plate (see Figure 42) was increased to 70 mm. A mild steel adapter ring was designed (see Figure 50) with a threaded outer diameter to fit the 70 mm threaded hole and an inner diameter hole with a 2 ” BSP pipe thread. By using an adapter instead of simply resizing the inlet hole a single change to the test rig front plate can accommodate many new inlet pipe diameters. If a different mass flow rate is required in the future a new adapter can be used to attach to the desired diameter pipe.

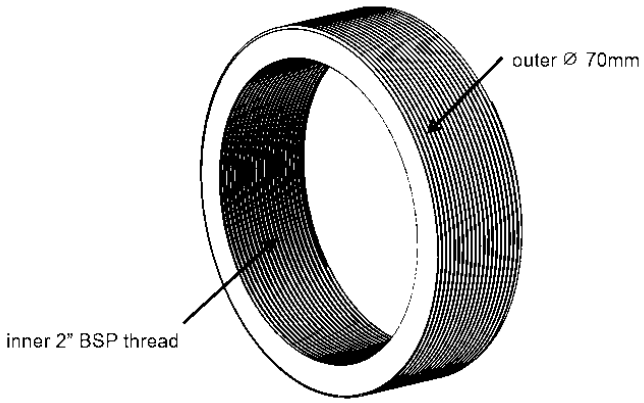

Figure 50: Leakage inlet 2” adapter

4.4.2. Shim Matrix and True Test Points

Each value of the geometric ratio *A* is achieved by finely adjusting the axial thickness of the fluidic curtain as described earlier in Section 4.4, by adjusting the axial position of the fluidic curtain by placing shims behind the labyrinth fin ring (see Figure 43). Pieces of shim material of thicknesses 0.5 mm, 0.1 mm, 0.025 mm, and 0.05 mm were used in various combinations to give curtain widths as close as possible to the nominal test values shown in Table 5. The actual values of curtain thickness (*a*) achieved with the various combinations of the shims compared to the test nominal values and the impact this has on the value of parameter *A*, is shown in Table 6.

.

Table 6: Shim combinations and resulting test values of *A*

Nominal test value of *A*	Nominal curtain width (mm)	Shim combination	Test curtain width (mm)	Test *A* achieved
6	0.833	1x 0.5mm 1x 0.05mm 1x 0.025mm	0.843	5.93
8	0.625	1x 0.5mm 3x 0.1mm 1x 0.05mm 1x 0.025mm	0.631	7.92
10	0.500	2x 0.5mm 1x 0.05mm	0.507	9.85
12	0.416	2x 0.5mm 1x 0.1mm 1x 0.05mm 1x 0.025mm	0.419	11.93
18	0.277	2x 0.5mm 3x 0.1mm 1x 0.05mm	0.295	16.93

4.4.3. Instrumentation

Pressure Transducers

Electronic pressure transducers were used to measure pressure data during tests and to monitor key pressures for test rig control purposes. A Labview program was used to run a PI controller which operated the Governing (Auto Control) Valve (Figure 38). This was used to maintain a constant curtain supply pressure in the outer curtain plenum (see Figure 42). This was achieved by opening Manual Control Valve 1 (see Figure 38) and using a pressure signal measured from the outer curtain plenum to control the Governing (Auto Control) Valve. The specifications of the transducers used are described in Table 7.

Table 7: Pressure transducers used in the experiment

Transducer	Make	Model	Range	Accuracy (% FSO)
Tank pressure	SensorTechnics	CTE8035GY0N	0 - 35 bar	0.10
Orifice plate 1 upstream	SpiraxSarco	EL2600	0 - 16 bar	0.05
Orifice plate 1 differential	SensorTechnics	BTE5002D1C	0 - 2 bar	0.20
Orifice plate 2 upstream	SensorTechnics	CTE8035GY0N	0 - 16 bar	0.10
Orifice plate 2 differential	SensorTechnics	BTE5001D1A	0 - 1 bar	0.20
Fluidic curtain outer plenum	SensorTechnics	BTE5010D1C	0 - 10 bar	0.20

The signals from the pressure transducers were logged by a National Instruments USB6218 data acquisition card. The Durham Software for Windtunnels software suite was used to control the

data acquisition process to log the voltage signal from each transducer at each of the planned test points. A known calibration for each transducer consisting of a multiplier and zero offset was then used by the software to turn the logged voltages into pressures. The quoted accuracies are given as a percentage of the full scale output (FSO).

Scanivalve

A DSA3217 Digital Sensor Array from Scanivalve Corp was used to measure the pressures at in the tests rig inlet and outlet plenums. This was also connected to the data acquisition system. This sensor array has an accuracy of 0.05 % FSO which is better than most of the available individual transducers. Due to the high accuracy of the Scanivalve, these measurements were used to determine the pressure ratios used when plotting results during post processing.

Analogue Pressure Gauge

The total pressure supplied by the inlet pipe to the inlet plenum chamber was measured by the total pressure port on the front face of the inner shaft cap (see Section 4.4.1). A pressure tap fitting on this pressure port was connected by flexible pressure tubing to an analogue 7 bar pressure gauge. This gauge was used to manually set the pressure at the leakage channel inlet by hand adjusting Manual Control Valve 2 (see Figure 38).

Thermocouple

The total temperature of the air in the blowdown tank was measured by a T type thermocouple, which has an accuracy of approximately +/- 1 °C. The thermocouple was connected to an SEM1610 temperature transmitter, which outputs a voltage signal for the thermocouple temperature. This voltage was logged by the data acquisition system in the same way as the pressure transducer signals. A suitable calibration coefficient was used to convert the voltage into a temperature within the Durham Software for Windtunnels programme. It was assumed that heat transfer from the pipework and the test rig to the surroundings was negligible and therefore that the stagnation temperature of the air in the blowdown tank could be used to determine the density of the air for calculating mass flow rates throughout the test facility.

Orifice Plates

Orifice plate 1 (see Figure 38) was used to measure the total mass flow to the test rig (i.e. seal inlet flow plus fluid curtain flow). By continuity this must also be a direct measurement of the total flow exiting from the test seal outlet. Orifice plate 1 had an orifice size of 18.72 mm. Orifice plate 2 was used to measure just the leakage channel inlet mass flow rate. Its orifice size was 25.44 mm. The fluidic curtain mass flow rate is the difference between the two orifice plate

measurements. This arrangement allows the mass flow rates across each of the three boundaries (seal inlet, fluid curtain and seal exit) of the test seal to be determined from the two mass flow measurements. Both orifice plates conformed to the British Standard; ISO:5167:2003 [**43**] [**44**].

Uncertainty in the mass flow rate measurements were calculated according to BS EN ISO 5167-1:2003 for the two orifice plates as a function of mass flow rate, plate geometry, and flow conditions, for a typical blowdown tank reservoir pressure of 10 bar. The orifice plate sizes described in the previous paragraph were selected to minimise uncertainty in the most important region of the tests where the seal is approaching the overblown condition. During tests the logging software automatically calculated an orifice plate uncertainty for each measured mass flow rate and this was used to plot error bars. Low mass flow rates have high uncertainty when measured by orifice plates; therefore the error bars on inlet mass flow at high *PR* are large. Curtain mass flow rates were calculated using inlet mass flow and so they also have large error bars for data points plotted at high *PR*.

4.5. Test Methodology

Before tests were carried out, the blowdown tank was charged by the air compressor to the maximum pressure used for the tests of 15 bara. The Scanivalve array was zeroed to the current atmospheric pressure; the input files for the Durham Software for Windtunnels programs were prepared; and atmospheric conditions in the lab were recorded. Then, the required 1.5 bara inlet pressure was set by manual control valve and the required curtain plenum pressure was set by the governing valve. Measurements were made for mass flow rates at orifice plate 1 and orifice plate 2, channel inlet pressure, and jet inlet pressure. The variation of mass flow rate across each boundary vs *PR* was then compared with the expected variation in mass flow rates vs *PR* obtained from CFD. The channel inlet pressure and *PR* was controlled by different relative settings between the manual valves to the channel inlet and the fluidic curtain inlet. Reversed flow was impossible using a single air supply, so the overblown condition where channel inlet mass flow is reversed could not be reached and seal performance could therefore only be evaluated over a range of *PR* values that were lower than that required for the overblow condition.

The outlet plenum chamber was open to atmosphere so the outlet pressure was always atmospheric. Atmospheric pressure was measured before each test so that the rig outlet pressure was always known. The pressure in the inlet plenum chamber was monitored using an analogue gauge. Rather than attempting to set the inlet pressure accurately to 1.5 bara, tests

were carried out by taking two sets of measurements, with the inlet pressure set to just over and just under 1.5 bara for the range of *PR* values tested. This provided two sets of data, and interpolation between these was used to determine a set of test data for the required inlet pressure of 1.5 bara. An example of this interpolation is shown in Figure 51.

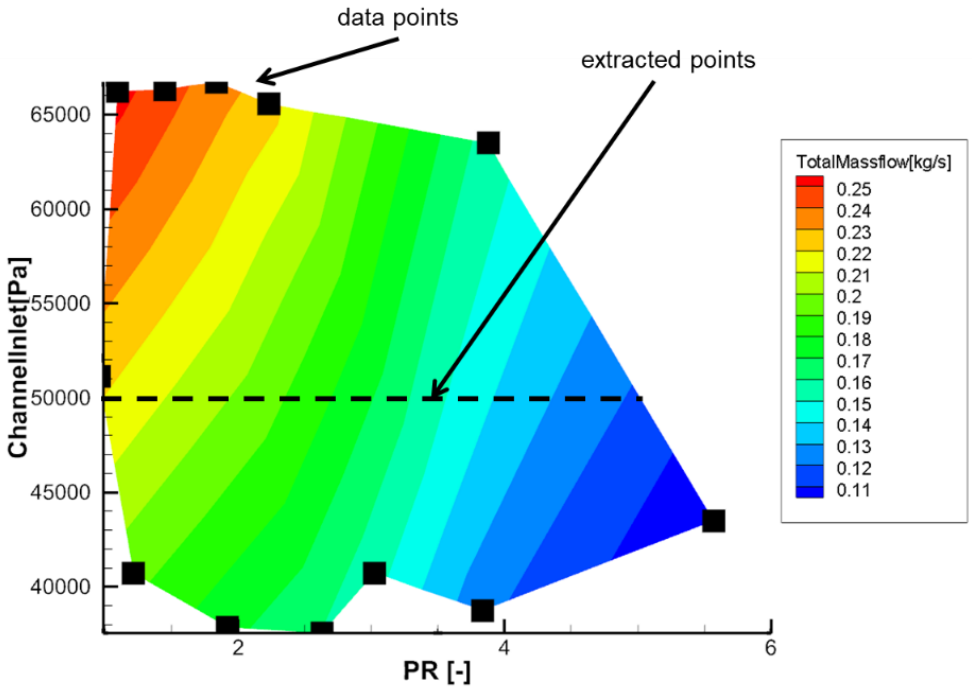

Figure 51: Contour of total mass flow rate as a function of *PR* and channel inlet gauge pressure

By plotting the mass flow rates measured using the orifice plates as contours against *PR* and channel inlet pressure, it was then possible to interpolate data for a channel inlet pressure of 1.5 bara. Test data for the variation in each mass flow rate vs *PR* for the case where the channel inlet pressure was exactly 1.5 bar was established using this method.

4.6. Results

The following plots show mass flow rates across each boundary of the fluidic curtain seal for both experimental and CFD results. The mass flow rates have all been non-dimensionalised relative to the respective CFD or experimental mass flow rates with no fluidic curtain present. This means that mass flow rates can be compared directly between geometries and between CFD and experiment (remembering that the CFD was a planar 2-D calculation predicting mass flows per unit channel width, whereas the tests were conducted using an axisymmetric geometry with very low channel radius ratio). Durham Software for Windtunnels used equations from BS EN ISO 5167-1:2003 to calculate orifice plate uncertainty for each data point based on geometry and flow conditions. These uncertainties were used to place error bars on the result plots. The uncertainties of the two orifice plates give the uncertainties in the mass

flow rates at the outlet and the leakage channel inlet. The uncertainty in the calculated mass flow rate in the fluidic curtain, i.e. the difference between these mass flow rates, was the sum of the two uncertainties. As *PR* increases and the seal moves toward the overblown condition the mass flow rate at the inlet decreases toward zero. For very low mass flow rates the uncertainty in the orifice plate calculation is large, so the error bars in the following results appear to grow large for the inlet and curtain mass flow rate data points at high *PR*. However the close fit between computational and experimental results and the small error bars in the measured total mass flow rate suggest the data can be trusted.

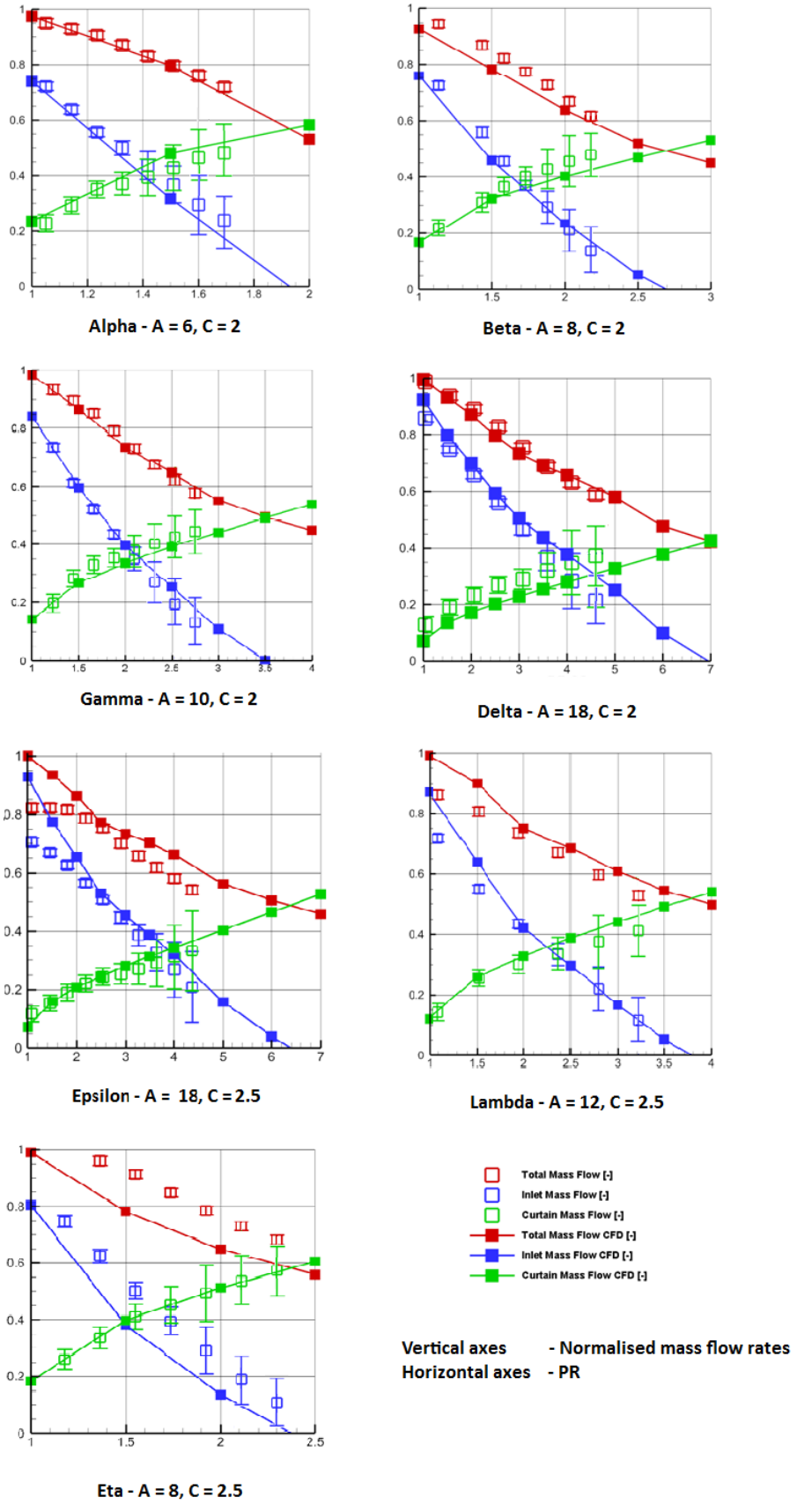

Figure 52: Summarised experimental results compared with corresponding CFD data points

4.7.Discussion

The results show generally good agreement between the experimental data and the CFD predictions. The Eta configuration shows higher inlet and outlet mass flow rates than expected from CFD, suggesting the curtain is performing less effectively for this geometry. Since the Eta geometry was tested last, this is possibly caused by repeated assembly and disassembly of the rig opening up the curtain inlet slot by a small fraction of a millimetre and forming a less effective curtain flow structure. As explained in Section 4.5 the overblown condition could not be reached using the experimental setup since the flow could not be reversed in the inlet piping. However the overblow pressure ratio and corresponding level of leakage reduction can be estimated by extrapolating the experimental data points to reach zero inlet mass flow rate. Sketching curves of best fit by hand was sufficient to estimate the overblow *PR* to an accuracy of ~0.1. Table 8 summarises these extrapolated results for maximum leakage reduction and maximum pressure ratio, and presents them with those which were predicted from the performance map in Figure 33.

Table 8: Comparison of results predicted by Figure 33 and extrapolated experimental results

Geometry	*A*	*C*	~$L_{expected}$	~L_{result}	~Max $PR_{expected}$	~Max PR_{result}
Alpha	6	2	40 %	45 %	2.0	2.0
Beta	8	2	45 %	45 %	2.5	2.5
Gamma	10	2	50 %	50 %	3.5	3.3
Delta	18	2	55 %	50 %	7.0	6.0
Epsilon	18	2.5	50 %	55 %	6.5	5.5
Lambda	12	2.5	45 %	50 %	4.0	3.7
Eta	8	2.5	40 %	35 %	2.5	2.5

For all data points the resulting leakage reduction and max *PR* were predicted well by the response surface. All resulting leakage reduction values were within 12.5 % of the predicted values, while all resulting *PR* values were within 15 % of those predicted. Most values matched much more closely. This demonstrates that the response surface created in Chapter 3 can be used to accurately predict the performance of a generic fluidic curtain incorporated into an existing labyrinth seal of known physical dimensions, as well as the supply pressure which would be required to operate it. The response surface is therefore validated as a design tool which may be used to estimate the performance characteristics of a new fluidic curtain seal design.

While most data points show the CFD prediction falling within the error bars on the experimental results, error bars are quite large in some cases at low flow rates. This is a consequence of the uncertainty of orifice plates at low mass flow rates; as the mass flow rate decreases the error increases gradually, and when the mass flow rate nears zero the uncertainty increases substantially to tens of percent. As the flow at the inlet boundary approaches zero, i.e. the perfect sealing condition, the increase in uncertainty gives large error bars for inlet mass flow. This also gives large error bars for the curtain mass flow rate since this was calculated using inlet mass flow rate. However, even with large uncertainty in individual data points, the overall trends seen in the experimental results match remarkably well with the CFD predictions.

4.8.Conclusion

The intent of the experimental campaign described in this chapter was to validate the CFD study in Chapter 3. The CFD study in Chapter 3 gives the performance map in Figure 33, which can be used to predict the basic performance of a fluidic curtain/labyrinth combination seal of a given geometry. A wide range of geometries were tested from the design space covered by Figure 33. The experimental results show good agreement with CFD predictions for all the generic fluidic curtain seal geometries tested. Good agreement was shown in both the optimum leakage flow reduction and the corresponding curtain supply pressure (*PR*) needed to achieve this. Therefore Figure 33 can be trusted as a design tool to be used to predict the performance of fluidic seal geometries of the generic type considered in this work. The validated response surface is used as the basis for developing fluid curtain seal designs for more representative turbomachinery applications in Chapter 5.

5. Adapting a Turbine Stage Shrouded Rotor Tip Seal to Incorporate a Fluid Curtain

The work described in Chapters 3 and 4 examines the relationship between seal geometry, performance, and required operating conditions. This information provides some fundamental design rules for applying fluidic curtains to improve sealing performance in turbomachinery applications.

The relationship between the principal geometric parameters and the performance benefit from using fluid curtains to reduce seal leakage is essentially captured in Figure 33 from Chapter 3. Figure 33 shows that the best leakage reduction occurs for small values of non-dimensionalised labyrinth fin clearance which presents a challenge incorporating a fluidic curtain into a typical labyrinth seal. The development of a turbine tip seal design, for a close-to-product model turbine test on a shrouded stream turbine rotor, is described in this Chapter. A shrouded tip seal is examined because the leakage path is a relatively simple axisymmetric annular channel and much of the existing literature such as Curtis et al [**9**] has focused on shrouded turbine blades. The study results in the new discovery that swirl in the seal inlet flow can have a significant adverse impact on the integrity of the fluid curtain, which compromises the leakage reduction performance compared to no-swirl conditions. This 'swirl-effect' is subsequently investigated further in the next two chapters of the thesis.

5.1. Achieving Low Ratios of Leakage Channel Height to Effective Seal Clearance (C) in Turbomachinery Seals

In this Chapter, the generic seal architecture incorporating a fluid curtain from Chapters 3 and 4 is referred to as the Generic Seal 1 (GS1) geometry. The work described in Chapters 3 & 4 showed how this generic geometry can yield high reductions in leakage flow rate, and operate at *PR* values where the fluid curtain could feasibly be supplied from within a single turbine stage. Performance is especially good when the labyrinth fin clearance is about half the height of the leakage channel. However, the labyrinth fin clearance in gas and steam turbine tip seal designs is typically much less than half of the leakage channel height. The ratio, *C*, of leakage channel height (*b*) to effective labyrinth fin clearance (*c*), for typical turbine tip labyrinth seals would normally be expected to be greater than 8, i.e. off the top of the vertical scale in Figure 33 and in a region of low/marginal performance benefit from applying fluidic curtains, regardless of the value selected for geometric parameter *A*. However, the leakage channel height which relates physically to the performance of a fluidic curtain is expected to be the

channel height in the region close to the location where the fluid curtain enters the leakage channel. If dimension *b* is defined as the local channel height at this location, then the ratio *C* can be decreased by lowering the value of *b* just in the region close to the fluid curtain injection plane. This approach has been used to develop the second generic seal design, GS2, shown in Figure 53. A fluid curtain has been applied upstream of a conventional 'long' labyrinth fin with a relatively small tip clearance compared to its length, whilst still achieving a low value of parameter *C* (= *b*/*c*).

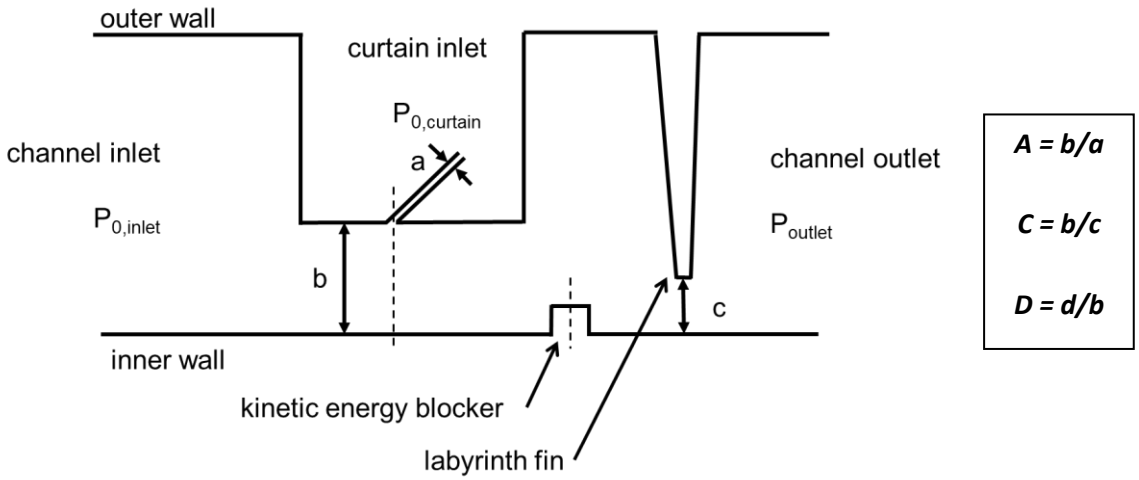

Figure 53: Generic Seal 2 (GS2) architecture. The channel height (*b*) and under fin clearance (*c*) are the same as those in the GS1 design, 1mm and 0.5mm respectively.

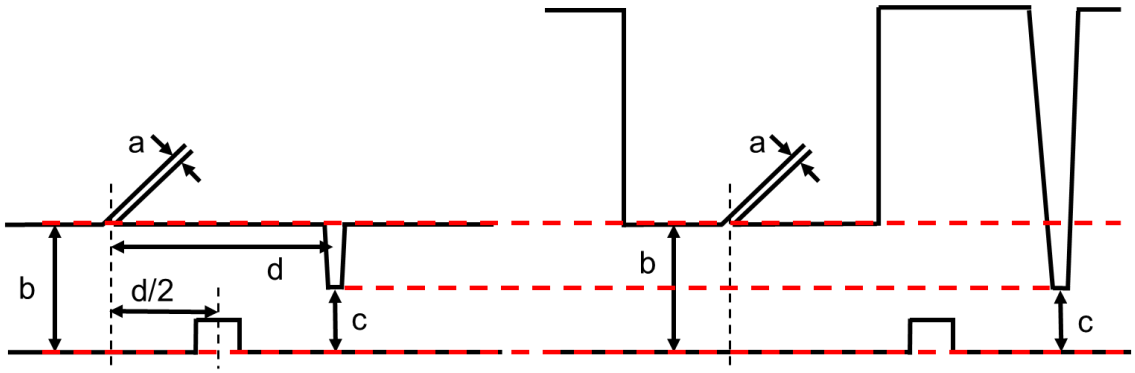

Figure 54: Comparison of GS1 (left) and GS2 (right) seal architectures.

For the geometry sketched in Figure 53, *C* = 2 because the labyrinth fin clearance height is half of the channel height at the fluidic curtain entry location. This geometry is compared with the GS1 generic seal geometry with *C* = 2 in Figure 54. Since the labyrinth fin clearance in both cases is identical; the leakage flow rate in the absence of any fluidic curtain flow is expected to

be approximately the same. The fundamental mechanism by which the presence of a fluid curtain reduces leakage flow (i.e. the pressure drop across the curtain needed to turn the curtain flow to the directions of the leakage flow) was expected to be essentially unaffected by the changes in geometry between GS1 and GS2. If this is correct then the performance map in Figure 33 for the GS1 design will also apply to the GS2 design. D was not considered as an independent variable when developing the GS2 design. For this geometry, *D* will always be significantly greater than unity and so the issue found with GS1 where the axial spacing between the fluid curtain and the kinetic energy blocker became problematic around *D* = 1 (see Section 3.5.4), will not apply to the GS2 design.

A CFD study was carried out to compare the performance of the GS1 and GS2 seal designs. Geometric parameter values of *A* = 12 and *C* = 2 were used in the study. The leakage channel height (*b*) was 1 mm. The mesh densities, boundary conditions, and the settings used in the CFD solver were the same as used in the CFD study in Chapter 3. Mass flow rates normalised by the flows for the no-curtain case across each boundary were plotted for both geometries against pressure ratio in Figure 55.

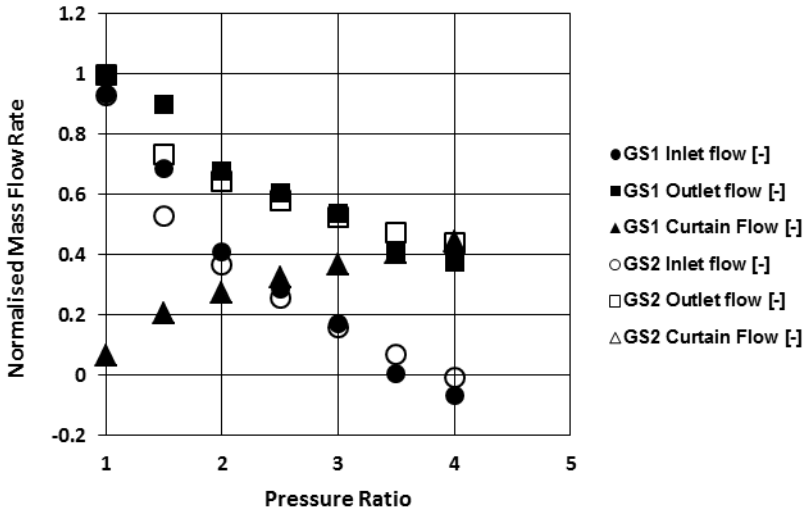

Figure 55 Mass flow rates vs *PR* for GS1 and GS2 seal architectures - *A* = 12, *C* = 2.

Figure 55 shows that the performance of the GS1 and GS2 seal designs are similar, as expected. Both designs have an optimum pressure ratio of approximately 4 and a maximum leakage flow reduction of 55 % at this value of *PR*. This is consistent with Figure 33 for the design point where *A* = 12 and *C* = 2. For low values of *PR*, there is a difference between the two designs, with GS2 initially showing a more rapid decrease in leakage flow rate as *PR* is increased.

However, at higher values of *PR*, as the overblown condition is approached, the performance of the two designs is essentially identical. This confirms that the performance map shown in Figure 33 can be used with confidence to predict the performance of other designs, when '*b*' is taken as the leakage channel height in the region where the fluid curtain is injected into the leakage channel.

5.2. Optimising the Flow Structure of the Interaction between the Fluid Curtain and Labyrinth Seal

Seals with the GS2 seal architecture have now been shown to have very similar performance characteristics as GS1 for the same non-dimensionalised seal geometry. Gas and steam turbine tip seals will generally have small labyrinth fin clearances compared to the height of the leakage channel but modifying the leakage channel height at the axial position of the fluidic curtain can still allow a small value of the non-dimensional fin clearance, *C* to be achieved in designs. A CFD study was carried out to simulate a fluidic curtain seal incorporated into a realistic high pressure steam turbine shrouded rotor tip seal application. The seal geometry shown in Figure 56 is representative of designs used for stages in high pressure and intermediate pressure steam turbines, with stage reactions of around 50 %. Steam turbine stages in the high pressure turbine, the intermediate pressure turbine, and first stages in the low pressure turbine will typically have a stage reaction of 50 % [**45**], so this type of turbine stage was selected as the basis for the seal design. The fluidic curtain replaced the first labyrinth fin in the three fin baseline seal design, which is shown in Figure 56. In what follows, the leakage flow calculated for this baseline design is compared with the leakage flow through modified designs under the same operating conditions.

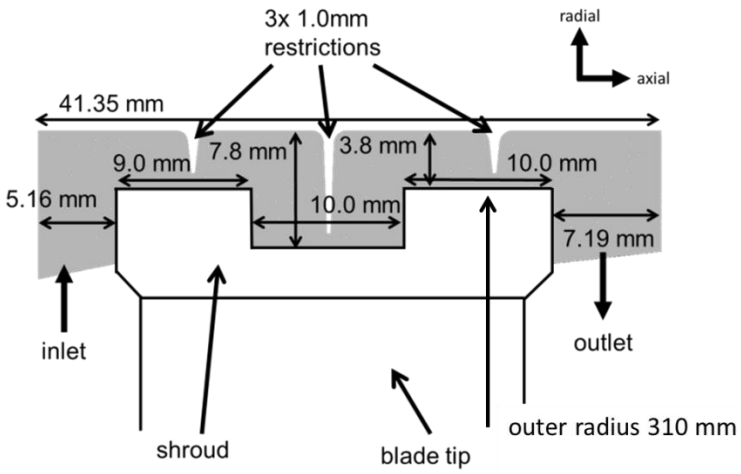

Figure 56: Dimensions of baseline tip seal

5.2.1. Fluid Curtain Seal Design

Design points were selected using the performance map in Figure 33. A = 8, C = 2 and A = 10, C = 4 were chosen due to the high leakage reductions predicted for these ratios and the low PR at which the fluidic curtain can operate. If the operating PR is sufficiently low then the curtain fluid can be supplied from within the same stage, using fluid bled from upstream of the fixed blade row preceding the rotor. At the optimum value of PR with zero leakage flow entering the rotor shroud seal over-tip leakage channel, the total pressure at the inlet to the over-tip leakage channel will be the static pressure upstream of the rotor blade tip plus the dynamic pressure due to swirl. This is indicated in Figure 57. The swirl that is present in the tip seal inlet cavity does nothing to drive leakage flow through the tip seal i.e. for an axisymmetric seal inlet cavity, there is no mechanism by which the swirl kinetic energy can be significantly recovered into static pressure to drive more flow through the tip seal. The pressure difference which drives tip leakage flow is therefore the difference in static pressure across the rotor at the tip of the blade. If there were no difference in static pressure across the rotor tip, then there would be no over-tip leakage flow regardless of the amount of swirl present in the flow in the tip seal inlet cavity. This means that the seal inlet total pressure which should be used to calculate PR for blade tip seal applications, is the static pressure in the seal inlet cavity, i.e. $P_{0,\text{inlet}} = P_{\text{rotor tip inlet}}$.

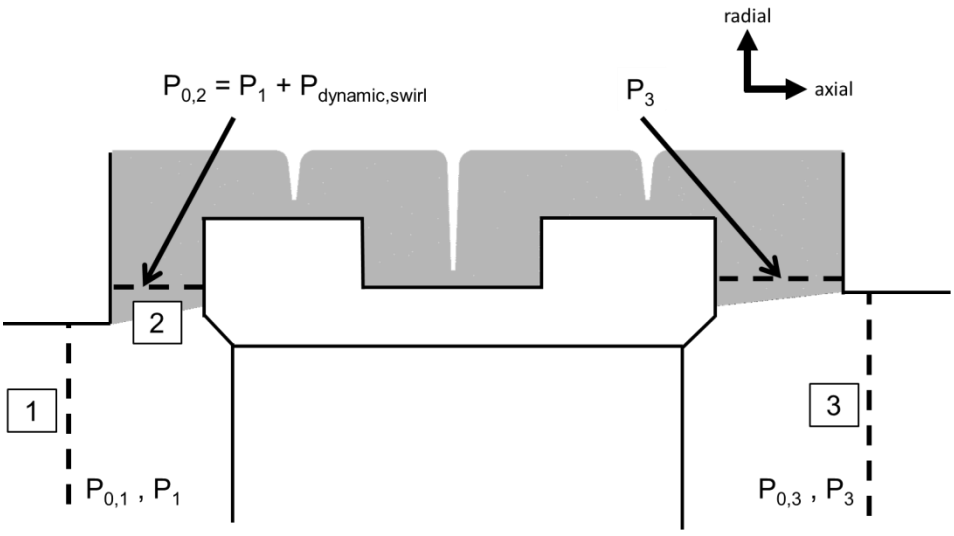

Figure 57: Inlet and outlet pressures to tip seal cavity

Making the assumption that fluid supplying the curtain is bled through holes or slots in the outer casing wall upstream of the fixed blades, the maximum pressure at which fluid can be supplied to the fluidic curtain from within a single turbine stage, is equal to the static pressure

at the stage inlet, i.e. $P_{0,jet} = P_{stage\ inlet}$ The static pressure at the blade tip seal outlet will be the static pressure at the turbine stage outlet, i.e. $P_{outlet} = P_{stage\ outlet}$. This means that for a rotor tip seal application, the value of pressure ratio PR is the reciprocal of the stage reaction, as shown in Equation 5.1.

$$PR = \frac{P_{0,jet} - P_{outlet}}{P_{0,inlet} - P_{outlet}} = \frac{P_{stage\ inlet} - P_{stage\ outlet}}{P_{rotor\ tip\ inlet} - P_{stage\ outlet}} = \frac{1}{Stage\ Reaction} \qquad (5.1)$$

Therefore, in a 50 % reaction turbine stage the maximum PR at which a fluidic curtain can be operated using a fluid supply from within the same stage is 2. Higher values of *PR* than this will be possible in lower reaction turbine stages. For this reason, the design points for this study were selected to have an optimum *PR* close to 2 and not exceeding 3.

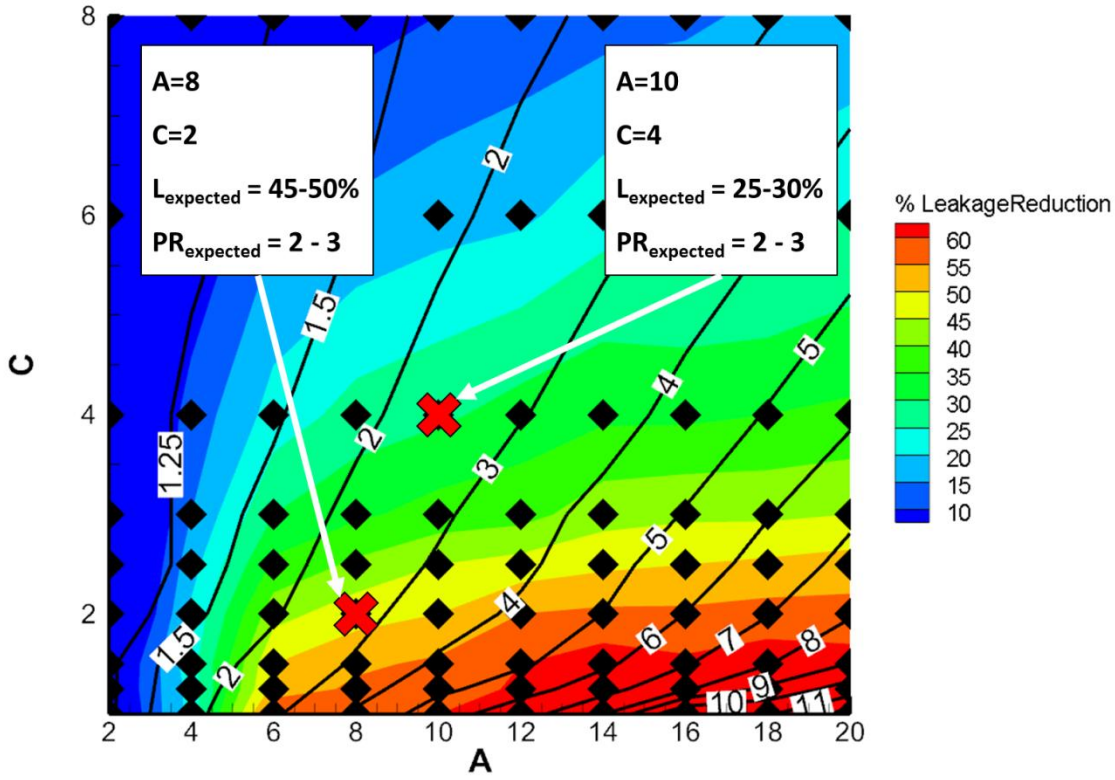

Figure 58: Design points selected for study on shroud seal design

If a fluidic curtain were to simply replace the first labyrinth fin in the baseline design shown in Figure 56 with the same rotor to casing clearance (channel height = 3.8 mm) at the location of the curtain, then the non-dimensional labyrinth fin clearance, *C*, would be calculated as shown in Equation 5.2. In this section it is assumed that any multiple fin labyrinth seal is equivalent to a single seal restriction with a clearance that is set to the clearance of the multi-fin seal divided by the square root of the number of restrictions. The single fin clearance can be thought of as

the ‘effective clearance’ of the multi-fin labyrinth seal. The work of Hendricks and Stetz [**17**], discussed earlier in Chapter 2, suggests that the number of restrictions raised to the power 0.4 (see Equation 2.1.), but 0.5 has been used for design purposes in this study, as this is the ‘rule of thumb’ often adopted by turbomachinery designers.

$$C = \frac{b}{c_{effective,single\ fin}} = \frac{3.8}{1/\sqrt{2}} = 5.37 \tag{5.2}$$

If *C* = 5.37 then it is clear from the Figure 65 that a *PR* of 2-3 will limit performance to ~ 25 % leakage reduction. Values of dimensionless curtain thickness, *A* (= *b*/*a*) ≈ 10 would be needed to achieve this performance, i.e. design curtain thickness *a* = *b*/10 = 0.38 mm. While it would be possible to design and manufacture a curtain of this thickness, the leakage performance improvement for this design is relatively low.

In order to reduce the value of *C* and therefore improve the performance of the fluid curtain seal, the channel height local to the fluidic curtain (*b*) was reduced as shown in Figure 53. Two design variants were considered. Shroud Seal 1, where the castellated rotor shroud is unchanged and the first labyrinth fin is replaced by a fluid curtain with a locally reduced rotor to casing clearance, and Shroud Seal 2, where the short and long fins are reversed and the rotor shroud design is changed so that the radius of the shroud is constant at the fluid curtain location and first downstream labyrinth restriction and then stepped down to a lower radius for the second restriction. Shroud Seal 2 includes a kinetic energy blocker on the shroud surface. A blocker was not included in the Shroud Seal 1 design, because the change in radius between the shroud surface where the fluidic curtain flow impinges and the shroud radius at the location of the first (‘long’) labyrinth restriction, would be sufficient to impede kinetic energy carry-over with this design. Four different designs (Shroud Seals 1 & 2 each at the two design points in Figure 65) incorporating a fluid curtain were therefore considered and their performance was compared to that of the baseline labyrinth design shown Figure 56. The values of channel height, *b*, and curtain thickness, *a*, needed to achieve the selected design point values for *A* and *C* are given in Table 9.

Table 9: Key dimensions of the fluidic curtain seal for selected design points

	***A* = 8** ***C* = 2**	***A* = 10** ***C* = 4**
individual fin clearance	1.0 mm	1.0 mm
***c* = effective fin clearance**	1/ √2 mm	1/ √2 mm
C	2	4
***b* (= *C* x *c*)**	1.414 mm	2.828 mm
A	8	10
***a* (= *b*/*A*)**	0.1768 mm	0.2828 mm
***p* (= 2*b*)**	0.3536 mm	0.5656 mm

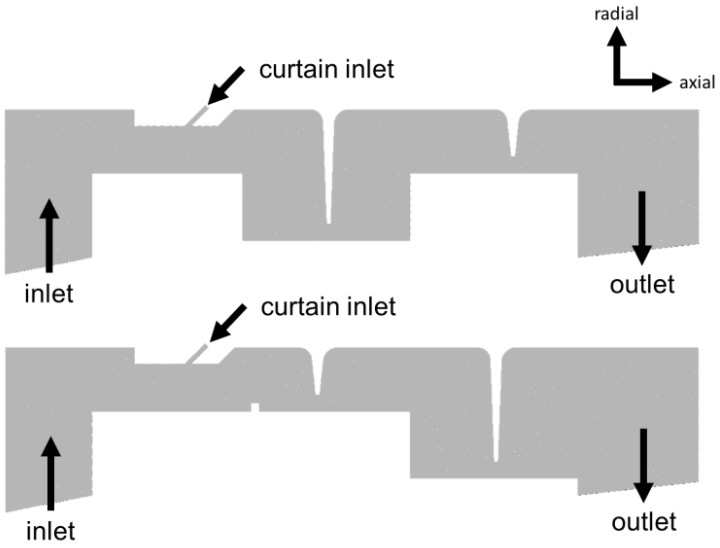

Figure 59: Shroud Seal 1 (top) and Shroud Seal 2 (bottom). Pictured where *A* = 10, *C* = 4 for comparison.

The labyrinth fin clearance heights in all geometries remain 1mm. If the effective single fin clearance is known, the required channel height local to the fluidic curtain, *b*, can be calculated for a given value of the ratio *C* as shown. Labyrinth fins are designed with tight clearances, normally less than 1 mm, and are expected to potentially see contact with rotating parts in service. If contact occurs then the labyrinth fin deforms without causing serious damage to the turbine. 'Hard' contacts such as the rotor shroud touching the casing must be avoided during operation. Turbines are designed with minimum allowed clearances to make sure hard contacts

never occur. These clearances are usually significantly greater than 1 mm. The decreased channel height local to the fluidic curtain is achieved by extending the casing radially inward, which reduces the clearance between the casing and the rotor shroud at this location. When selecting the design point for a steam or gas turbine seal, care will need to be taken to ensure that the desired value of *C* gives a local channel height which is sufficient to ensure that design rules for hard contacts are not violated. The minimum allowed hard-on-hard design clearance will set the limit on how small the value of *C* can be made, and will therefore set the limit on sealing improvement. Similarly, knowing channel height *b* and ratio *A* means that fluidic curtain width, *a*, can also be calculated.

Earlier work described in Section 3.5 has shown that the development of the two vortex structure between the fluid curtain injection and the first labyrinth fin, which is needed for good sealing performance, can be impeded for designs with shorter axial spacing between the curtain inlet and the kinetic energy blocker. This was shown to result in reduced leakage reduction benefit from the presence of the curtain. This does not impact the Shroud Seal 1 design because there is no kinetic energy blocker. In the Shroud Seal 2 design, the axial distance *p* between the end of the surface through which the curtain issues and the first labyrinth restriction (see Figure 60) was maintained at twice the leakage channel height at the curtain entry location, i.e. $p = 2b$ in all of the designs calculated. The values of *p* needed to achieve this design are also included in Table 8. The kinetic energy blocker was placed half way between the start of the increase in channel height and the labyrinth fin. This was intended to create a similar flow structure to the two large vortices seen previously between the curtain and the labyrinth fin. The 1.75 mm distance shown in Figure 60 between the curtain inlet and the end of the surface through which the curtain issues, ensured that the curtain flow will have fully crossed the leakage channel and impinged on the rotor shroud surface, before the channel height starts to increase.

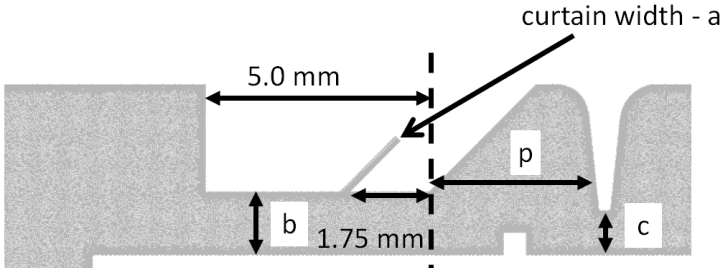

Figure 60: Key dimensions indicated on close up of fluidic curtain section. Unknowns depend on *A* and *C*

5.2.2. Setup of CFD Calculation Comparing Shroud Seal 1 and 2

The settings and boundary conditions used in the CFD study are given in Table 10 and the study was carried out in with the same method as the one described in Chapter 3; the inlet and outlet pressures were kept fixed with mass flow rates at each boundary calculated as *PR* is increased in increments by raising the fluidic curtain inlet total pressure. Boundary conditions are representative of a turbine stage half way through the high pressure section of a typical subcritical large steam turbine set. The shroud geometry in Figure 56 is from a model turbine test stage and so the speed of rotation used in the calculations is equal to the speed of the scale test turbine on which the seal geometry is based. The working fluid is high pressure superheated steam modelled as an ideal gas. The channel inlet total pressure is equal to the static pressure upstream of the rotor as discussed in Section 5.2.1. This essentially means that any swirl in the flow entering in the inlet cavity of rotor tip seal, is not included in the axisymmetric CFD calculations described in this section.

Table 10: Settings used in CFD study on realistic tip seal

Cell count	~450 000
Simulation type	RANS steady state, pressure based
Format	2D, axisymmetric
Viscosity model	k-epsilon realisable
Wall functions	Fluent enhanced wall treatment y+ ~ 1
Working Fluid	Water vapour – ideal gas laws
Channel inlet boundary	Total pressure = 92.4 bar Total Temperature = 440°C
Channel outlet boundary	Static pressure = 86.0 bar
Curtain inlet boundary	Pressure increased in steps according to Eq. 1 Total Temperature = 440°C
Rotating wall (shroud)	Rotating wall – 1300 rpm
Solver	Ansys Fluent version 15.0

5.2.3. CFD Results

Cases were run using Ansys Fluent version 15.0 for the baseline seal geometry and each of the four designs incorporating the fluid curtain, described in the previous section. These included cases with no supply to the fluidic curtain and cases for a range of *PR*. The maximum operating *PR* and the corresponding leakage reduction obtained for each seal design was determined from the CFD model. The leakage flows modelled for the designs in Figure 59 incorporating the fluidic curtain, were compared to leakage flows modelled both the baseline geometry (3 labyrinth fin design – Figure 56) and with the designs shown in Figure 59 but with the fluidic

curtain turned off (the no-curtain case). Figure 61 to Figure 64 show mass flow rate vs *PR* for the seal designs investigated. The leakage mass flow rate for the baseline tip seal design (Figure 56) was calculated to be 3.62 kg/s for the steam conditions given in Table 10.

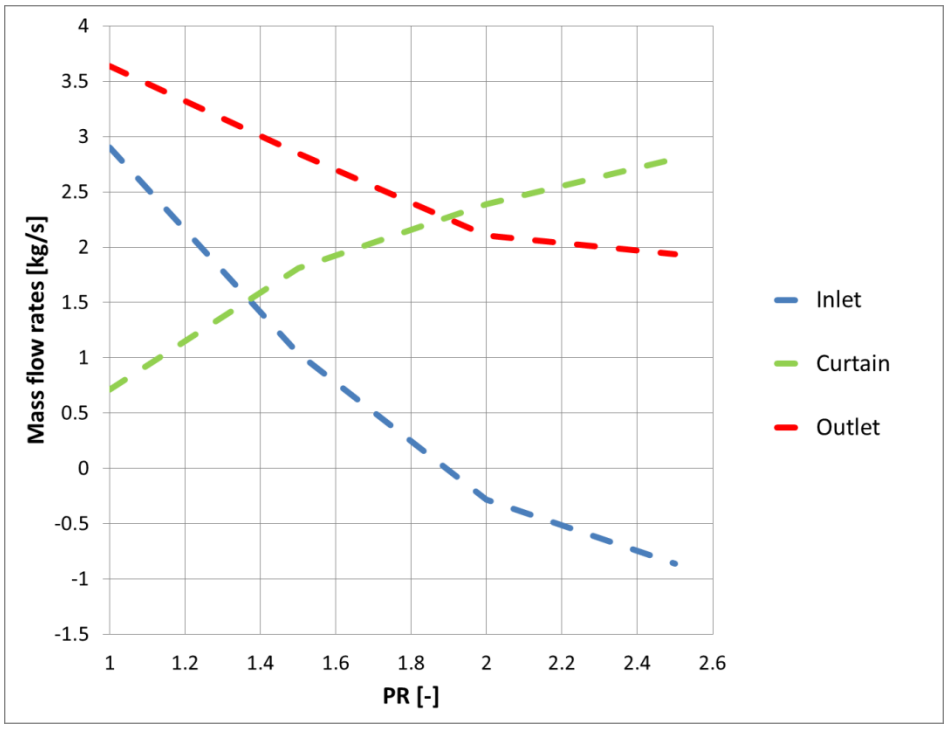

Figure 61: Mass flow rate vs *PR*

***A* = 8, *C* = 2, Shroud Seal 1 layout**

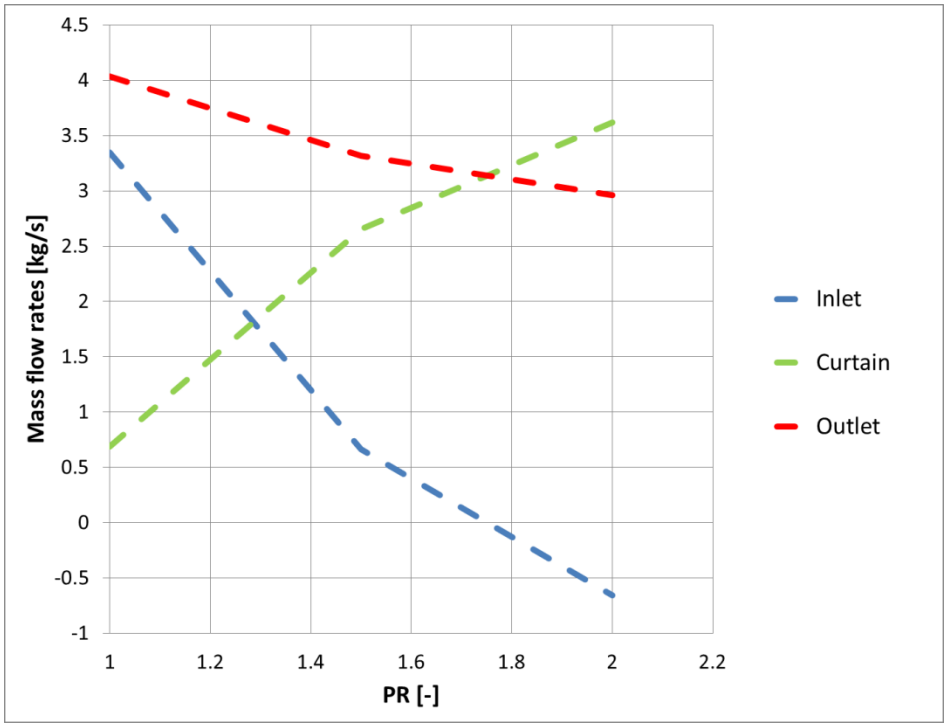

Figure 62: Mass flow rate vs *PR*

***A* = 10, *C* = 4, Shroud Seal 1 layout**

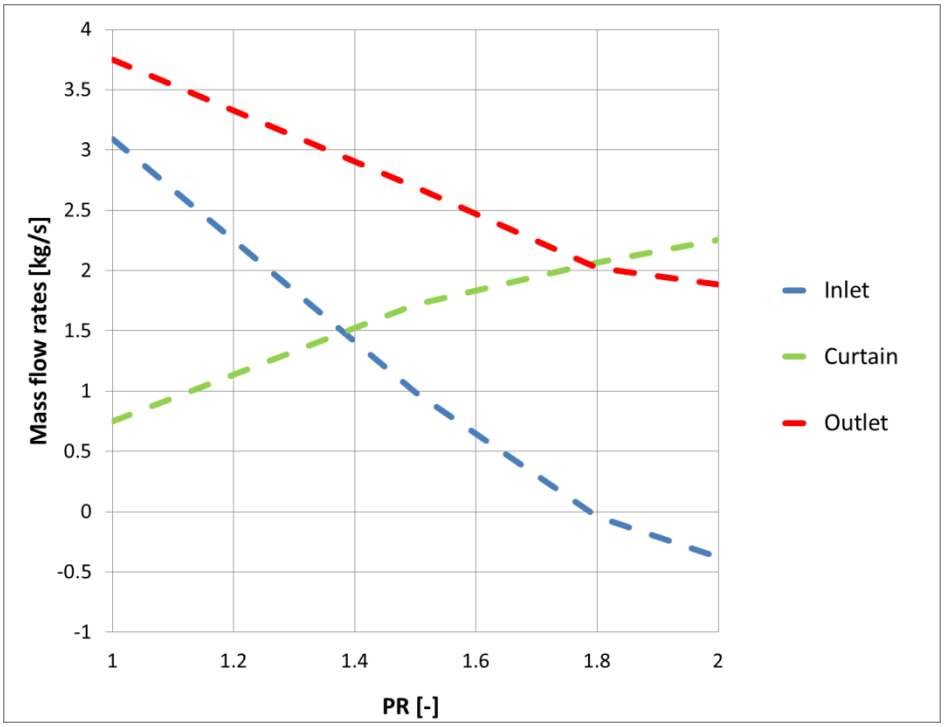

Figure 63: Mass flow rate vs *PR*

***A* = 8, *C* = 2, Shroud Seal 2 layout**

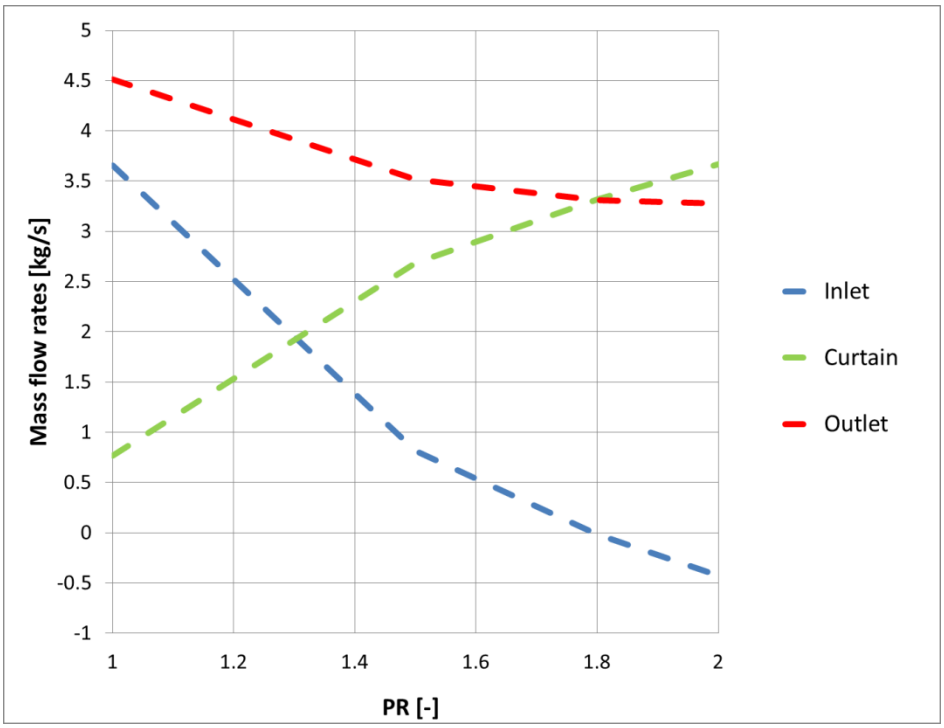

Figure 64: Mass flow rate vs *PR*

***A* = 10, *C* = 4, Shroud Seal 2 layout**

As discussed earlier, the desired operating point with the fluid curtain is that which gives the maximum reduction of total (outlet) leakage mass flow rate without overblowing the seal. This point can be found from Figure 61, Figure 62, Figure 63, and Figure 64 by interpolating to find the value of *PR* where the inlet mass flow reaches zero. At this value of *PR*, the curtain mass flow rate is equal to the outlet mass flow rate. It should be noted that *PR* = 1.0 does not correspond to the no curtain flow case, because there will be a pressure drop along the leakage channel which will cause the local static pressure at the curtain injection point to be lower than the pressure at the leakage channel inlet. This can be seen in all results where the fluidic curtain flow is greater than zero at *PR* = 1.0. The best design is the one where the action of the fluidic curtain at its optimum *PR* gives the biggest reduction in outlet mass flow rate compared to the baseline case. In this study, the best performance is seen where *A* = 8 and *C* = 2 for the Shroud Seal 2 layout where the presence of the fluidic curtain reduces the leakage flow exiting the seal to just over half of the leakage of the baseline design. The results are summarised in Table 11 with the best results highlighted in bold.

Table 11: Performance summary of the four seal designs (expected = values inferred from Figure 33).

		***A* = 8** ***C* = 2**	***A* = 10** ***C* = 4**
Shroud Seal 1	Overblow PR	2.0 (2 - 3 expected)	1.7 (2 - 3 expected)
	Leakage reduction w.r.t no-curtain	40.1 % (45 – 50 % expected)	20.4 % (25 – 30 % expected)
	Leakage reduction w.r.t baseline	35.1 %	8.3 %
Shroud Seal 2	Overblow PR	**1.8** (2 - 3 expected)	1.8 (2 - 3 expected)
	Leakage reduction w.r.t no-curtain	**52.5 %** (45 – 50 % expected)	26.7 % (25 – 30 % expected)
	Leakage reduction w.r.t baseline	**44.1 %**	8.5 %

5.2.4. Discussion

Both design points were expected to have similar optimum operating *PR*s of between 2 and 3 based on Figure 58 (i.e. Figure 33). The CFD results show that for the Shroud Seal 2 layout the overblow *PR*s are both approximately 1.8, so just less than the value of 2 expected for these seal design geometries incorporating fluid curtains which are quite different to the GS1 generic seal design used to develop Figure 33. This again demonstrates that Figure 33 is a useful generic design guideline for developing different types of seal designs that incorporate fluid curtains. It should also be noted that good agreement exists between the leakage reductions predicted by CFD for all four of the fluid curtain seal designs investigated, and the leakage reductions from Figure 33 for the design points used.

As discussed in Section 5.2.1, if a fluidic curtain were to be fed with fluid from the main gas path upstream of the previous stator row, then the maximum *PR* that can be supplied in a 50 % reaction turbine stage is 2. Both of the designs could therefore feasibly be incorporated into a 50 % reaction turbine stage with the curtain flow supplied passively from within the stage.

The performance for the Shroud Seal 1 design was lower than that for the Shroud Seal 2 layout. In order to explain the difference in performance between the two shroud architectures, a detailed examination of the flow structure was undertaken. Since all fluidic curtain dimensions and boundary conditions were identical in the CFD investigations of the two layouts, the difference in performance was attributed to the difference in flow structure from the fluid curtain inlet slot to the first downstream labyrinth restriction.

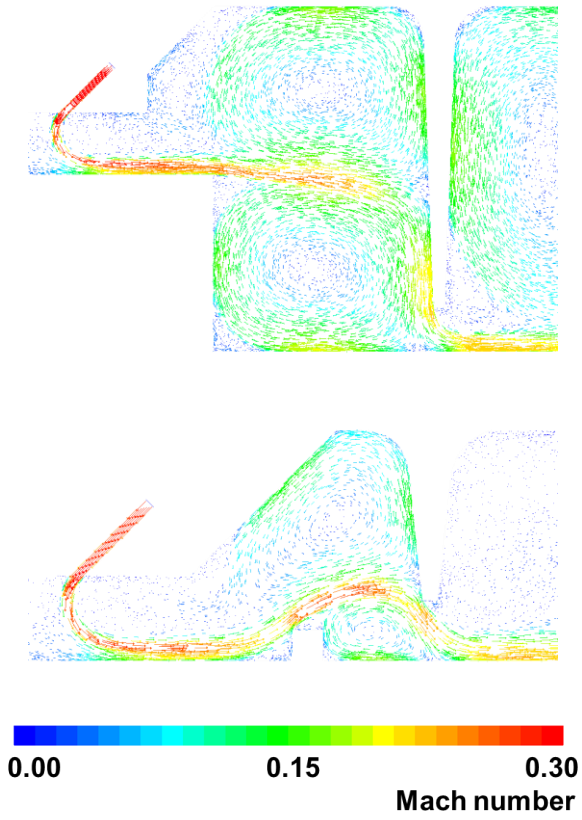

Figure 65: Velocity vectors where *A* = 8, *C* = 2, *PR* = 1.5
Comparing Shroud Seal 1 (top) with Shroud Seal 2 (bottom)

In the velocity vector plot shown in Figure 65 it can be seen that as the fluidic curtain moves downstream it divides as it impinges on the front face of the labyrinth fin, forming two vortices. In the Shroud Seal 1 layout both vortices are large and the high kinetic energy stream decelerates as it turns in the lower vortex to flow down the front face of the labyrinth fin. In the Shroud Seal 2 layout the lower vortex is smaller and the high kinetic energy stream decelerates while turning through a smaller radius. This flow structure gives a tighter turning radius close to the tip of the labyrinth fin and appears to be responsible for the increase in sealing effectiveness of Shroud Seal 2 compared to Shroud Seal 1 where *A* = 8 and *C* = 2. This observation is supported by the lack of similar improvement between the two shroud designs

for the other design point considered where *A* = 10 and *C* = 4. Figure 66 shows the same comparison between shroud designs where *A* = 10 and *C* = 4. With the Shroud Seal 2 layout the high kinetic energy stream impinges on the labyrinth fin at the root, and forms two similar size vortices. This gives similar flow structures close to the tip of the labyrinth fin for both shroud layouts and therefore similar sealing performance.

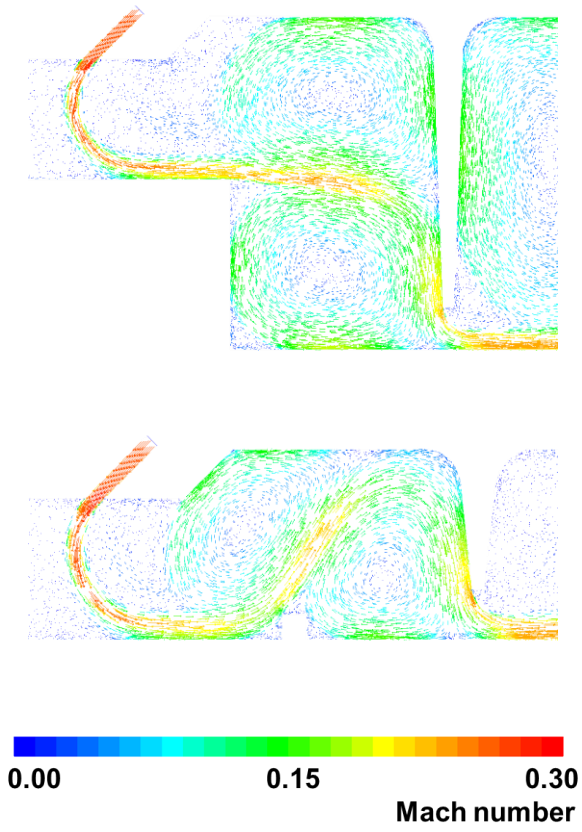

Figure 66: Velocity vectors where *A* = 10, *C* = 4, *PR* = 1.5
Comparing Shroud Seal 1 (top) with Shroud Seal 2 (bottom)

As expected, the leakage reduction with respect to the baseline case is lower than with respect to the no curtain case for each design, but still significant in the context of reducing turbine tip leakage. This confirms that a fluidic curtain brings a greater increase in performance than an extra labyrinth fin placed in the same position.

5.2.5. Optimum Vortex Structure

If the high performance of the Shroud Seal 2 design where *A* = 8, *C* = 2 was due to the flow structure between the fluidic curtain and the downstream labyrinth fin, then creating a similar flow structure where *A* = 10, *C* = 4 would be expected to increase the performance of that design as well. The Shroud Seal 2 design was modified to give a similar flow structure, with a

larger vortex followed by a smaller, faster vortex. This was achieved by moving the first downstream labyrinth fin forward axially by 1 mm. This modified design is referred to as Shroud Seal 2A Figure 67 shows a velocity vector plot coloured by Mach number for both Shroud Seal designs for comparison. The main vortices have been highlighted in the figure to show the change in flow structure with the Shroud Seal 2A design vortex system now being similar to the *A* = 8, *C* = 2 case (see Figure 65 Shroud Seal 2), with a smaller, faster vortex preceding the first labyrinth fin downstream from the fluidic curtain.

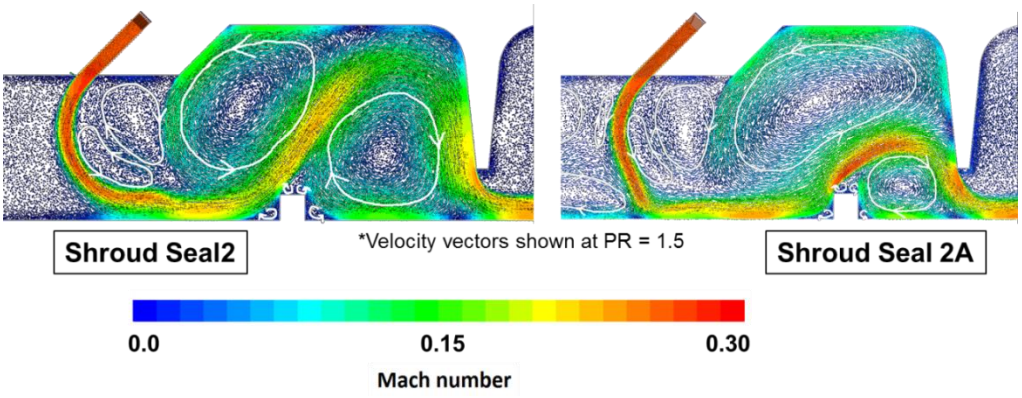

Figure 67: Comparison of flow structure between Shroud Seal 2 and Shroud Seal 2A where A=10 and C=4.

The CFD results showed that switching from the Shroud Seal 2 to the Shroud Seal 2A design increased the leakage reduction factor compared to the baseline from 8.5 % (see Table 11) to 22.9 %. This further confirms that the type of flow structure shown in Figure 65 for Shroud Seal 2 appears to be important when maximising the pressure drop due to the fluidic curtain.

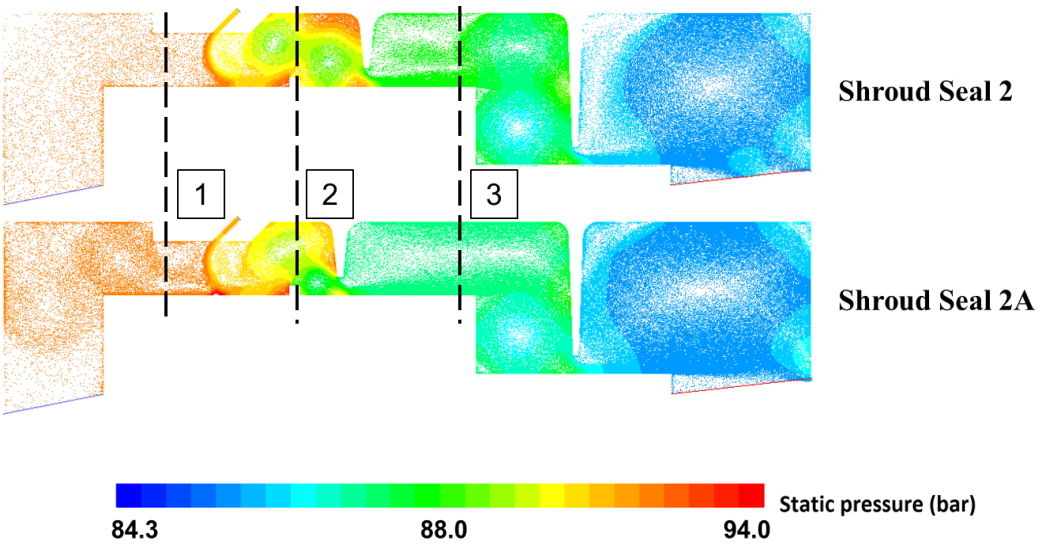

Figure 68: Shroud Seal 2 and Shroud Seal 2A – Velocity vectors coloured by static pressure. *PR* = 1.5.

Figure 68 shows the static pressure distributions in the leakage flow for Shroud Seals 2 and 2A. Three monitoring planes are indicated in the figure. The static pressure drop between stations 1 and 2 will show the pressure drop due to the fluidic curtain, while the static pressure drop between stations 2 and 3 will show the pressure drop across the first labyrinth fin. These pressure drops are given in Table 12 and are calculated using the mass weighted static pressure from the CFD solutions at the three stations. In the case of the fluidic curtain a theoretical value is also given, which has been calculated using the model in equation 2.4.

Table 12: Comparison of pressure changes between each of the stations indicated in Figure 68

		$\Delta P_{1\text{-}2}$	$\Delta P_{2\text{-}3}$
Shroud Seal 2	**Theoretical**	-223000 Pa	-
	CFD	-196000 Pa	-156000 Pa
Shroud Seal 2A	**Theoretical**	-217000 Pa	-
	CFD	-212000 Pa	-235000 Pa

The pressure drop across the fluid curtain ($\Delta P_{1\text{-}2}$) predicted both by the CFD and by the analytical model is similar in all cases in Table 11. The data in the table shows that the increase in performance by switching from the Shroud Seal 2 to Shroud Seal 2A design for $A = 10$, $C = 4$, is due to the increased static pressure drop across the downstream labyrinth fin. So, by modifying the flow structure so that there is a tighter higher velocity vortex immediately upstream of the fin, the static pressure drop across the fin is increased (by 50 %) and the overall sealing performance of the design is significantly enhanced as a result.

5.3.The Effect of Inlet Swirl on the Performance of Fluid Curtain Seals

The previous two sections of this chapter have shown how fluid curtains can be incorporated into turbomachinery seal designs achieving the values for the dimensionless geometry parameters *A* and *C* needed for good leakage reduction performance guided by Figure 33, and the importance of controlling the flow structure between the fluid curtain injection and the first seal restriction, in order to maximise the performance improvement achieved.

This section describes work that was undertaken to use this new knowledge to incorporate a fluid curtain into a turbine stage rotor tip seal for a model turbine test, which was planned to

be carried out on GE's Grace model turbine test facility at their research laboratories in Rugby. The intention was to modify the tip seal on an existing model turbine stage to incorporate a fluid curtain. This has the twin advantage of minimising cost and also eliminating the need for a new baseline test, as the data from GE's tests already carried out on the chosen test stage provides the baseline data needed for the unmodified rotor tip seal build.

A GE proprietary 3-D through-flow method (HAZE [**46**]) was used to calculate the rotor tip seal inlet and outlet flow conditions (including swirl), that are used as boundary conditions for the high fidelity 2D axisymmetric CFD calculations carried out in this study to modify the tip seal to incorporate a fluid curtain.

5.3.1. Grace Seal Design

A fluidic curtain seal design was created as a modification to an existing three fin labyrinth tip seal on a turbine test stage that had been previously tested by General Electric on their two stage Grace model turbine test facility. This test rig uses the refrigerant R134a as a working fluid to achieve test Reynolds numbers that are representative of those in high pressure steam turbines. Representative Reynolds numbers range from 10e3 to 10e6 [**47**], so testing using steam as the working fluid would require representative steam turbine pressure in order for the density, and therefore Reynolds number, to be accurate. R134a has a high density and allows safer testing at lower temperature and pressure while still providing representative Reynolds numbers. Basic information on the Grace rig is given in Table 13.

Table 13: Grace test rig basic information

Stages	2
Working fluid	R134a
Typical inlet pressure	~4 bar
Typical outlet pressure	~3 bar
Operating temperature	30-40°C (room temperature)
Typical Reynolds number	1e6 – 2e6
Blade root diameter	265 mm
Blade height	~38 mm
Rotational speed	~1400 rpm

A section view of the Grace turbine is shown in Figure 69. Due to the greater accessibility of the first stage labyrinth seal from the outside, the seal modification was intended for use on the first stage.

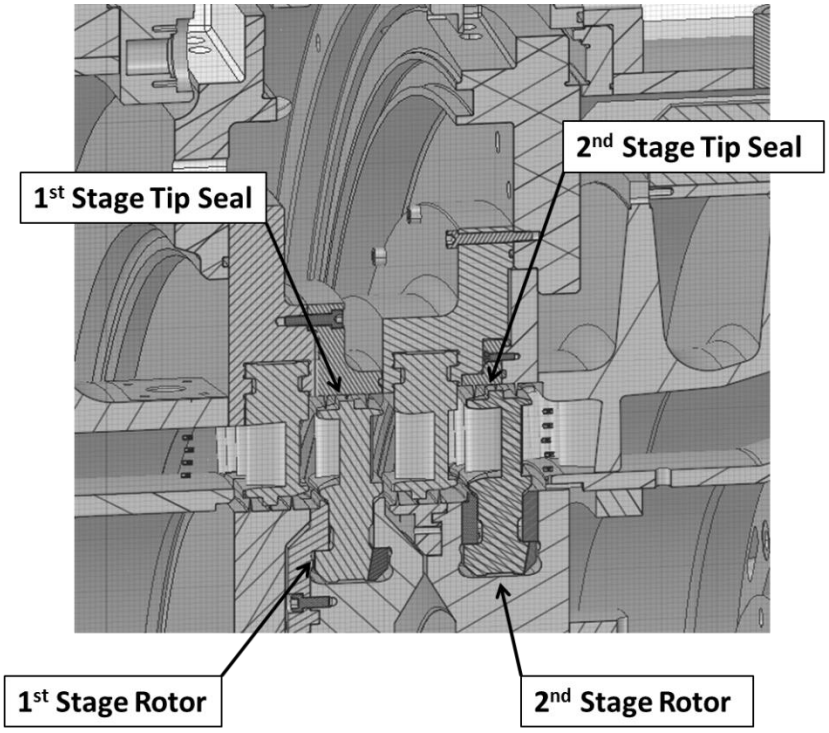

Figure 69: Grace test turbine general arrangement

Figure 70 shows the original three fin stepped labyrinth tip seal design and the proposed modification to incorporate a fluid curtain. It was possible to retain three labyrinth restrictions in the modified seal design. Detailed dimensions of the modified seal design in the region of the curtain injection and first labyrinth restriction are shown in Figure 77.

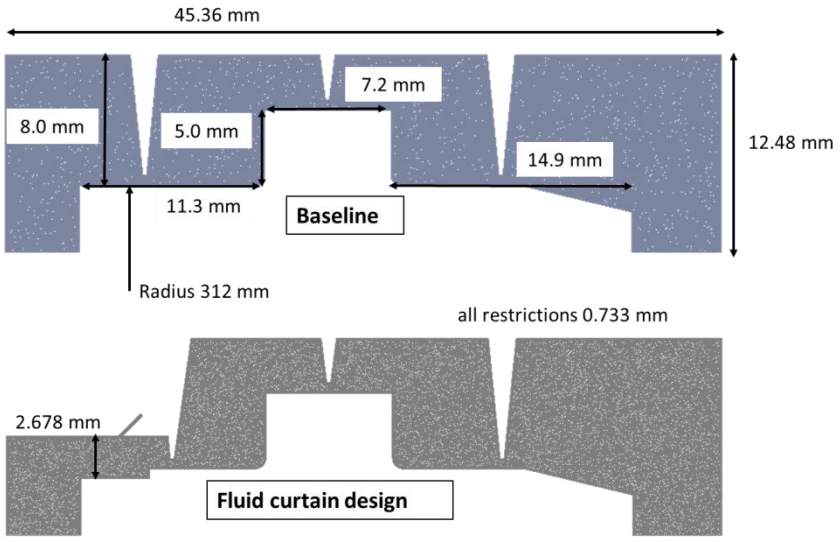

Figure 70: Comparison of baseline seal design with the design employing a fluidic curtain seal

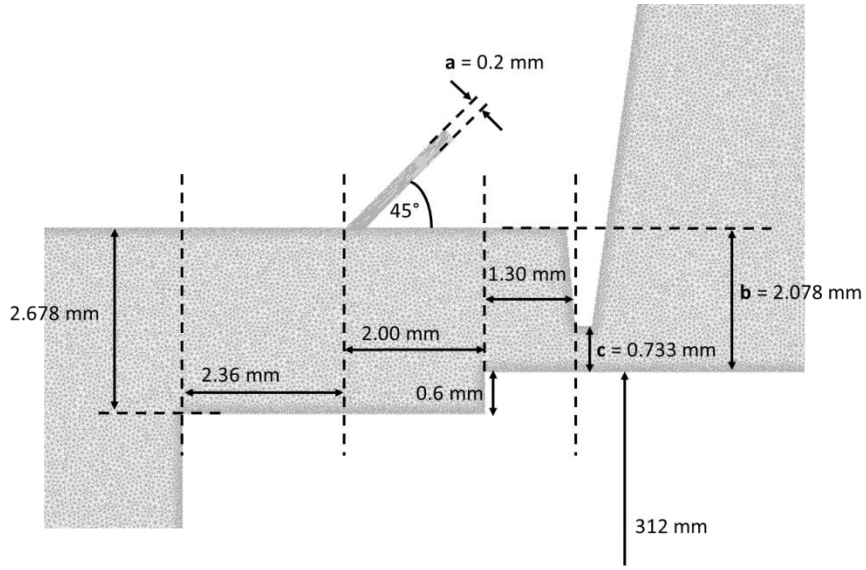

Figure 71: Dimensions of the Grace seal design.

In the modified seal design, a step in the shroud surface acts as a kinetic energy blocker in order to create a similar flow structure to the Shroud Seal 2A design from Section 5.2.5, with a small vortex in front of the labyrinth fin. The individual tip clearance of the labyrinth was 0.733 mm in both the baseline and the modified designs. The channel height, *b*, at the curtain injection was set to 2.678 mm based on GE's design rules for the minimum allowable clearance between hard components. The curtain width, *a*, was set to the minimum manufactureable inlet slot width of 0.2 mm. These dimensions resulted in a seal design where *A* = 13.4 and *C* = 6.3. Figure 33 shows that this design would be expected to give a leakage reduction of approximately 25 % at a pressure ratio of between 2 and 3. These dimensions and the expected performance benefit are summarised in Table 12.

Table 14: Important dimensions and geometric ratios in seal design

Variable	Value	Comment
Individual tip clearance	0.733 mm	Nominal clearance
Number of downstream restrictions	3	Downstream of fluidic curtain and upstream of exit plane
Effective single restriction equivalent of the 3 restriction seal, *c*.	0.423 mm	Divide individual clearance by square root of number of restrictions
Channel height at fluidic curtain entry slot *b*	2.678 mm	Allowable minimum 'hard on hard' clearance for this design of 2.0 mm based on GE rules.
Fluidic curtain width *a*	0.2 mm	Minimum manufactureable curtain slot width

***A* (=*b*/*a*)**	13.4	Calculated from *a* and *b*
***C* (=*b*/*c*)**	6.3	Calculated from *c* and *b*
Expected optimum PR	2 - 3	Read from Figure 33
Expected maximum L	25%	Read from Figure 33

5.3.2. Setup of CFD Calculation Investigating the Grace Tip Seal Design

Whereas previously the seal was simulated without swirl in the inlet flow, in the new model detailed information about the leakage channel inlet and exit conditions were extracted from a GE HAZE throughflow calculation of the test stage and used as the boundary conditions in the CFD simulation. This included (for the first time) the swirl velocity at the leakage channel inlet. As discussed in Section 5.2.1 the total pressure at the inlet to the leakage channel was the sum of the static pressure between the fixed and rotating blades and the dynamic pressure due to swirl. The fluidic curtain supply pressure was set to the static pressure upstream of the fixed blades in the same stage, as this is the maximum pressure which could be used to supply the curtain flow passively from within the turbine stage and therefore represents the best possible sealing from the fluidic curtain. This gives a maximum operating *PR* of 1.75. As this value of *PR* is lower than that needed to deliver the optimum performance benefit from the fluid curtain according to Figure 33, it was expected that the Grace performance test of the modified seal would result in less than the 25 % leakage reduction compared to the baseline design indicated in Table 12. Details of the CFD calculations and boundary conditions are summarised in Table 15.

Table 15: Settings and boundary conditions used in CFD simulations of the baseline and modified Grace rotor tip seal design.

Cell count	~450 000
Simulation type	RANS steady state, pressure based
Format	2D, axisymmetric
Viscosity model	k-epsilon realisable
Wall functions	Fluent enhanced wall treatment y+ ~ 1
Working fluid	R134a – NIST real gas model
Channel inlet boundary	Total pressure = 3.757 bar + Swirl dynamic pressure Static Pressure = 3.757 bar Total Temperature = 36°C
Channel outlet boundary	Static pressure = 3.606 bar
Curtain inlet boundary	Total pressure = 3.870 bar
Rotating wall (shroud)	Rotating wall – 1300 rpm
Solver	Ansys Fluent version 15.0

Figure 72 and Figure 73 show static pressure contours for the baseline seal design and for the design incorporating a fluidic curtain seal. Each figure compares the flow with and without the swirl component, and gives the mass flow rates and pressures at each boundary. Leakage reductions are given with respect to the baseline case with the same swirl velocity.

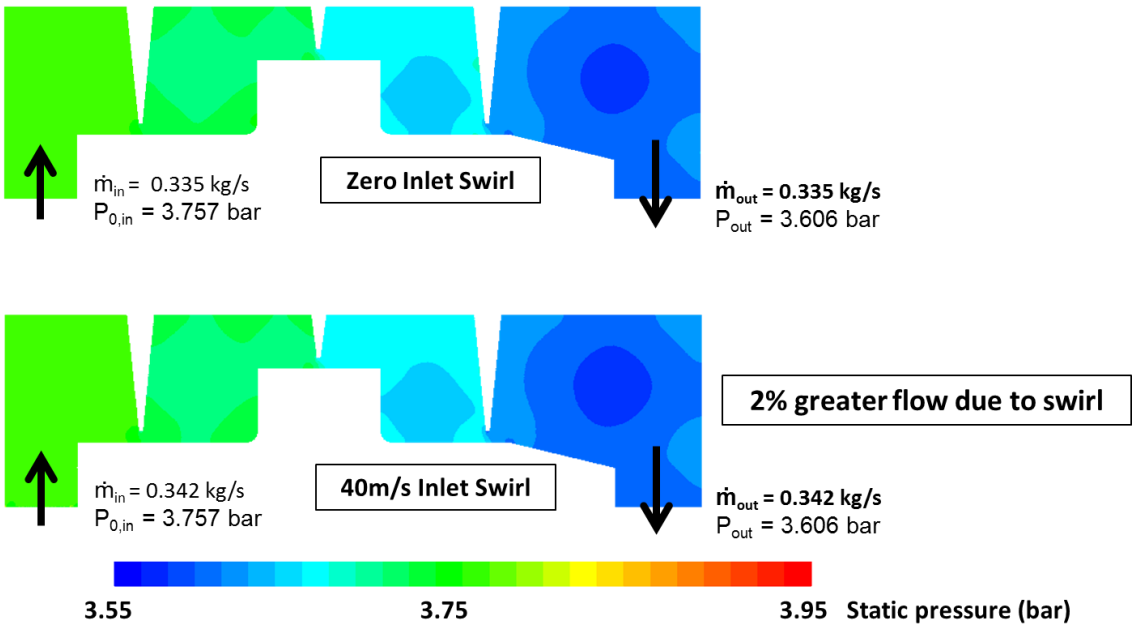

Figure 72: Comparison of the baseline seal at zero and 40m/s inlet swirl

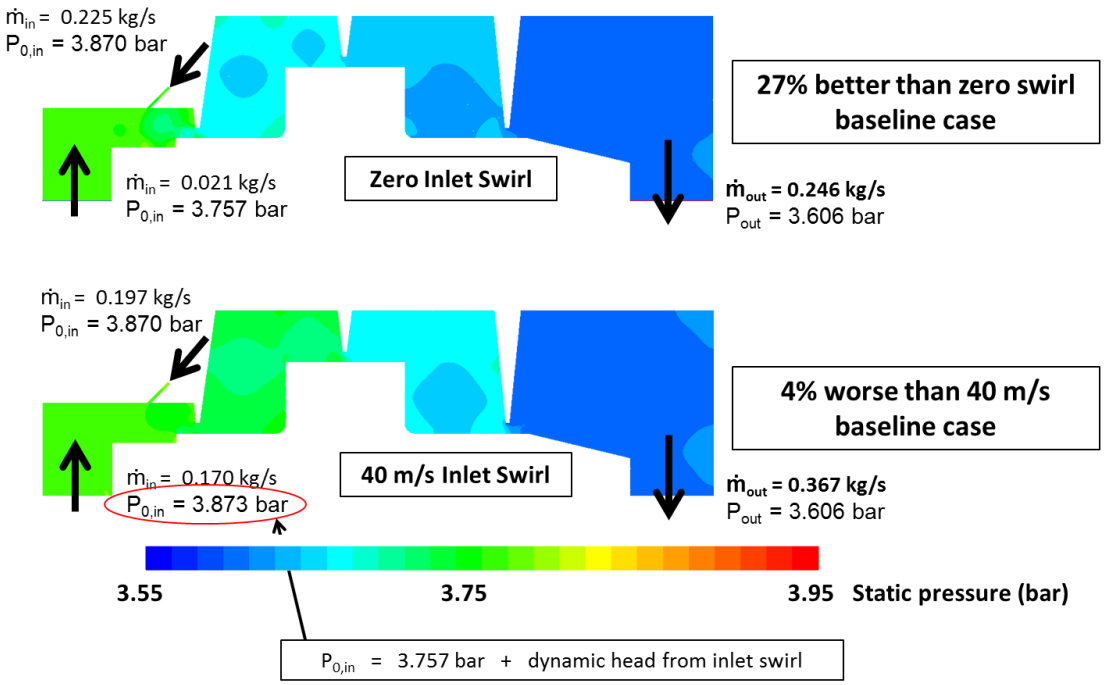

Figure 73: Comparison of the modified seal at zero and 40m/s inlet swirl

The baseline labyrinth seal had a leakage mass flow rate of 0.335 kg/s with no inlet swirl and 0.342 kg/s with inlet swirl. This shows a small increase in flow rate (~2 %) due to the addition of the swirl dynamic pressure. The flow increases by 2 % while the total to static pressure difference across the leakage channel increases by 77 % in the presence of swirl. This is not unexpected since the swirl dynamic pressure does not directly drive flow through the leakage path. Operating without swirl, the seal reduced tip leakage by 27 % over the zero swirl baseline design. This was close to the expected maximum leakage reduction of 25 % and occurred at a *PR* of 1.75, which was slightly lower than the expected optimum *PR* of 2 - 3. It was found that when the swirl velocity component at the inlet to the seal was included in the simulation, the performance of the seal was severely reduced at the same pressure ratio. The inlet flow to the leakage channel decreased, but not to near zero as in the no swirl case. The total outlet mass flow saw a marginal increase.

As stated earlier, the greater swirl dynamic pressure does not drive much extra flow through the seal so the increase in leakage is not simply due to an increased pressure difference across the seal. It can be concluded that the swirl must have had some other impact on the effectiveness of the fluidic curtain. Figure 73 shows that there is a smaller drop in static pressure across the first labyrinth fin in the case with swirl than without. Section 5.2.5 describes how the fluid curtain can create a flow structure which maximises the pressure loss through the next downstream restriction. A reduced pressure drop through this restriction suggests that the presence of swirl diminishes this effect of the fluid curtain. This results in a higher total to static pressure difference across the remaining two labyrinth fins and therefore a higher leakage flow rate.

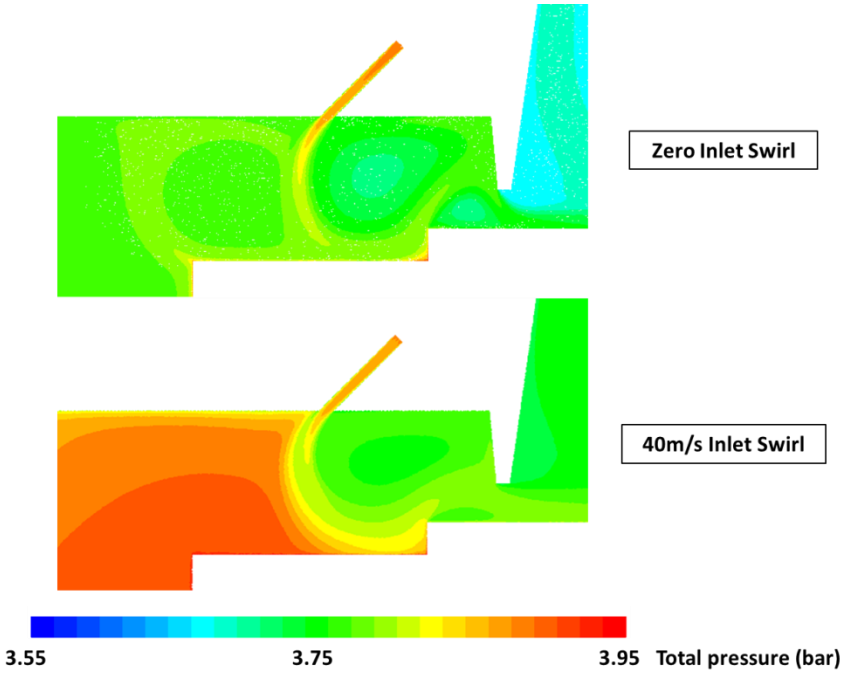

Figure 74: Comparison of flow structures between fluid curtain inlet and first labyrinth fin.

It can be seen in Figure 74 that the swirling leakage flow sheared the curtain flow and made it more diffuse in the region between the curtain inlet and the first restriction. In this region the vortex structure has a strong effect on the seal effectiveness, as discussed in Section 5.2.5. Shearing the curtain prevents it from maximising the pressure loss across the first restriction and reduces the leakage reduction which can be achieved over the baseline leakage flow rate. The effect of this inlet swirl on the effectiveness of the fluidic curtain seal is explored in detail in the next chapter.

5.3.3. Comparison with Previous Work

The experiment carried out by Curtis et al [**9**] showed a net leakage reduction of approximately 30 % when the inlet leakage flow was reduced to zero by using a fluid curtain. This is a similar level of leakage reduction to the seal design discussed in this chapter and occurred with swirl present at the leakage channel inlet. It is estimated in Haylock [**48**] that in the Curtis design where the rotational speed is 1100 rpm, the leakage channel sees a swirl velocity of ~110 m/s at the inlet.

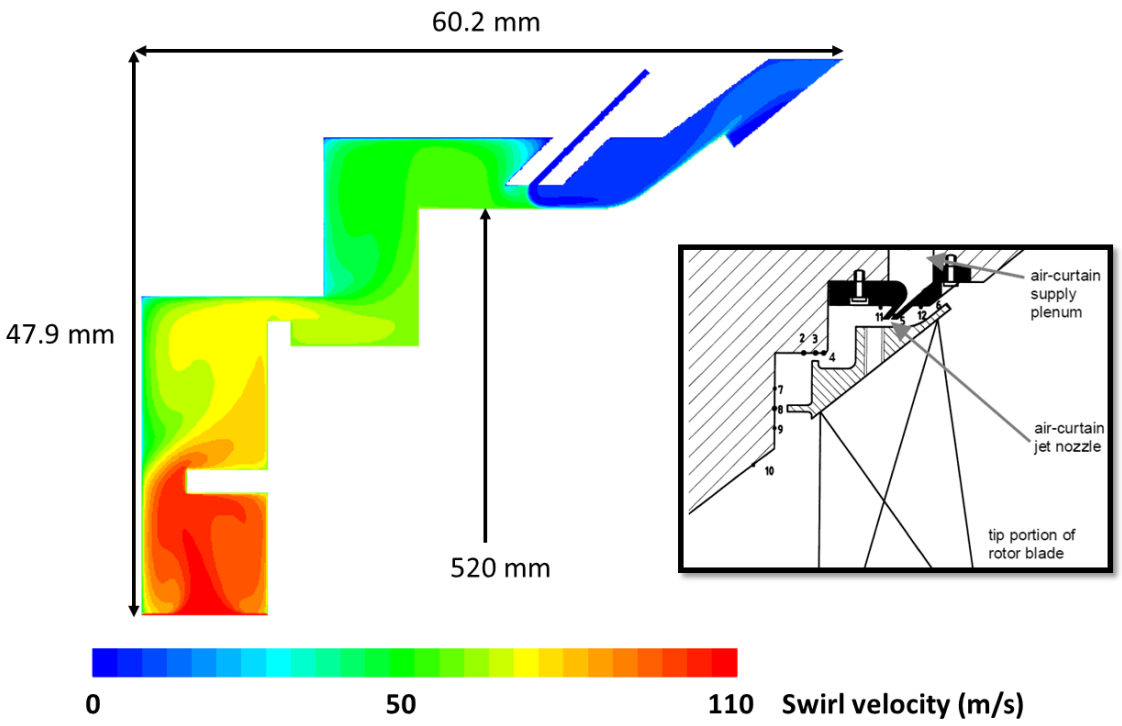

Figure 75: Swirl velocity in Curtis seal design (CFD by Dr Richard Williams, 2019)

With the seal architecture described so far, the position of the fluid curtain is close to the leakage channel inlet and so the level of swirl in the leakage flow is approximately the same as at the inlet. If this were the case in the Curtis design then a loss of effectiveness of the fluid curtain would be expected, but a leakage reduction of 30 % is still achieved compared to when the curtain is switched off. CFD studies carried out by Haylock as well as Dr Richard Williams [**49**] found that swirl decayed to ~50 m/s by the time the leakage flow reached the curtain, see Figure 75. This reduced the negative effect of swirl and ensured significant leakage reduction was still possible. The decrease in swirl velocity through the leakage channel is due to a combination of losses passing through the restrictions which the flow passes and the conservation of momentum with the increasing radius between the leakage channel inlet and the curtain.

5.4. Summary

The fundamental study on improving turbomachinery sealing performance by incorporating fluid curtains into conventional seals from Chapters 3 and 4 has been extended in this Chapter to begin to address how the technology can be applied to shrouded turbine rotor tip seal designs.

In the first part of the Chapter it has been shown that the generic seal geometry, GS1, that was used to develop the design map in Figure 33, can be modified to a new generic seal geometry, GS2, which has essentially the same performance characteristics as GS1 but which makes it more straightforward to incorporate fluid curtains into turbomachinery seals with the geometry needed to achieve significant leakage flow reduction in accordance with Figure 33.

The next section in the Chapter describes an investigation of the flow structure between the fluid curtain injection plane and the first seal restriction. This provides insights into the type of flow structure that designers should aim for in order to achieve the maximum benefit from applying a fluid curtain.

The final part of the Chapter describes a study where the aim was to take all of the new information from Chapters 3, 4 and 5 and use it to design a modification to a rotor tip seal geometry on a GE model turbine (Grace) test stage, in order to validate the performance benefit that could be achieved from applying fluid curtains. This study is the closest to product investigation in the thesis so far, including accounting for swirl in the inlet flow through the seal for the first time. It has long been established that in conventional turbomachinery labyrinth seals, swirl in the seal inlet flow has essentially no effect on the leakage performance of the seal. Swirl is often included in labyrinth seal studies that investigate its impact on rotordynamic stability, but its effect on leakage in second order at best. Indeed, well established methods for predicting the leakage flow through labyrinth seals, such as Martin's correlation [**19**] (Equation 2.2), do not include swirl for this very reason. However, the work on the Grace turbine test stage showed that for seals that incorporate a fluid curtain, if the swirl in the leakage flow approaching the curtain is high, the circumferential shear force that this exerts on the non-swirling curtain flow acts to mix and dissipate the curtain flow weakening it. This can significantly reduce the performance benefit from applying the curtain. In the case of the seal design for the Grace test, the effect was found to be so strong that it completely eliminates any performance benefit from applying the fluid curtain.

It has been demonstrated previously in tests that it is possible to achieve performance benefits from applying fluid curtains to the seals in turbine stages where there is swirling leakage flow. For example: the model turbine tests described in the paper by Curtis et.al [**9**]. The effect of swirl on the fluid curtain flow is examined further in Chapters 6 & 7, in order to develop a new design rule to allow the effect of swirl to be taken into account when incorporating fluid curtains into turbomachinery seal designs.

6. Investigation of the Effects of Swirl on Fluidic Curtain

The rotor shroud tip seal design incorporating a fluid curtain that was described in the previous chapter was intended for testing on GE's model turbine test facility, Grace. As detail was added to the simulation of the seal it was found that the swirl velocity of the fluid entering the leakage channel acts to significantly decrease the leakage blocking effect from the fluid curtain. The flow that enters any axial flow turbine tip seal will have high levels of swirl from passing through the upstream fixed blades. The effect on fluid curtain seal performance caused by swirl in the incoming leakage flow therefore needs to be investigated further.

This chapter explores the effect of swirl on fluidic curtain seal performance by using CFD to model the turbine tip seal design with a fluid curtain that was described in Section 5.3, with a range of levels of swirl applied to the leakage flow entering the seal. The inlet swirl velocities ranged from zero to the expected upstream swirl velocity at the blade tip for the turbine test stage operating at design conditions. At each inlet swirl velocity the overall leakage reduction due to the fluidic curtain was calculated. This study was carried out using testing conditions for the test stage described in the previous chapter in Table 15 using R134a as the working fluid and for conditions that are representative of a mid-stage in the expansion through a high pressure steam turbine with superheated steam as the working fluid. Finally, a non-dimensional parameter to characterise the effect of inlet swirl on fluidic curtain performance is proposed.

6.1. Setup of CFD Calculation to Investigate the Effect of Swirl on Grace Fluidic Seal Design

The tip seal incorporating a fluid curtain described in Section 5.3 includes three labyrinth fin restrictions downstream of the curtain injection. The design had the geometric ratios A = 13.4, C = 6.3, see Section 5.3.1 for definitions. As described previously the baseline seal design has been previously tested by the project sponsor, GE, on the Company's Grace two-stage model turbine test facility. See Section 5.3.1 for a full description of the baseline seal and the modified seal geometry. The seal inlet and exit flow boundary conditions were taken from a GE through-flow simulation of the test stage supplied by the Company. The baseline and modified seal designs were simulated using CFD at various levels of inlet swirl, with the modified geometry using a single curtain supply pressure for all cases. Inlet swirl was increased in increments from zero up to the representative tip seal inlet swirl velocity for the test stage. The static pressure at the inlet to the leakage channel, static pressure at exit from the seal and total pressure of the injected curtain flow, were all kept constant. Constant static pressure at seal inlet for different inlet swirl levels was achieved in the CFD simulations, by setting the total pressure of the seal

inlet flow to the desired static pressure plus the dynamic pressure due to the swirl component of the velocity at the seal inlet, in each of the calculations. The leakage reduction was calculated as the proportional change in total leakage compared to the baseline design at the same inlet conditions, that is, the same inlet swirl velocity. The simulation was first carried out using R134a as the working fluid and known model turbine test operating conditions from the Grace test turbine facility. To provide a comparison of the effect of inlet swirl between test rig conditions and high pressure steam turbine conditions, a set of simulations was also carried out using the same geometry but with superheated steam replacing the R134a test gas and boundary conditions that are representative of a high pressure steam turbine mid-expansion stage. Table 16 gives the parameters used for the CFD study. In both cases, the supply pressure for the fluidic curtain was set to the static pressure upstream of the stationary blades in the same turbine stage, see Section 5.2.1. This gave operating *PR* values of 1.75 for R134a cases and 1.40 for the superheated steam test cases. Table 16 shows the settings used in the CFD solver, these were the same as those used in the study described in Chapter 5, except for including swirl.

Table 16: Settings used in CFD study on realistic tip seal

Cell count	~450 000
Simulation type	RANS steady state, pressure based
Format	2D, axisymmetric-swirl
Viscosity model	k-epsilon realisable
Wall functions	Fluent enhanced wall treatment y+ ~ 1
Material	R134a – NIST real gas model Steam – Water vapour, ideal gas
Channel inlet boundary	Static Pressure (R134a) = 3.757 bara Total Temperature (R134a) = 36°C Static Pressure (Steam) = 92.4 bara Total Temperature (Steam) = 440°C
Channel outlet boundary	Static pressure (R134a) = 3.606 bara Static pressure (Steam) = 86.0 bar

Curtain inlet boundary	Total pressure (R134a) = 3.870 bara Total pressure (Steam) = 95 bar
Rotating wall (shroud)	Rotating wall – 1300 rpm
Solver	Ansys Fluent version 15.0

Table 17 and Table 18 show the set of swirl velocities which were used in this CFD study. Each swirl velocity represents one data point comparing baseline leakage with modified seal leakage at that level of inlet swirl. The columns in the tables show the swirl velocity, the swirl component of dynamic pressure at that inlet swirl level and the inlet total pressure this gives when the swirl dynamic pressure component is added to the inlet flow static pressure from Table 16. The axial and radial components of the inlet velocity were negligible compared to swirl velocity.

Table 17: Levels of inlet swirl simulated using R134a as the working fluid

Swirl Velocity (m/s)	Swirl Dynamic Pressure (bara)	Total Pressure (bara)
0	0.000	3.757
7	0.039	3.761
15	0.181	3.775
20	0.322	3.789
25	0.503	3.807
30	0.725	3.829
40	1.289	3.886

Table 18: Levels of inlet swirl simulated using high pressure steam as the working fluid

Swirl Velocity (m/s)	Swirl Dynamic Pressure (bara)	Total Pressure (bara)
0	0.000	92.400
20	0.056	92.456
50	0.350	92.750
70	0.686	93.086
90	1.134	93.534
120	2.016	94.416
200	5.600	98.000

The study was carried out for each geometry and working fluid. First, each case was solved with zero swirl velocity by specifying the inlet flow to be normal to the inlet plane. Second, this solution was used as a starting point for the lowest level of inlet swirl. The total pressure setting at the inlet was increased and the direction vector for flow across this plane was set with an axial component of zero, a radial component (i.e. normal to the inlet plane) of 1, and a trial

value used for an initial guessed tangential direction vector component. A converged solution was obtained with the guessed flow direction vector. The predicted static pressure and swirl velocity of the seal inlet flow were then compared with the static pressure predicted by GE's test stage throughflow calculation and the target inlet swirl velocity. These values were used to adjust the tangential component of the velocity direction vector in order to obtain a new solution closer to the throughflow calculation static pressure and the target swirl velocity at the seal inlet plane. This process was continued until a solution was found where the mass weighted average total and static pressure and swirl velocity simultaneously matched the desired values to within 0.005 bar and 2 m/s respectively for R134a cases and within 0.3 bar and 5 m/s for steam cases. This process was repeated for each of the swirl levels in Table 17 &

Table **18**, for the baseline and fluid curtain geometries and for the two different working fluids, giving four sets of solutions. Each set of baseline solutions was then compared with its corresponding set of fluidic seal solutions to show the change in leakage reduction as inlet swirl increases for both the model test conditions and for the representative HP steam turbine conditions.

6.2.CFD results

Increasing the level of inlet swirl resulted in a small increase in the leakage mass flow rate through the seal for the baseline cases. This is caused by the radius increase from the seal inlet plane to the radius of the clearance under the first labyrinth restriction (see Figure 70). Conservation of swirl momentum results in a lower swirl velocity at the first restriction compared to the swirl at the inlet plane. This results in some of the inlet swirl dynamic pressure being recovered increasing the static pressure immediately upstream of the first restriction (and hence the pressure drop driving the leakage through the labyrinth restrictions) when swirl is present, compared to the no-swirl case.

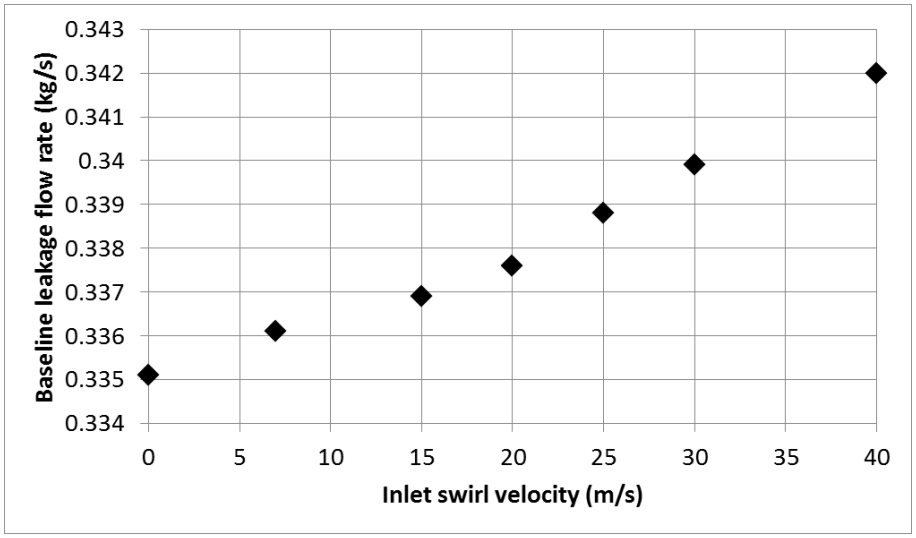

Figure 76: Baseline leakage flow rate vs inlet swirl (R134a)

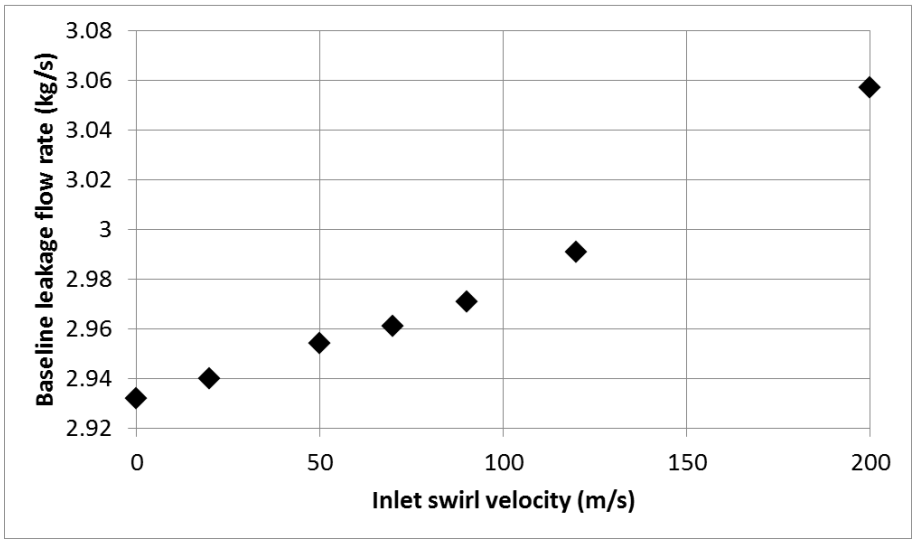

Figure 77: Baseline leakage flow rate vs inlet swirl (High pressure steam)

Figure 76 and Figure 77 show the increase in baseline leakage flow as swirl velocity increases. In the case of R134a at 40 m/s swirl the flow rate is 0.342 kg/s i.e. 2.1 % higher than the no-swirl case. For the high pressure turbine superheated steam cases, the maximum swirl condition gave an increase in leakage of 4.2 % over the no-swirl case. These small percentage increases in leakage flow rate as swirl increases can be accounted for by considering angular momentum conservation. The leakage flow enters the leakage channel across the inlet plane at a radius of 306 mm (see Figure 76). The radius of the first labyrinth restriction is 312.5 mm at mid clearance height.

$$\tau_{r\theta} = \dot{m}\,\omega\,r^2 \qquad (6.1)$$

$$\dot{m}_1\,\omega_1\,{r_1}^2 = \dot{m}_2\,\omega_2\,{r_2}^2$$

Where:
$\tau_{r\theta}$ = Angular momentum flux in the radial direction (kg.m^2/s^2)
$\dot{m}$ = Mass flow rate (kg/s)
ω = Rotational speed (rad/s)
r = Radius (m)

Consider the R134a case at 40 m/s inlet swirl. Using Equation 6.1, since mass flow rate is the same at both positions it can be shown that the swirl velocity decreases by a factor 0.979 due to the described change in radial position. Since dynamic pressure is proportional to the square of velocity and here the inlet swirl velocity is much greater than the axial or radial velocities, this gives a drop in dynamic pressure by a factor 0.959. Calculating a new dynamic pressure and assuming no loss in total pressure gives a new static pressure upstream of the first restriction of 3.761 bara. This is within 0.001 bara of the mass weighted static pressure in the CFD result at that location. Applying the adjusted Martin equation shows that with the same outlet pressure, an inlet pressure of 3.761 bara increases leakage flow by 1.6 % compared to an inlet pressure of 3.757 bara. This quick estimate of the effect is close to the 2.1 % increase in leakage flow seen in the CFD solution. For the steam case at maximum swirl, the same calculation predicts an increase in flow rate of 5.9 %, close to the 4.2 % increase which was observed at 200 m/s swirl. The agreement of these calculations with observed CFD results confirms that the angular momentum effect causes the increase in baseline leakage flow as swirl velocity increases.

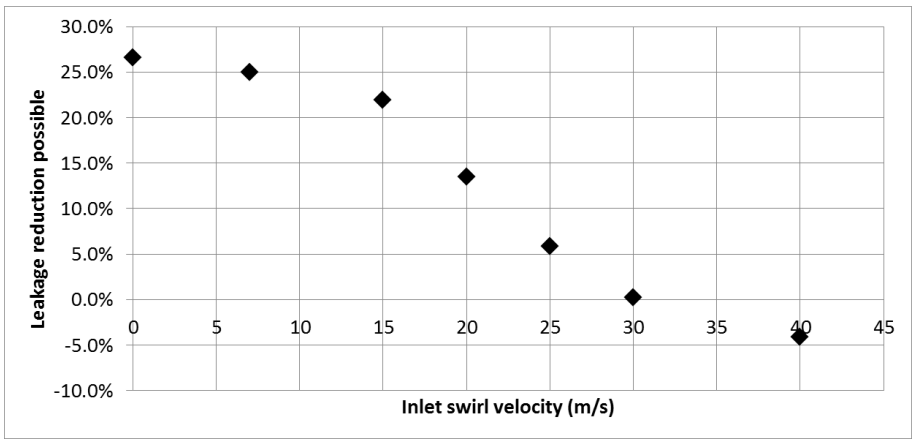

Figure 78: Maximum leakage reduction vs inlet swirl (R134a)

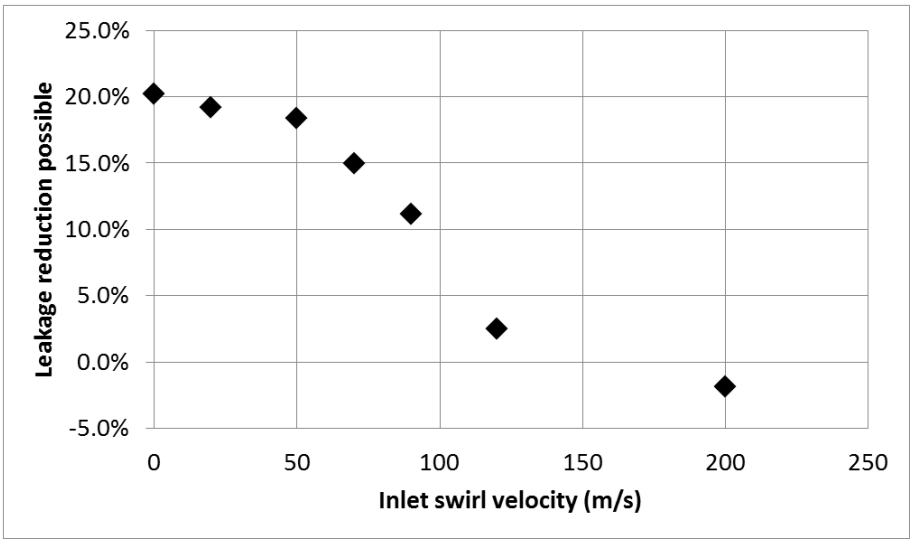

Figure 79: Maximum leakage reduction vs inlet swirl (high pressure steam)

Using the performance map in Figure 33, and the geometric ratios *A* = 13.4, *C* = 6.3 the leakage reduction at zero inlet swirl was expected to be 25 % for an optimum curtain supply pressure ratio of *PR* = 2.5. This is close to the leakage reduction seen in the R134a results shown In Figure 78 for the zero swirl case. As noted in Section 6.1, the results in Figure 78 are for *PR* = 1.75, as this is the maximum value of *PR* that can be achieved using fluid extracted from the inlet of the test stage. The results for the test stage with superheated steam in Figure 79 show a lower leakage reduction of 20 % for the fluid curtain seal in comparison to the baseline. For the steam cases, the operating PR using stage inlet steam was lower at *PR* = 1.4, which explains the reduced leakage reduction for no swirl compared to the R134a results.

Despite the very different absolute swirl levels at design conditions at inlet to the tip seal in the R134a (40 m/s) and superheated steam (200 m/s) simulations, Figure 78 and Figure 79 show similar trends for both working fluids as inlet swirl is increased. In both cases, a significant reduction in leakage flow for the fluid curtain seal compared to the baseline labyrinth design is maintained for inlet swirls of up to about 25 % of the stage design values. After this, the performance benefit from applying the fluid curtain drops off rapidly, essentially reducing to zero benefit when the inlet swirl is increased to approximately 75 % of the stage design condition. Between 75 % and 100 % of the design condition seal inlet swirl, the fluid curtain seal has a poorer performance than the baseline design. At the high swirl levels in the seal inlet flow, the fluid curtain no longer has a positive impact on the performance of the seal and instead, the presence of the curtain flow simply adds to the total leakage flow through the seal. The flow physics behind these observations are explored in the next section.

6.3.Characterisation of the Effect of Swirl on Grace Fluidic Seal Design

The results from the study show that as the swirl velocity at the leakage channel inlet increases, the leakage reduction provided by a fluidic seal decreases. For both R134a at scale test conditions and steam at high pressure steam turbine conditions, the leakage reduction compared to the baseline seal design was reduced to below zero percent (leakage flow increased) when the stage design tip seal inlet swirl level was applied. The mechanism by which swirl causes a loss in performance of the fluidic curtain seal is investigated in this section by examining the flow structure around the fluidic curtain and first labyrinth restriction. A new dimensionless design parameter is then proposed to characterise this effect.

6.3.1. Effect of Swirl on Fluid Curtain

In Chapter 5 it was shown that the leakage reduction performance of a fluidic curtain is highly dependent on the flow structure between the fluidic curtain and downstream labyrinth restriction. This flow structure consists of a pair of vortices, which are produced as the fluidic curtain flow splits when it impinges on the upstream face of the first labyrinth fin. To maximise leakage reduction the radius of the vortex closest to the labyrinth restriction must be minimised relative to the vortex closest to the curtain inlet. The effect of this flow structure on performance and the reduction in performance due to swirl suggests that the presence of high swirl changes this flow structure in such a way that sealing capability is lost. Figure 80 and Figure 81 show total pressure and static pressure contours respectively, illustrating how this flow structure changes for the R134a cases between zero swirl, medium swirl (20 m/s), and stage design seal inlet swirl (40 m/s).

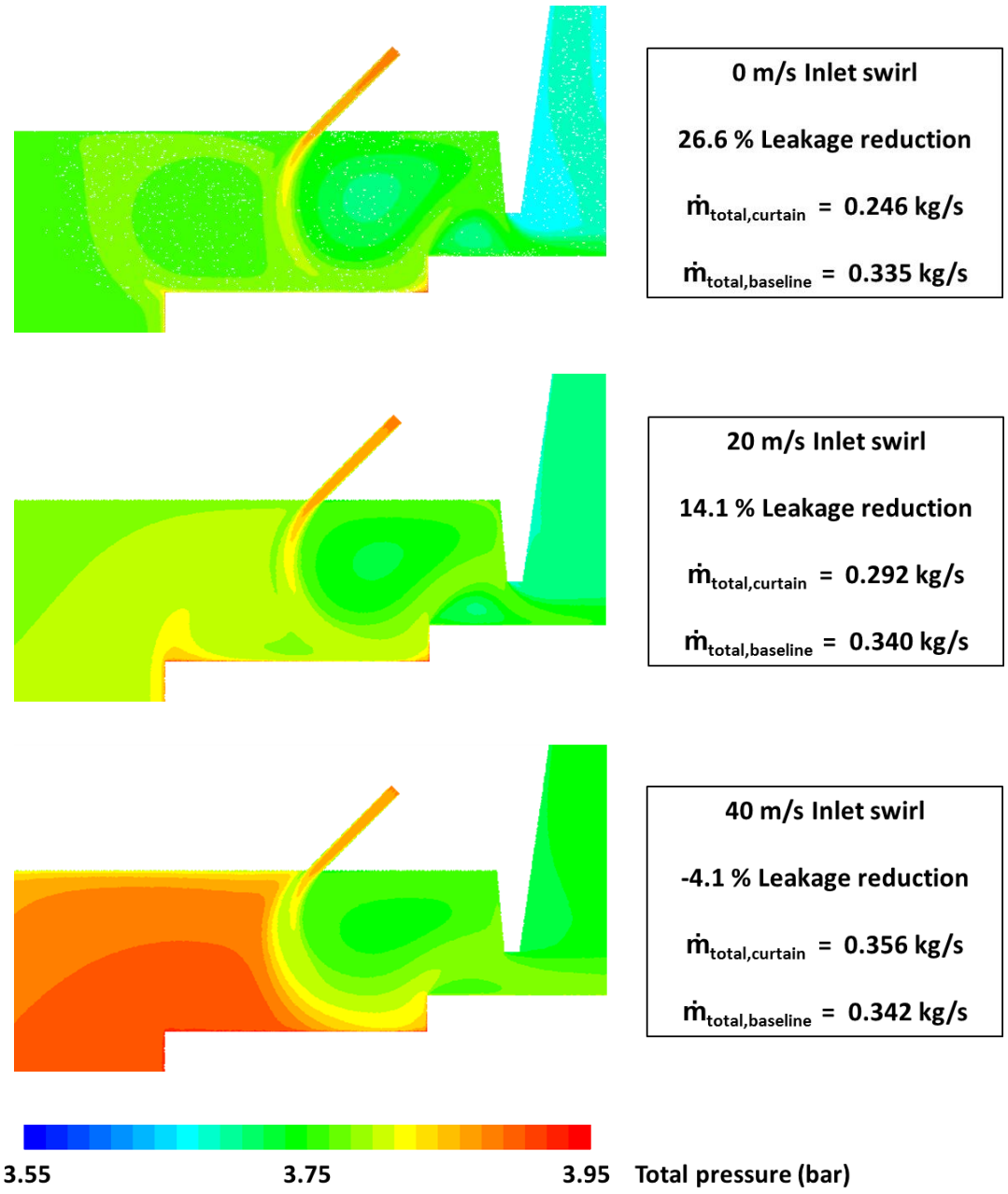

Figure 80: Total pressure contours on fluidic curtain for low, medium, and high swirl (R134a)

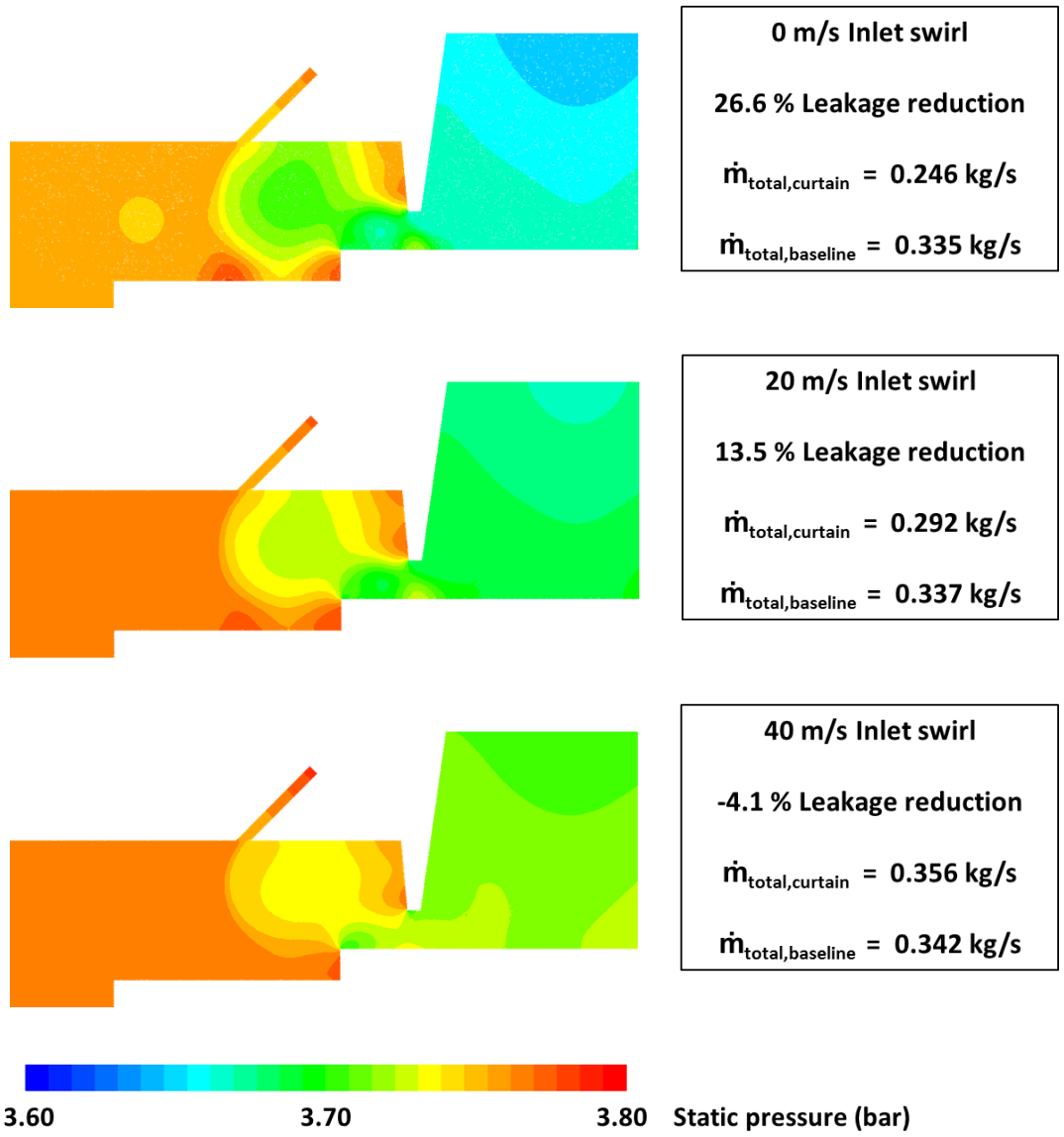

Figure 81: Static pressure contours on fluidic curtain for low, medium, and high swirl (R134a)

The fluid curtain is clearly visible in the pressure plots. Where swirl is zero, the width of the fluidic curtain remains approximately equal to the thickness of the inlet slot as it crosses the leakage channel. As swirl velocity increases the curtain becomes more diffuse and widens as it crosses the channel. After the curtain has impinged on the rotor shroud surface, it is deflected by the step in the shroud; the more diffuse curtain flow does not travel as far radially outward before it impinges on the labyrinth fin closer to the fin tip. Impinging closer to the fin tip means the flow does not need to turn as tightly to pass through the restriction, thereby increasing the effective clearance of the labyrinth restriction and causing more kinetic energy carry over through it. This effect is visible in the contours in Figure 80 which show the increase in the size of the vena contracta of the first labyrinth restriction as the inlet swirl is increased. Both the

increase in effective clearance and the kinetic energy carry over contribute to the reduced curtain seal performance when swirl is added to the seal inlet flow.

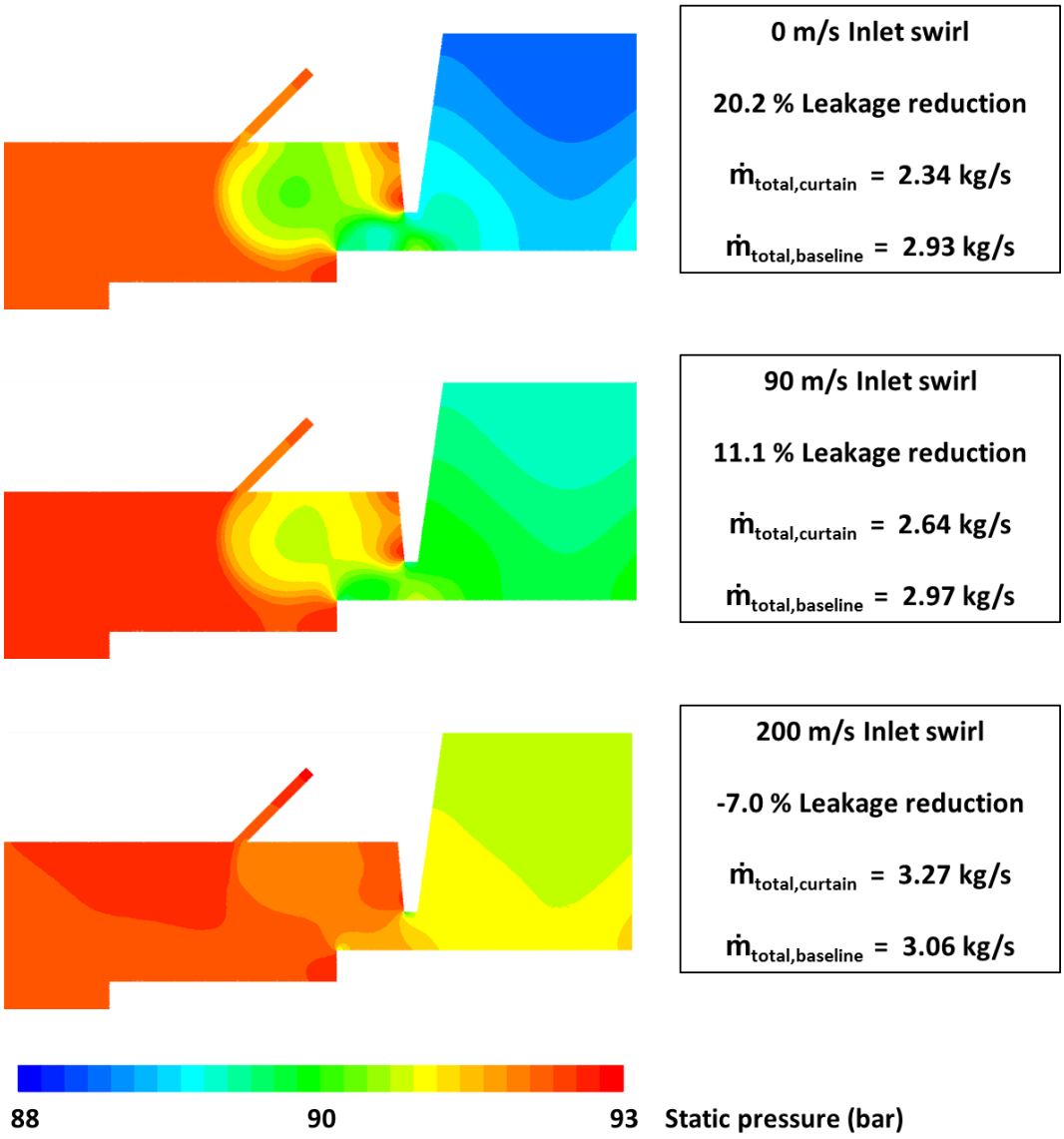

Figure 82: Static pressure contours on fluidic curtain for low, medium, and high swirl (high pressure steam)

Figure 82 shows the comparison of flow structures with increasing swirl levels for the superheated steam cases, using static pressure contours. The absolute swirl velocities are much higher that they are for the R134a cases, but so are the mass and momentum flow rates with superheated steam. So, the greater swirl shear acting across the fluid curtain with superheated steam is mitigated by the higher momentum flus of the curtain flow. So, it is still possible to achieve an 11 % performance improvement for the fluid curtain seal over the baseline design with 90 m/s of swirl in the seal inlet flow, whereas in the R134a cases, the performance benefit from the fluid curtain was completely destroyed at swirl levels higher than one third of this

value (as shown previously in Figure 78 & Figure 79). In the highest swirl case of 200 m/s shown in Figure 89, the shear resulting from the swirling inlet flow has made the curtain flow become so diffuse that it no longer crosses the leakage channel fully and misses the step. This results in an even greater increase in the leakage flow rate over the baseline seal design for design swirl conditions in the superheated steam case (7.0 % increase in leakage), compared to R134a (4.1 % increase in leakage).

6.3.2. Non-Dimensionalising Shear Incident on Fluidic Curtain

The primary effect of inlet swirl is to diffuse the fluid curtain through shear. The shear force arises due to the difference in tangential velocity where the leakage flow meets the curtain. This effect will be maximised at the optimum *PR* for the fluid curtain seal. Under these conditions, the seal inlet flow is reduced to zero and only the curtain flow passes through the downstream labyrinth seal and forms the seal exit flow. If the curtain flow is injected without swirl (as is the case for all of the fluid curtains considered in this thesis), at optimum *PR* there will be essentially zero swirl acting on the downstream side of the fluid curtain and the full swirl in the seal inlet flow acting on the upstream curtain face. The shear force exerted across the fluid curtain caused by the inlet swirl will be maximised for the seal at these inlet and exit conditions and the action of this shear force in diffusing the fluid curtain flow will be greatest.

The results described in Section 6.3.1. show that both the swirl shear force acting on the curtain flow and the linear momentum of the curtain flow have an important influence on the ability of the curtain flow to withstand the effect of the shear caused by the inlet swirl. By non-dimensionalising this shear force it may be possible to compare the effect of swirl between seals with different working fluids, mass flow rates, and swirl velocities. A new parameter *F* is proposed to characterise this as defined by Equation 6.2. The parameter *F* is the ratio of shear force acting on the upstream side of the fluid curtain flow to the momentum flux of the curtain inlet flow. The equation assumes that the curtain velocity is uniform, swirl distribution is uniform, and that the frontal area of the curtain is equal to the annular area of the leakage channel. For the seal geometries which have been researched in this body of work these assumptions are reasonable. However, if for instance the curtain width is a large proportion of the leakage channel height or the inlet swirl velocity is non-uniform then *F* will give a less meaningful impression of the shear force acting on the curtain. The equation should only be used to compare shear forces for a given geometry under different flow conditions.

$$F = \frac{\mu \cdot W_{upstream} \cdot A}{\dot{m}_{curtain} \cdot u_{curtain} \cdot t} \quad (6.2)$$

Where:

μ *= Dynamic viscosity (kg/m.s)*

$W_{upstream}$ *= Swirl velocity immediately upstream of curtain (m/s)*

A *= Annular area of fluidic curtain, i.e. annular area of leakage channel (m²)*

$\dot{m}_{curtain}$ *= Curtain mass flow rate (kg/s)*

$u_{curtain}$ *= Velocity in core of curtain half way across leakage channel (m/s)*

t *= Curtain thickness (m)*

New plots were created showing leakage reduction using parameter *F* on the horizontal axes. Each of the data points from the new CFD study were placed on these plots to produce similar plots to those in Figure 78 and Figure 79. All data points are applicable to the same geometry (modified 3 fin tip seal where *A* = 13.4, *C* = 6.3) where the leakage reduction is calculated at a *PR* close to the optimum *PR*.

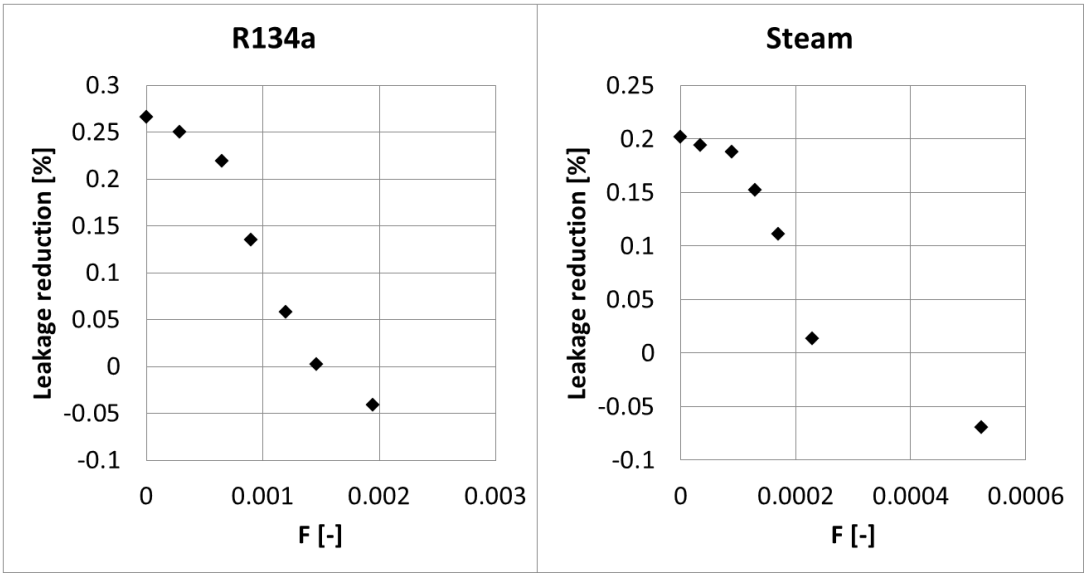

Figure 83: Plot showing expected leakage reduction varying with parameter *F*

A given leakage reduction is not unique to a particular value of *F*. That is to say a new geometry or operating *PR* would require a revised set of data points to be calculated to show the variation in leakage reduction as *F* changes. One of the recommendations for future work discussed in Section 8.4 is to find an expression using *F* and other parameters which might allow a unique value of leakage reduction to be calculated analytically. This would allow the above graphs to be plotted without the need for CFD.

6.4.Conclusions

The previous chapter demonstrated that swirl in the seal inlet flow has a negative impact on the performance of a fluidic curtain seals. This chapter has investigated this effect by examining sealing behaviour over a range of inlet swirl conditions using CFD. The study was carried out using the GE Grace model turbine test stage described in Section 5. Model turbine conditions were simulated using R134a as the working fluid as well as superheated steam turbine conditions that are representative of conditions mid-way through the expansion in a typical steam turbine high pressure cylinder. In both cases, it has been demonstrated that the stage design levels of swirl in the seal inlet flow, prevents the fluidic curtain from improving the sealing performance over the baseline seal. This is caused by the shearing effect of the swirl, which diffuses the curtain flow and prevents it from forming the characteristic flow structure shown in previous chapters to be responsible for effective leakage reduction. A new design parameter, *F*, has been defined as a means of characterising the influence of swirl on the curtain flow structure. In the existing literature, this is the first investigation into the effect of swirl on the behaviour of a fluidic curtain seals. It has been seen that this effect is important and must be taken into consideration if fluidic curtain seals are to be reliably designed for seal applications in turbomachines.

7. Experimental validation of findings on the effect of swirl

It has been found in previous chapters that swirl velocity in the inlet to the leakage channel reduces fluidic curtain seal performance by shearing the curtain and reducing its ability to induce a drop in pressure. The relationship between level of inlet swirl and loss of fluidic curtain performance was examined in the previous chapter using CFD and a new parameter, *F*, was created as a non-dimensional measure of the shearing force on the fluid curtain. A better understanding of how seal performance varies as a function of inlet swirl velocity and of parameter *F* will be important in the design of fluidic curtain seals intended for use in applications where swirl velocity is high. This chapter describes an experiment to validate the effect and explore further the impact of shear from inlet swirl on fluid curtain performance with the aim of confirming the phenomenon observed using CFD. An existing rotating turbomachinery seal test rig was modified to test fluidic curtain designs at various mass flow rates and inlet swirl velocities. This produced test conditions with a range of swirl velocities and values of the parameter *F* in the test section.

7.1. Seal Geometric Parameters and Test Points

To validate the findings on the effect of swirl in Chapter 6, a single fluidic curtain geometry was tested at a range of values of swirl velocity and the parameter *F*. As in the experimental validation described in Chapter 4, this validation focused on the most promising region of the design space illustrated in Figure 33. That is, the value of *C* (=*b*/*c*) was to be small enough that the leakage reduction could reach 40 – 50 %. The design point was selected to have a greater operating pressure ratio than the geometries studied in the previous chapter. The performance of a fluid curtain is dependent on *PR*, see Equation 3.1. Where the overblow *PR* is low, a given change in curtain pressure produces a greater change in *PR* as a proportion of the overblow *PR* compared to where the overblow *PR* is high. This means the performance, that is the leakage reduction, of a seal geometry with a higher overblow *PR* is less sensitive to uncertainty in supply pressure measurements. For example, a seal with an inlet pressure of 2 bar, an outlet pressure of 1.8 bar, and an overblow *PR* of 2 will operate optimally with a curtain supply pressure of 2.2 bar. Since a *PR* of 1 is expected to give approximately no leakage reduction, the seal operates in the *PR* range of 1-2. A 5000 Pa error in the curtain pressure could reduce the actual *PR* to 1.75. This means the error in curtain pressure would have reduced the seal performance on the order of 25 % of its operating range. If the seal had an overblow *PR* of 6 then the same 5000 Pa error would only reduce performance by 5 % of the operating range. Since the experiment aims to capture potentially small changes in performance due to the effect of swirling inlet flow, a seal with an overblow *PR* of ~6.5 was selected. This was done to

minimise apparent changes in seal performance caused by small errors in pressure transducer measurements. The point selected for testing is indicated by the cross in Figure 84. The seal geometry had the same layout as the seal designs in Chapter 6 with new values selected for the clearance size and the fluid curtain thickness, giving a new design point on the performance map developed in Chapter 3, Figure 33. To give the desired combination of large leakage reduction and high optimum operating *PR*, the selected value of *C* was 3.12 and the value of *A* was 19.5. This was expected to give a seal which operates best at a *PR* of 6 - 7 and which would give 40 – 45 % leakage reduction with the fluid curtain switched on. The set of seal dimensions selected to give these geometric ratios are given in Table 19.

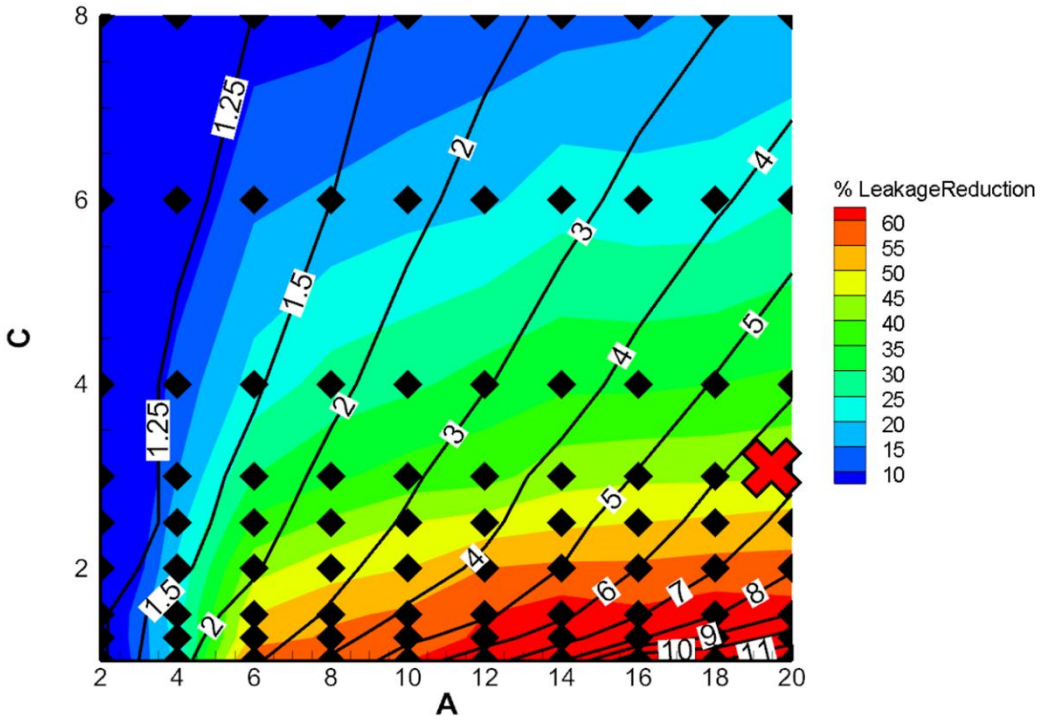

Figure 84: Response surface from Chapter 3 – The red cross indicates the set of geometries included in the experimental validation

Table 19: Summary of seal parameters

Leakage channel height	*b*	3.9 mm
Non-dimensional curtain thickness	*A*	19.5
Curtain thickness	*a (=b/A)*	0.2 mm
Non-dimensional labyrinth fin clearance	*C*	3.12
Labyrinth fin clearance	*c (=b/C)*	1.25 mm
Expected leakage reduction	40 - 45 %	
Expected optimum *PR*	6 - 7	

7.2. Seal Test Rig Modification

To test the impact of swirl, the fluidic curtain design described in the previous section was incorporated into a turbomachinery seal test rig. *A* circumferential pre-swirl chamber was added, to generate a range of swirl velocities in the leakage channel upstream of the fluidic curtain seal. This section describes the design of the modified test rig, how upstream swirl was generated, and test instrumentation.

The existing test rig was supplied from the Durham Blowdown Facility described in Section 4.2. The test rig was developed for an earlier PhD study and is fully described in the thesis by Messenger [**39**]. It consists of a ~370 mm diameter rotor placed between inlet and outlet plenum chambers to simulate a turbomachinery leakage path (see Figure 85). Air is supplied to the inlet plenum chamber through a single inlet port connected to the Durham Blowdown Facility compressed air tank. The outlet plenum chamber vented to the atmosphere through six holes. The outer surface of the rotor had an axial length of 130 mm and formed the inner wall of the seal test section. The outer casing comprised a set of concentric rings which held the seal test section and instrumentation. The rotor was driven by an electric motor with a maximum speed of 1500 rpm. All the main components of the test rig were manufactured from structural steel.

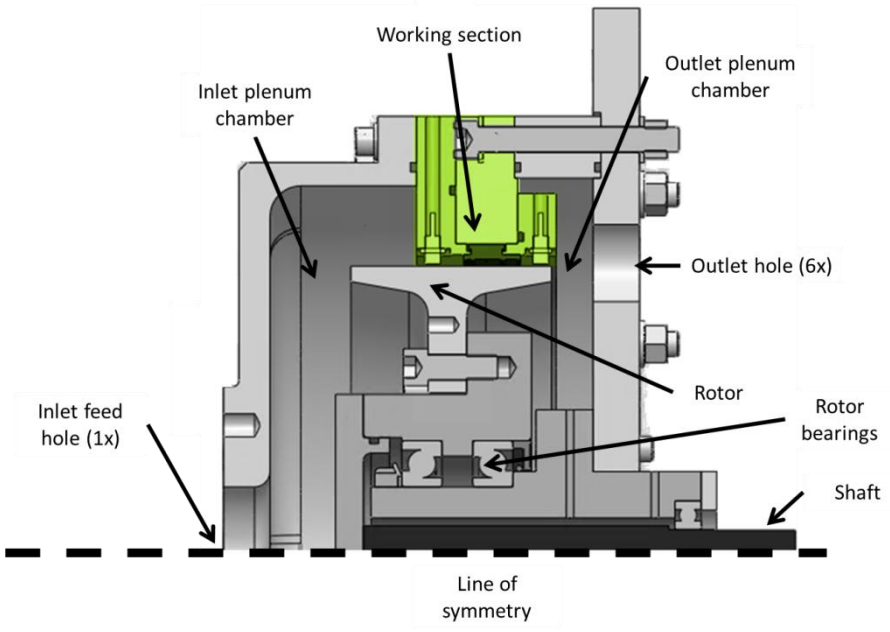

Figure 85: Cross section view of the rotating seal test rig before modification.

The rig was modified for the experiment described in this chapter by modifying the rotor, redesigning the concentric rings which formed the outer wall of the test section, and changing

the pipework and instrumentation. The three casing components, which were replaced with the new working section and upstream swirl chamber, are coloured green in Figure 85.

In total, five main modifications were made to the test rig:

1. A fluidic curtain seal was built into the test section.
2. A swirl generating inlet chamber was added to the casing. This used multiple inclined inlet jets to swirl the flow in a large circumferential chamber before it entered fluidic curtain test section.
3. The inlet pipework was divided to feed both the swirl chamber and the fluid curtain. Hand valves and orifice plates were placed in both branches to control the inlet pressure to each branch and measure each of the mass flow rates.
4. The downstream exhaust ports were combined into a single outlet pipe containing a hand valve and orifice plate to control downstream static pressure and measure the outlet mass flow rate.
5. The existing pipework to the inlet plenum chamber was disconnected from the air tank and used as a vent, to discharge air from upstream of the test section to atmosphere, on the opposite side of the swirl chamber. This additional outlet caused a higher mass flow rate to enter the swirl chamber for a given pressure difference between it and the downstream outlet. This allowed the velocity of the flow in the inclined jets to be increased to the levels needed to achieve the swirl levels within the swirl chamber that were needed for the tests (see Table 24).

The connection of the test rig to the blowdown tank and the connections to the test rig outlets are shown schematically in Figure 86. A control valve and an orifice plate were included in a bleed pipe system connected to the vent port on the front of the inlet plenum, so that the bleed flow can be controlled.

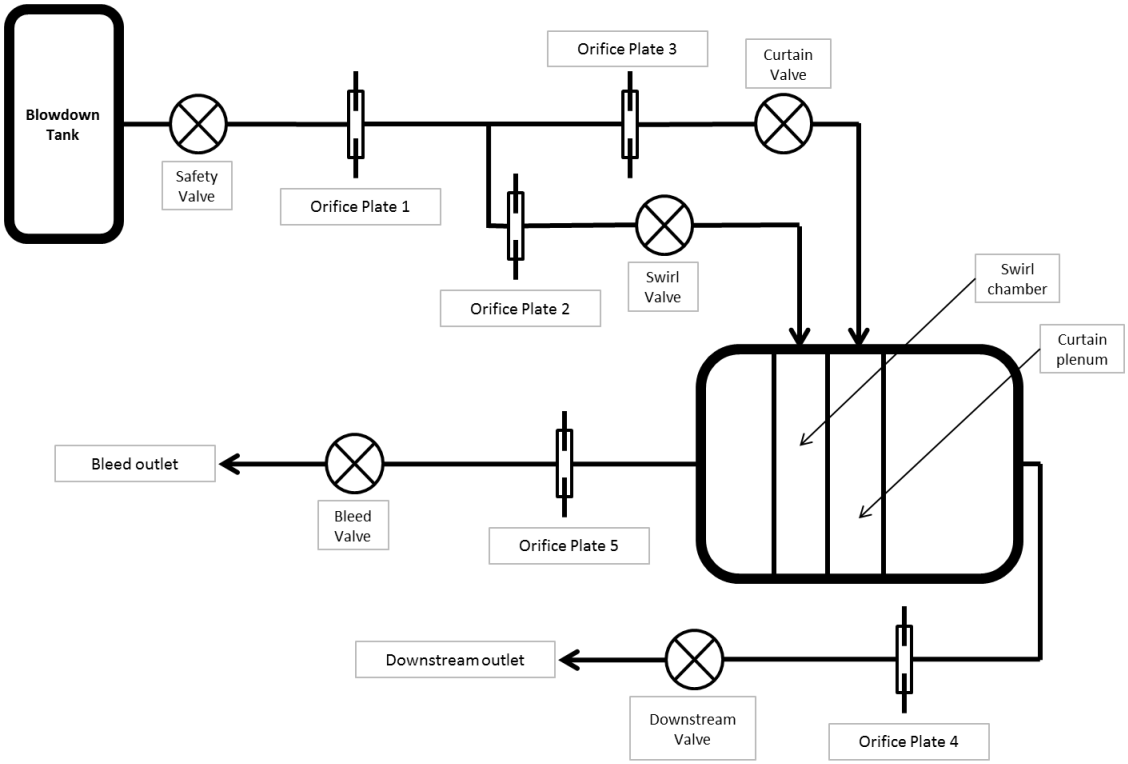

Figure 86: The rotating seal test rig schematic design

7.2.1. Fluidic Curtain Seal Design

New outer casing components were built to house the fluidic curtain plenum chamber and the curtain supply slot. A step was also machined into the rotor to create a kinetic energy blocker in the same way as in the Grace design discussed in Section 5.3.1. The seal geometry had the same generic architecture as the seal in Chapter 6 (i.e. a fluid curtain issuing through the outer wall of an axisymmetric leakage channel upstream of a single labyrinth fin restriction with a clearance to the inner wall), but with new dimensions of the curtain inlet slot and the labyrinth fin clearance as shown in Table 19. Similar to the static test rig in Chapter 4, the fluidic curtain was supplied from an internal plenum chamber within the casing. Similarly to the static rig, the fluid curtain supply slot was formed by front and rear concentric seal rings which were bolted together. These components also formed an inner curtain supply plenum chamber, as shown in Figure 87. The inner plenum chamber was connected to an outer plenum chamber by 12 radial holes, each with a diameter of 10 mm spaced circumferentially around the front seal ring.

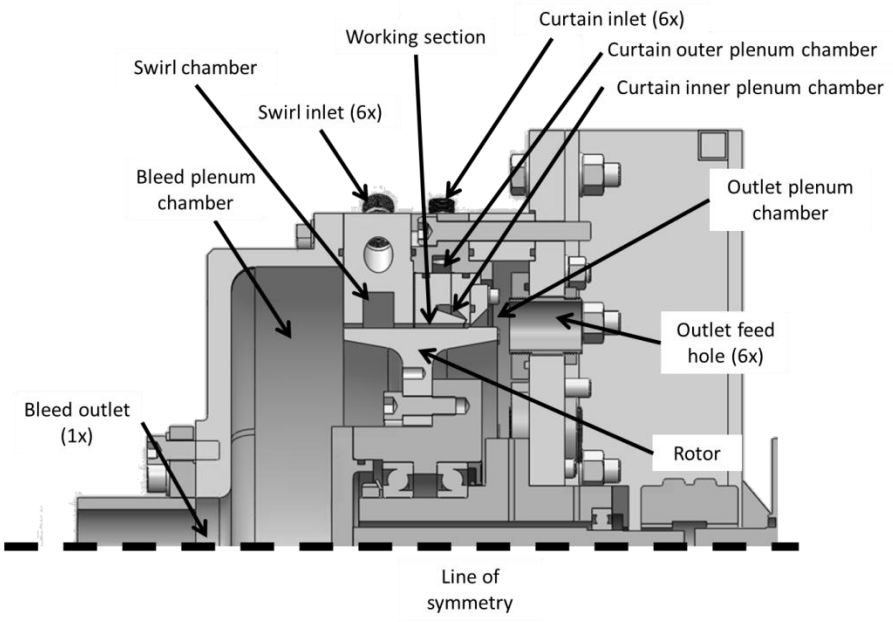

Figure 87: Section view of the modified test rig

The outer plenum chamber was fed by six 0.5 inch diameter radial holes that were equally spaced around the outer wall. The feed holes were connected by pipe fittings to six flexible hoses which were connected to the fluidic seal supply branch of the inlet pipework as shown in Figure 86. An additional ring was used to form a downstream labyrinth fin restriction by bolting it to the rear seal ring. Figure 88 shows a detailed view of the seal geometry used in the tests including key dimensions.

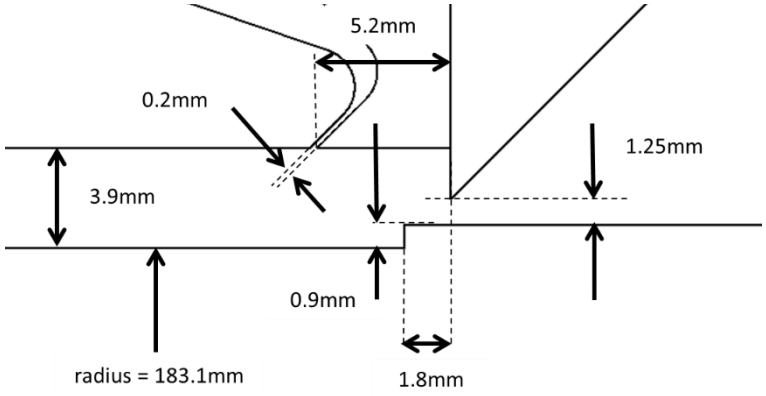

Figure 88: Fluidic curtain seal key dimensions

7.2.2. Swirl Chamber Design

The swirl chamber was formed by a ring with a deep circumferential groove in its inner circumference. On either side of the groove, the inner diameter of the swirl chamber ring was the same as the inner diameter of the front seal ring. The groove was fed by six 0.75 inch holes, inclined at 62 degrees to the swirl chamber's tangential direction at the point that the jets meet

the inner groove. The six holes were connected by flexible hoses to the swirl chamber branch of the inlet pipework (see Figure 86); in a similar manner to the fluid curtain feed holes.

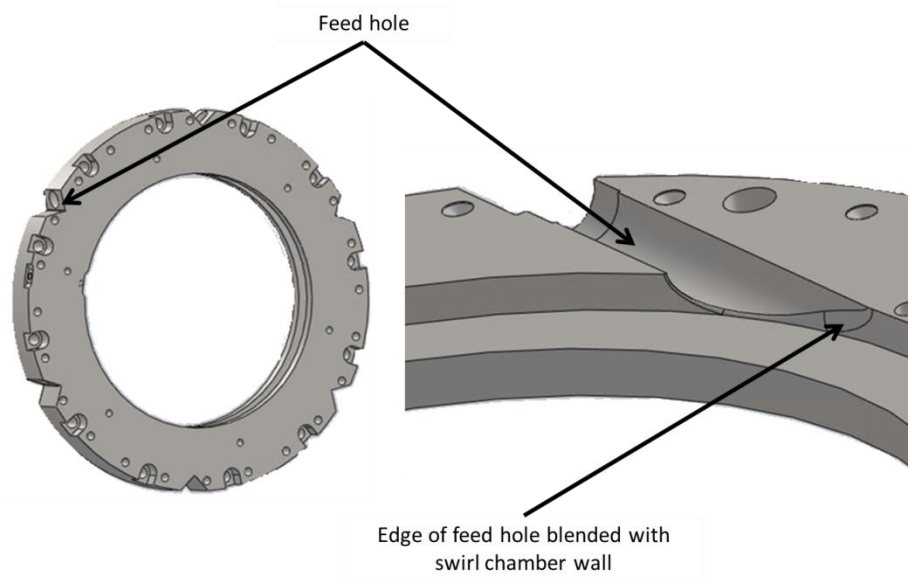

Figure 89: View of the swirl chamber – the view on the right is a mid-axial section view showing an inclined feed hole.

CFD was used to optimise the final design of the swirl chamber. The simulations were used to test the ability of the swirl chamber design to generate the range of swirl velocities needed for the tests (Table 21), by varying the mass flow rate through the bleed plenum chamber. The velocity distribution in the leakage channel at the axial location where the fluid curtain is injected was also investigated, to check its uniformity and that the swirl velocity around the annulus was essentially constant immediately upstream of the test seal.

A 3D mesh of the inside of the test rig was created for an internal flow geometry that included the interior of the swirl chamber and the leakage channel up to but not including the fluid curtain and labyrinth fin. A 60 degree periodic section which included one of the swirl chamber feed ports was used to reduce computing time (as shown in Figure 90). In the calculations, the flow entering through the swirl chamber feed port was allowed to exit either from the downstream end of the leakage channel or from the plane of the front face of the swirl chamber ring into the bleed plenum chamber (not modelled).

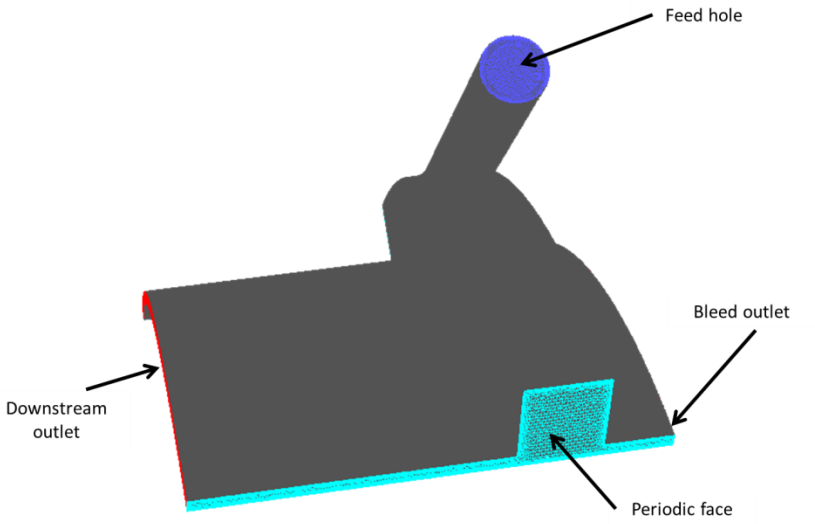

Figure 90: The CFD mesh for the optimised swirl chamber design

A total pressure of 2 bara was applied at the inlet to the swirl chamber feed ports, and the two outlets were given mass flow rates as boundary conditions. The planned inlet pressure for the tests was 2 bara (see Table 23 and Table 24) since this was high enough to give appropriate pressure ratios across the seal while avoiding additional pressure regulations for the internal volume of the test rig, that is the rig would not be pressurised to more than 250 bar litres [**50**]. The downstream outlet was set to one of the expected mass flow rates through the seal, 0.18 kg/s, while the mass flow rate through the bleed was given a range of values from zero to 0.24 kg/s. This simulated a range of possible conditions which could be created by opening the bleed valve to a range of positions in the test rig.

Table 20: Parameters used in the swirl chamber CFD study

Cell count	~5.5 million
Simulation type	RANS steady state, pressure based
Format	3D
Viscosity model	k-epsilon realisable
Wall functions	Standard wall functions y+ > 30
Working Fluid	Air – ideal gas laws
Swirl chamber inlet	Pressure inlet Total pressure = 2.0 bar Total Temperature = 15°C
Downstream outlet boundary	Mass flow outlet 0.18 kg/s
Bleed outlet boundary	Mass flow outlet 0.00-0.24 kg/s
Rotating wall (shroud)	Rotating wall – 1500 rpm
Solver	Ansys Fluent version 15.0

Designs were simulated to show their ability to generate a suitable range of swirl velocities on the downstream outlet plane as the mass flow rate through the bleed was varied. The distribution of swirl velocity in the downstream outlet plane was also important since the swirl incident on the fluid curtain should be as constant as possible around the entire annulus in order to assess the effect of swirl on seal performance.

Table 21: Results from swirl chamber CFD

	Mass flow rate (kg/s)		
Curtain swirl (m/s)	**Swirl inlet**	**Bleed**	**Downstream**
25.0	0.18	0.00	0.18
37.0	0.24	0.06	0.18
44.8	0.30	0.12	0.18
49.6	0.36	0.18	0.18
60.0	0.42	0.24	0.18

The CFD results confirmed that six 0.75 inch diameter swirl chamber feed ports would be sufficient to provide the desired swirl velocity control. It was also shown that to minimise the variation in swirl velocity the feed hole must be blended into the swirl chamber groove, as shown in Figure 89. This feature prevented the jets issuing from the feed holes from fully separating from the outer surface of the groove and therefore reduced turbulence in the swirl chamber, giving a more even swirl distribution.

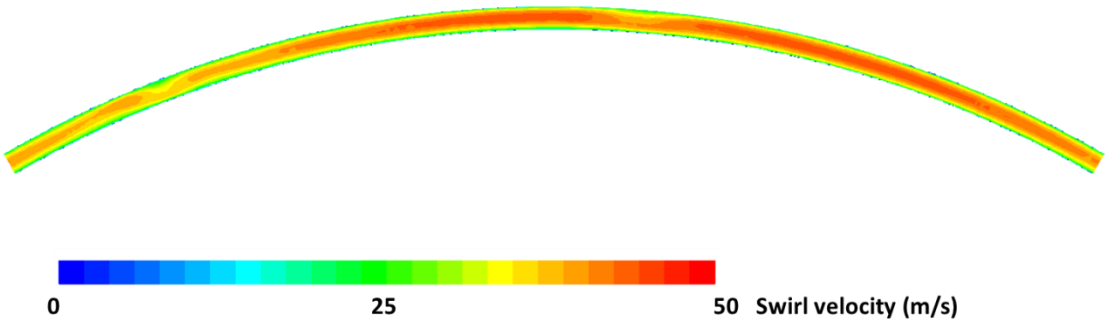

Figure 91: Contour plot showing the variation in swirl velocity at the position of the fluidic curtain – result corresponds with the second row in Table 21

7.2.3. Swirl Probe Design

To establish the impact of swirl it was important to accurately measure the characteristics of the swirl. The key to this was measuring the velocity and swirl angle at the inlet to the test section. To measure these parameters, a total pressure probe and a static pressure tapping in the downstream side of the swirl chamber was used to measure the velocity and swirl angle of the flow as it leaves the swirl chamber and enters the leakage channel, as shown in Figure 92.

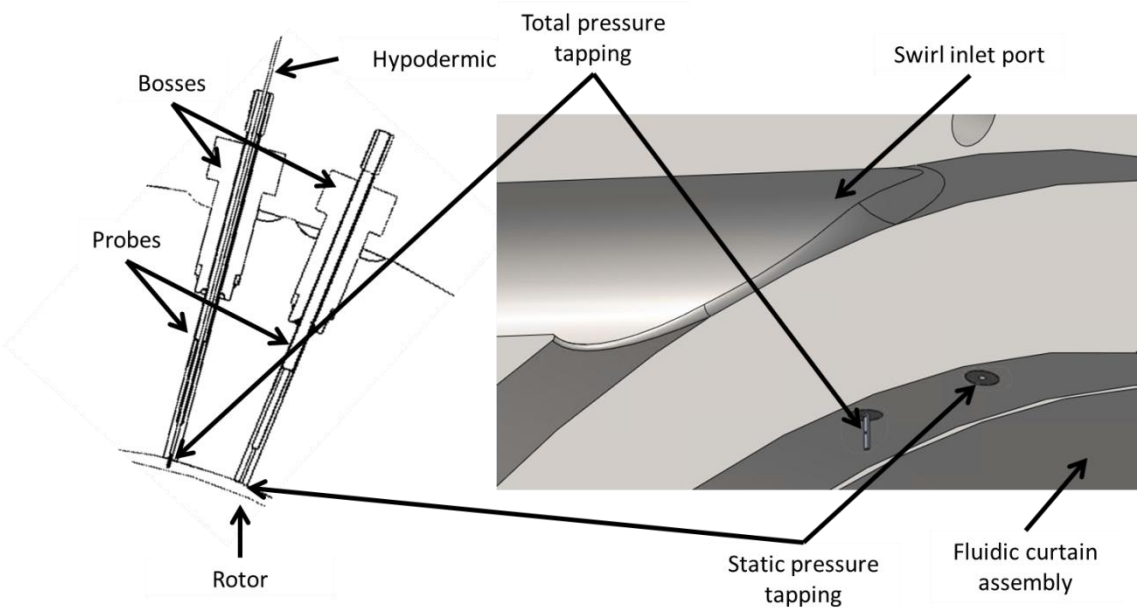

Figure 92: Section views of swirl chamber pressure measurement ports – left image shows rig-axial view of pressure probes reaching the leakage channel, right image shows a close up oblique view of pressure tappings

The CFD simulations had confirmed the change in the swirl velocity field along the leakage channel leading up to the test seal was negligible. The total pressure probe was formed from a piece of 1.1 mm diameter hypodermic tube sealed with epoxy resin at its open end and flattened on one side with a 0.2 mm hole drilled through the flat face (see Figure 93).

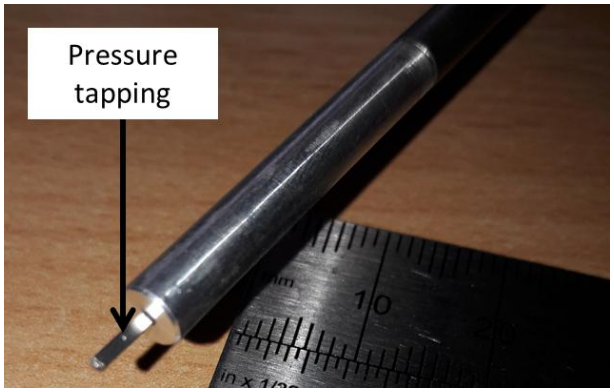

Figure 93: Tip of the swirl probe showing the total pressure tapping in the side of the hypodermic tube

The tube was secured in the tip of a 5 mm diameter probe, flexible tubing was used to connect the hypodermic tube to the pressure transducers. The 5 mm probe was mounted in a radial hole through the swirl chamber outer wall. The hole was sealed using a boss which screwed into the outer face of the swirl chamber and squeezed an o-ring against the 5 mm probe. When located, the tip of the swirl probe extended into the leakage channel on the downstream side

of the swirl chamber with the total pressure tapping located halfway between the inner and outer walls. A turntable with a stepper motor was used to rotate the swirl probe (see Figure 94). When the probe was rotated, the maximum pressure measurement (which is also the total pressure of the flow), occurs when the pressure tapping in the probe is aligned with the velocity vector of the flow as it leaves the swirl chamber and enters the leakage channel section. The total pressure was used together with the local wall static pressure measurement to calculate the magnitude of the flow velocity vector. The angle at which the total pressure was set provided swirl angle measurement. This allowed the swirl velocity to be calculated from these two measured values.

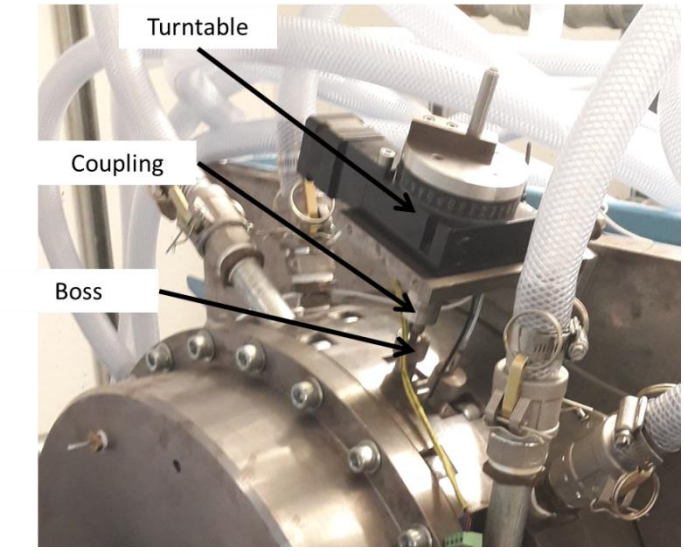

Figure 94: The swirl probe positioned in the swirl chamber ring and connected to the turntable

7.2.4. Instrumentation

Measurements of pressure and temperature were made using the same methods and instrumentation that were used in the experiments described in Chapter 4 (see Section 4.4.3). A range of pressure transducers and a Scanivalve sensor array were used to measure pressures in the plenum chambers and in the test section. Additional transducers were used to monitor and control pressures in the test rig in real time. Orifice plates were used to measure all mass flow rates at locations shown in Figure 86. Total temperature of the inlet flow was measured by the thermocouple located in the blowdown facility compressed air tank. The signals from all of the instrumentation were logged using the same data acquisition hardware and software as described for the earlier static rig tests in Chapter 4. Table 22 summarises the measurements made in the experiments and lists the details of the instrument used for each.

Table 22: Instrumentation summary

Measurement	Instrument	Range	Accuracy
Fluid curtain inner plenum chamber pressure – position 1	Scanivalve DSA3217	0 – 6.8 bar	0.05 %
Fluid curtain inner plenum chamber pressure – position 2			
Swirl chamber outlet total pressure measured by swirl probe			
Swirl chamber upstream pipework pressure			
Test section outer wall 18mm upstream of curtain – position 1			
Test section outer wall 18mm upstream of curtain – position 2			
Bleed plenum chamber pressure			
Downstream plenum chamber pressure			
Orifice plate 1 upstream pressure	SpiraxSarco EL2600	0 – 16 bar	0.05 %
Orifice plate 1 differential pressure	SensorTechnics BTE5002D1C	0 – 2 bar	0.2 %
Orifice plate 2 upstream pressure	SensorTechnics CTE8035GY0N	0 – 16 bar	0.1 %
Orifice plate 2 differential pressure	SensorTechnics BTE5010D1C	0 – 10 bar	0.2 %
Orifice plate 3 upstream pressure	SpiraxSarco EL2600	0 – 16 bar	0.05 %
Orifice plate 3 differential pressure	SensorTechnics BTE5010D1C	0 – 1 bar	0.2 %
Orifice plate 4 upstream pressure	SensorTechnics CTE8020GY1N	0 – 20 bar	0.2 %
Orifice plate 4 differential pressure	SensorTechnics BTEM50350D1C	0 – 0.35 bar	0.2 %
Orifice plate 5 upstream pressure	SensorTechnics CTE8010GY7	0 – 10 bar	0.1 %
Orifice plate 5 differential pressure	SensorTechnics BTE5001D1A	0 – 1 bar	0.2 %
Swirl chamber outlet total pressure measured by swirl probe – real time	Cynergy3 IPS-G1002-6	0 – 10 bar	0.25 %
Swirl chamber outlet static pressure – real time	SensorTechnics CTE8010GY7	0 – 10 bar	0.1 %
Fluid curtain inner plenum chamber pressure – position 1 – real time	SensorTechnics CTE8025GV7N	0 – 25 bar	0.2 %
Downstream plenum chamber pressure – real time	SpiraxSarco EL2600	0 – 16 bar	0.05 %
Tank pressure	SensorTechnics CTE8035GY0N	0 – 35 bar	0.2 %
Tank temperaure	Type – T thermocouple	−200 – 350°C	+/- 1 °C

7.3. Test Methodology

The test rig was designed to operate a fluid curtain seal with or without swirl in the leakage channel. Operating the seal without swirl was expected to give the performance predicted by Figure 33 and previously reproduced experimentally using non-swirling air. It was not possible to test with no swirl in the leakage flow if flow was supplied through the inlet ports in the swirl chamber. So, the test rig was designed to switch easily between two configurations in order to be able to carry out tests with and without swirl.

In the swirl configuration, inlet hoses were attached to the six inclined feed holes in the swirl chamber (as described in Section 7.2.2) and the bleed chamber was vented through a valve to the atmosphere via an orifice plate. To operate the test rig with no inlet swirl, the flexible hoses were disconnected from the swirl chamber and the feed holes were sealed using blank pipe connectors. The bleed plenum chamber exit pipe (see Figure 86) was removed and an inlet manifold was attached to the front face of the bleed plenum chamber over the vent hole used in the swirl configuration. Four of the six flexible hoses that supplied the swirl chamber inlet jets in the swirl configuration were then connected to the inlet manifold and used to supply air to the leakage channel. This reconfiguration of the test facility essentially changed the bleed plenum chamber into a test section inlet plenum chamber. Photographs of the test facility in these two configurations are shown in Figure 95 and Figure 96.

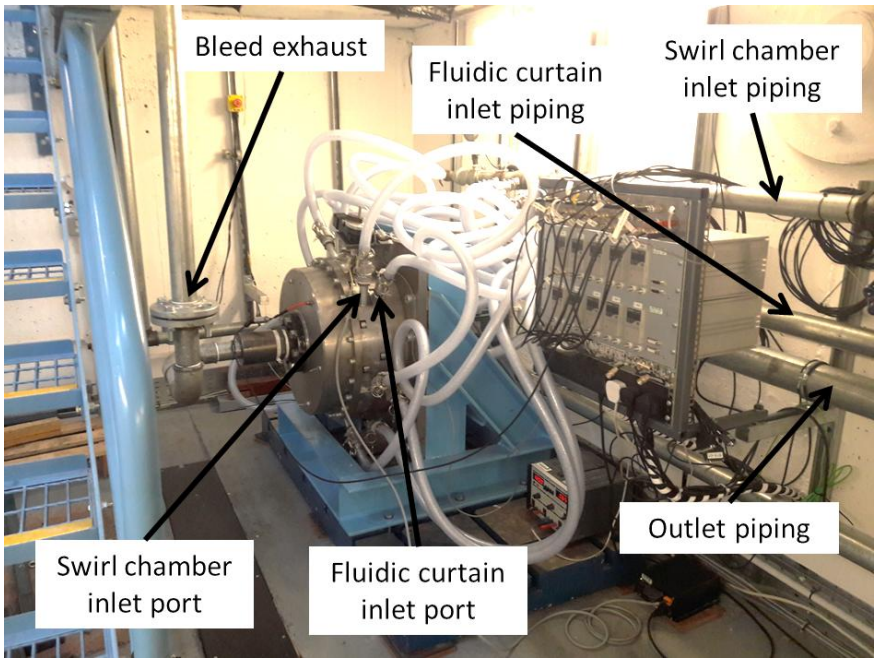

Figure 95: Test rig in swirl configuration

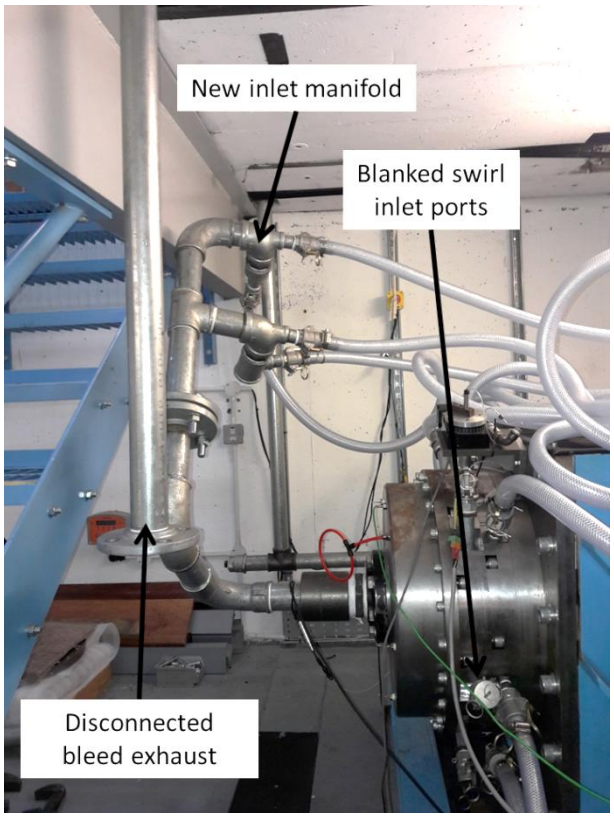

Figure 96: Test rig in no-swirl configuration

Before tests were carried out with swirl added to the seal inlet flow, validation tests were carried out to confirm that the performance of the fluid curtain seal design used in the tests was consistent with that expected according to Figure 33. All of these tests used a leakage channel inlet absolute total pressure of 2.0 bar. Tests were carried out with *PR* values up to the expected optimum *PR* = 6, which was expected to deliver a leakage reduction factor *L* = 40 % (values approximated for the test point shown in Figure 91). The test points selected are listed in Table 23. For all no-swirl tests the pressure difference between the leakage channel inlet and outlet was set to 0.2 bar, giving in an inlet to outlet pressure ratio of 1.11.

Table 23: Test points measured with zero swirl velocity

PR	$P_{0,in}$ **(bara)**	P_{out} **(bara)**	$P_{0,curtain}$ **(bara)**
0	2.00	1.80	0.00
1	2.00	1.80	2.00
2	2.00	1.80	2.20
3	2.00	1.80	2.40
4	2.00	1.80	2.60
5	2.00	1.80	2.80
6	2.00	1.80	3.00

For the tests with swirl added to the leakage channel inlet flow, test points were selected for a range of values for *F* by independently varying both the inlet flow swirl velocity and by changing the curtain flow momentum. Equation 6.2 can be amended using mass continuity to give Equation 7.1. The fluid properties and the geometry are fixed in the tests and so the momentum of the curtain flow is a function of the square of its mass flow. Therefore, it was relatively easy to change the value of *F* in the tests whilst holding the inlet swirl level constant, by changing the curtain mass flow rate.

$$F = \frac{\mu \cdot W_{upstream} \cdot A \cdot \pi \cdot d_{slot} \cdot \rho}{\dot{m}_{curtain}{}^2} \tag{7.1}$$

Where:

μ *= Dynamic viscosity (kg/m.s)*

$W_{upstream}$ *= Swirl velocity immediately upstream of curtain (m/s)*

A *= Annular area of fluidic curtain (m²)*

$\dot{m}_{curtain}$ *= Curtain mass flow rate (kg/s)*

d_{slot} *= Diameter of fluid curtain inlet slot (m)*

ρ *= Density of fluid curtain*

The approach taken to varying the curtain mass flow rate, whilst maintaining the optimum operating value of *PR*, was to simultaneously change both the curtain supply total pressure and the pressure drop along the leakage channel by controlling the static pressure of the leakage channel exit flow.

The same complication as noted earlier in Section 6.1 for the CFD study, is also encountered in the tests when swirl is added. The dynamic pressure of the axial and radial velocity components in the leakage channel upstream of the test seal are small compared to the dynamic pressure of the swirl velocity when this is added. In the absence of swirl in the inlet flow, the total and static pressure of the leakage channel inlet flow are essentially equal, because the dynamic pressure of the leakage flow is negligibly small. When swirl is added, the total pressure at the leakage channel inlet will be significantly higher than the static pressure because of the relatively large dynamic pressure from the inlet swirl. However, the presence of swirl will not affect the static pressure drop that is driving leakage flow through the seal. So, for the tests with swirl, it is the static pressure at the leakage channel that was maintained at 2.0 bara rather than the total pressure, in order to maintain a value of *PR* = 6.0 which was comparable with the no swirl tests.

In order to determine the test conditions for the 'with swirl' tests the following approach was used. The leakage channel inlet static pressure was fixed at 2.0 bara. A value of leakage channel exit pressure was selected for the test point. The supply total pressure for the curtain flow was then determined for *PR* = 6.0 using the inlet flow static pressure rather that total pressure, as discussed in the previous paragraph. Equation 2.3 was then used to estimate the leakage flow through the seal in the absence of the curtain flow. Figure 84 has shown that the seal design that has been selected for has its optimum performance at *PR* = 6.0 when the curtain flow is estimated to reduce leakage to 60 % of that without the curtain. At this condition the inlet flow will be reduced to zero and all of the flow exiting the seal comes from the curtain. 60 % of the leakage flow calculated from Equation 2.3 was therefore used to provide an estimate of the curtain mass flow at *PR* = 6.0. This estimated curtain flow was then used with a range of selected values of leakage channel inlet swirl, in order to calculate expected values for parameter *F* for the test points in Table 24. The maximum swirl velocity that could be achieved in the test facility was 45 m/s and so swirl levels of 15 m/s, 30 m/s and 45 m/s were used in the tests. This produced swirl angles ranging from ~65 degrees to ~80 degrees.

For each level of inlet swirl, the static pressure difference between the leakage channel inlet and outlet was set to four levels ranging between 0.1 bar to 0.25 bar. This gave inlet to outlet pressure ratios across the channel of between 1.05 and 1.14. This range of pressure ratios resulted in curtain mass flow rates which gave estimated values of *F* for the test in the range from 0.0006 up to 0.0018. This spans the range of values of *F* calculated from the CFD results in Chapter 6 and was therefore expected to be sufficient to demonstrate an effect on seal performance.

Table 24: Planned test points at various levels of swirl velocity and *F*

Swirl level	***PR***	$P_{stat,in}$ **(bara)**	P_{out} **(bara)**	$P_{0,curtain}$ **(bara)**	$F\ (x10^{-5})$
Low (~25m/s)	6	2.00	1.90	2.50	103
Low (~25m/s)	6	2.00	1.85	2.75	78
Low (~25m/s)	6	2.00	1.80	3.00	66
Low (~25m/s)	6	2.00	1.75	3.25	60
Medium (~30m/s)	6	2.00	1.90	2.50	126
Medium (~30m/s)	6	2.00	1.85	2.75	96
Medium (~30m/s)	6	2.00	1.80	3.00	82
Medium (~30m/s)	6	2.00	1.75	3.25	74
High (~45m/s)	6	2.00	1.90	2.50	180
High (~45m/s)	6	2.00	1.85	2.75	137
High (~45m/s)	6	2.00	1.80	3.00	117
High (~45m/s)	6	2.00	1.75	3.25	105

7.3.1. No-Swirl Conditions

Laboratory atmospheric conditions were recorded and the pressure measurement equipment was zeroed to the current atmospheric pressure. The swirl probe was turned so that the pressure tapping faced directly upstream since the flow is axial in the no-swirl case. An estimate of the required positions of the fluid curtain inlet valve and rig outlet valve were made and the valves set. The test rig was powered up and the upstream control valve was opened until the computer terminal indicated the desired upstream static pressure at the inlet to the leakage channel. Fluidic curtain inner plenum chamber pressure and downstream plenum chamber pressure were noted and the upstream control valve was closed. Based on the plenum chamber pressures, the fluid curtain inlet valve and rig outlet valve were adjusted to correct these pressures. This process was carried out iteratively until the pressures at all inlets and outlets matched the desired pressures. When all valve positions were set correctly, the rotor was spun up to maximum speed, the upstream control valve was used to set the inlet pressure, and the logging program was run to record the transducer measurements.

The results which were output for these tests were the mass flow rates over a range of values of *PR*. These were plotted in the same way as in Chapter 4 and are presented in Section 7.4. In all cases, both with and without swirl the mass flow rates are normalised by multiplying by a correction factor. The correction factor is the ratio between the leakage flow rates calculated using Equation 2.3 for the planned channel inlet and outlet pressures, and for the actual measured channel inlet and outlet pressures.

7.3.2. Swirl Conditions

Laboratory atmospheric conditions were recorded and the pressure measurement equipment was zeroed to the current atmospheric pressure. The bleed valve was set as required. An estimate of the required positions of the swirl chamber inlet valve, fluid curtain inlet valve and rig outlet valve was made and the valves set. The test rig was powered up and the upstream control valve was opened until the computer terminal indicates the desired upstream static pressure at the inlet to the leakage channel. Fluid curtain inner plenum chamber pressure and downstream plenum chamber pressure were noted and the upstream control valve was closed. Based on the noted plenum chamber pressures the swirl chamber inlet valve, fluid curtain inlet valve, and rig outlet valve were adjusted to correct these pressures. This process is carried out iteratively until the pressures at all inlets and outlets matched the desired pressures.

The entire process was carried out once with the fluid curtain switched off and once with it switched on. In each case, two logging programs are run:

1. The test section inlet static pressure is set to the required value using the upstream control valve and the swirl probe is turned through 2.5 degree steps over a 70 degree angle, logging total and static pressure at the channel inlet for each step. The rig is stopped and the flow angle and flow velocity are determined from the data collected by the swirl probe. These values are used to calculate the swirl velocity.
2. The swirl probe orientation was then set to align the probe with the swirling leakage flow which provides a measure of total pressure in the inlet to the leakage channel. The rig was restarted and the leakage channel inlet static pressure was again set using the upstream control valve while pressures at all locations in the test rig are logged.

The leakage reduction factor was then the percentage change in total mass flow rate where the fluidic curtain is on compared to when the fluidic curtain is off. The shearing force, *F*, was calculated using Equation 7.1. This calculation used the swirl velocity obtained where the curtain is switched on and the mass flow rate measured in the curtain inlet orifice plate. The density term in Equation 7.1 is calculated using the measured fluid curtain plenum chamber pressure and blowdown tank temperature. By plotting the leakage reduction factor against *F* the effect of non-dimensional shearing force can then be seen.

7.4.Results

This section presents the main findings from the experimental campaign. First, mass flow rates at each leakage channel boundary are plotted against pressure ratio as seen previously in Chapter 4 for both swirl and no-swirl conditions. Second, leakage reduction for a single pressure ratio is plotted against both swirl velocity and parameter *F*.

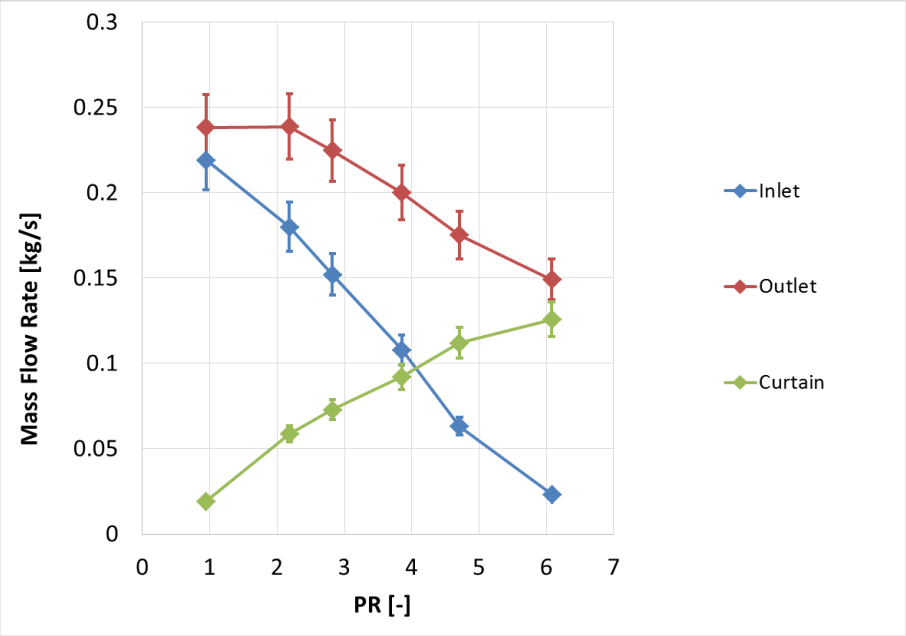

Figure 97: Mass flow rates vs *PR* for the no-swirl condition

For the no-swirl condition, the seal behaved as expected. In Figure 97, as the *PR* increased the incoming leakage flow decreased, and the total flow leaving the channel was reduced. With no fluidic curtain, no swirl, and a pressure difference of 0.2 bar across the seal, the baseline leakage flow rate was 0.23 kg/s. With a fluidic curtain operating at a *PR* of 6.1 the leakage flow at the inlet to the leakage channel was reduced by 90 % and the total leakage flow was reduced by 36 %. For the same reason as in the experiment in Chapter 4, conditions could only approach the overblown condition with the test rig set to the no-swirl configuration, but from Figure 97 the maximum leakage reduction factor at the point of overblowing the seal can be extrapolated to be ~40 % at a *PR* of 6.5. This matches well the leakage reduction factor of 40 – 45 % and *PR* of ~6.5 predicted by Figure 33. This further validates the findings in Chapter 3 with new seal geometry. As long the seal contains the main features positioned correctly relative to each other (such as the relative positions of the kinetic energy blocker, curtain slot, and labyrinth restriction) Figure 33 is a good design tool for predicting seal performance from its geometric proportions.

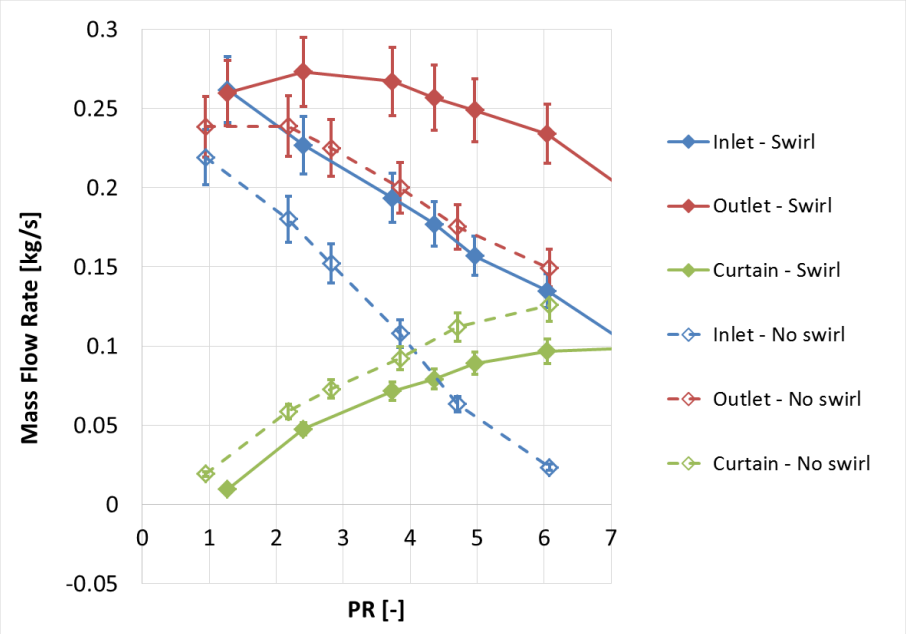

Figure 98: Mass flow rates vs *PR* with inlet swirl

With the bleed valve fully open, the inlet swirl changed the behaviour of the fluid curtain seal. Results for the three mass flow rates are plotted against *PR* in Figure 98. The inlet and outlet mass flow rates show that the fluidic curtain still reduces flow through the simulated leakage channel, but the decrease in leakage is much smaller for any given *PR* value when in the presence of swirl. For example at a *PR* of 6, the seal becomes almost overblown with no swirl, but the inlet mass flow rate only decreases by a factor of 2 when the swirl velocity is ~45 m/s. This clearly confirms the observations made in Chapter 6 are physically valid: as inlet swirl velocity is added, the leakage reducing effect of the fluidic curtain is reduced for the same *PR*.

As discussed in detail in sections 5.2.1 and 6.2, the addition of swirl velocity increases baseline leakage flow by only a small amount. The swirl dynamic pressure component is therefore neglected from the channel inlet total pressure in the calculation of seal *PR*, see Equation 5.1. In the maximum swirl cases the swirl dynamic pressure did not exceed 2 kPa. If this pressure is added to the channel inlet pressure in Table 23 where no swirl is present, then the curtain pressure would need to increase by 12 kPa to maintain a pressure ratio of 6 and keep the inlet flow close to zero. However, when the pressure is added in the form of swirl it was found experimentally that to eliminate inlet leakage flow the curtain pressure had to be increased by over 200 kPa. This corresponded to a *PR* of 17. In a turbomachinery application this would require the fluid curtain to be supplied from higher pressure fluid elsewhere in the cycle, making its overall performance benefit less clear. This confirms that the swirl affects the

function of the fluidic curtain by a mechanism which is stronger than simply raising the effective inlet pressure.

The inlet mass flow was that which entered the simulated leakage channel from the upstream swirl chamber, i.e. the swirl chamber mass flow rate minus the flow measured through the bleed. The bleed had a minimum flow area of ~2000 mm^2 and the simulated seal had a minimum flow area of ~4600 mm^2, this meant that as the flow through the seal decreased the flow through the bleed would not increase by the same amount and the rate of flow entering the swirl chamber had to decrease slightly. The swirl velocity was dependent on the mass flow rate through the swirl chamber feed ports and therefore decreased as *PR* increased for a constant bleed valve setting. This means that Figure 98 shows how performance changes while both *PR* and swirl velocity change. However over the *PR* range shown in Figure 98 the mass flow entering the swirl chamber decreased by 11 %, giving only a small drop in swirl velocity from ~50 m/s to ~45 m/s.

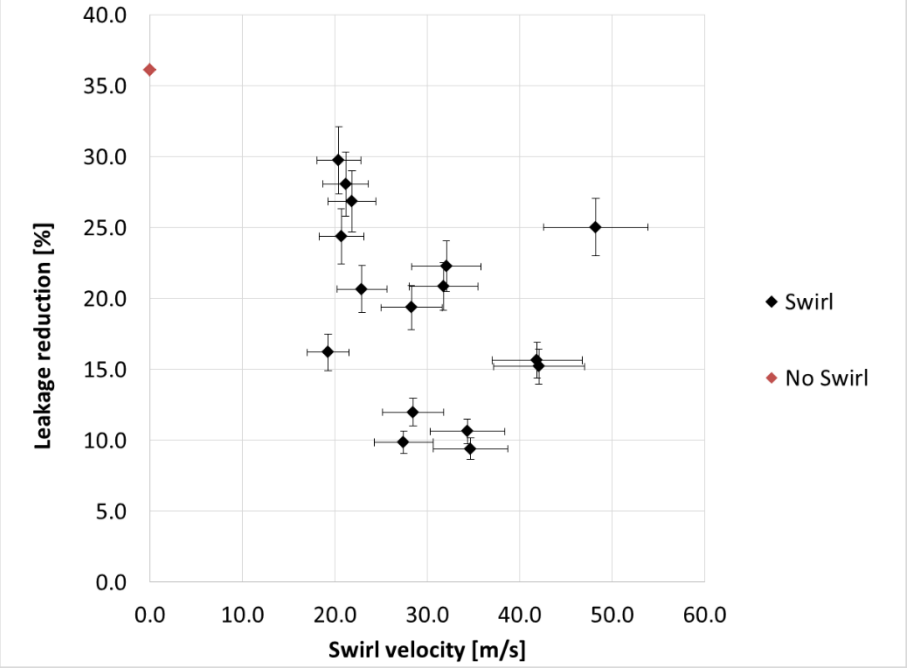

Figure 99: Experimental results for leakage reduction over the range of swirl velocity

Figure 99 shows the results taken at a *PR* of 6, see Table 24. The leakage reduction factor was obtained by comparing curtain on and curtain off cases back to back and then was plotted against swirl velocity. The range of swirl velocities and mass flow rates gave swirl angles ranging from ~70 degrees to ~80 degrees, close to the expected range. The result for the no-swirl condition is shown for comparison. These results show that the leakage reduction cannot easily

be estimated knowing only the swirl velocity for a given *PR*. Figure 100 shows that knowing the value of parameter *F* would allow a much more accurate estimation of seal performance.

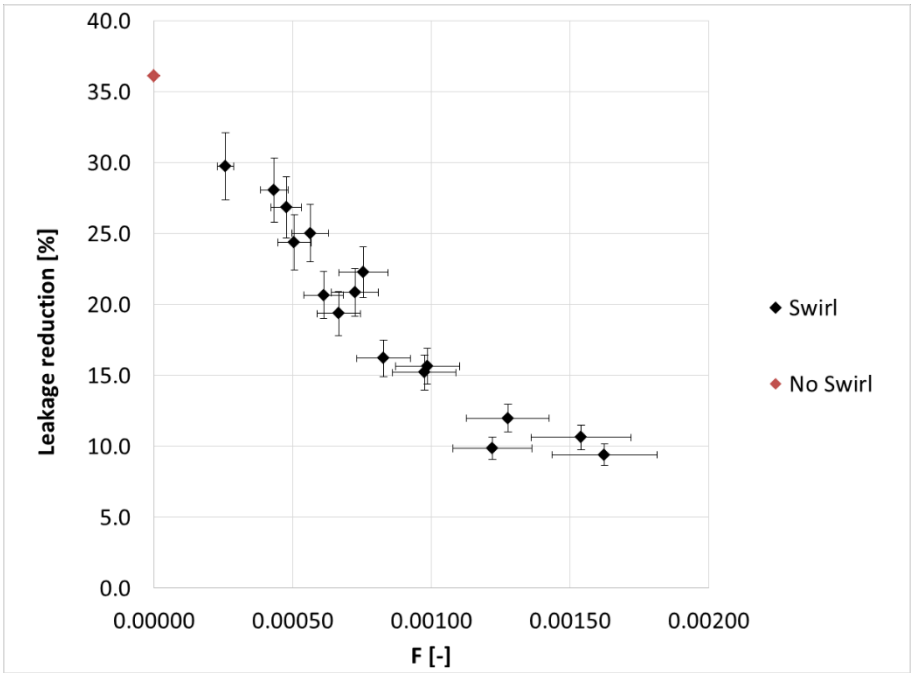

Figure 100: Experimental results for leakage reduction over the range of parameter *F*

The leakage reductions are shown again in Figure 100, this time plotted against parameter *F*. Values of *F* were generated in the test rig ranging from zero to 0.00163, spanning most of the planned range of values for *F*; zero to 0.00180.

The maximum leakage reduction occurs where *F* = 0 at zero swirl velocity. As *F* increases, the leakage reduction achievable with the same curtain *PR* decreases as expected from earlier analysis. The plot clearly shows that the no-swirl performance lies where it would be expected if a trend line were extrapolated to the vertical axis. At the maximum value of parameter *F*, the leakage reduction given by the fluid curtain drops to less than 10 %. This means the high swirl condition has reduced leakage reduction capability by more than 60 % compared to the 36 % leakage reduction for the case for zero swirl velocity.

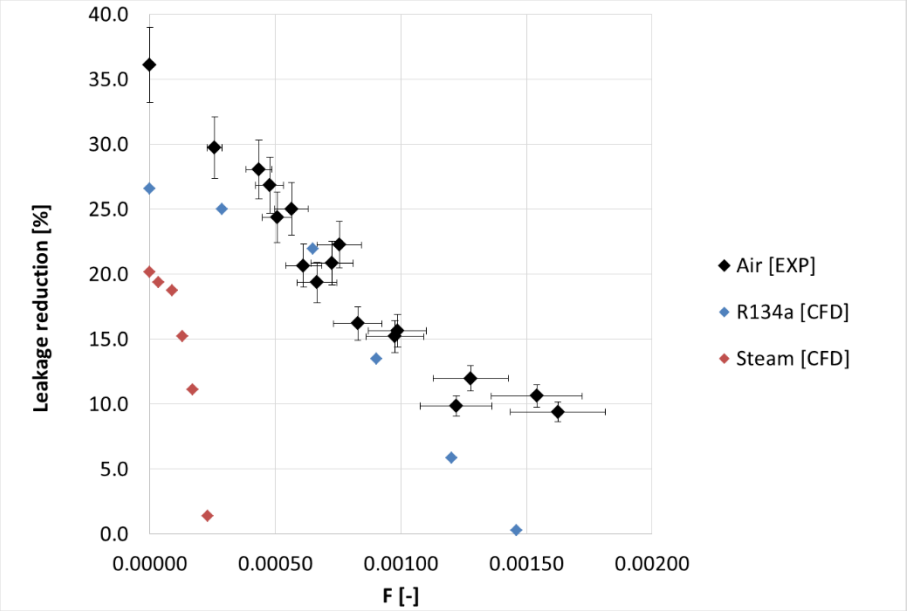

Figure 101: Comparison between experimental results and CFD results from Chapter 6

Comparing the experimental results with CFD results from the previous study on the effect of swirl showed that the effect of swirl on leakage reduction cannot be estimated by knowing only the value of *F*. Leakage reduction is plotted against *F* in Figure 101. The CFD study was carried out using a different geometry with a different operating *PR* and different working fluids were simulated. All three sets of data show similar trends and cover a similar decrease in leakage reduction over each range of *F*. However, these decreases in leakage reduction occur over different ranges of *F*. There must therefore be another factor affecting seal performance as well as *F*.

The difference between plotted experimental results for air and CFD results for R134a is smaller than the difference between these two data sets and the CFD results for high pressure steam. This suggests that the additional factor is similar in the cases of the experiment and R134a CFD, while significantly different in the case of the steam CFD.

7.5.Conclusion

The intent of the experimental campaign described in this Chapter was to validate the effect of swirl in the leakage flow on the performance of the fluid curtains, which has been observed in the CFD studies described in Chapter 6. An existing seal test rig was modified to produce various swirl velocities at the inlet to an annular leakage channel. A fluid curtain seal of the same generic design as the one investigated using CFD was built into the leakage channel. The test rig was run at a range of flow velocities and mass flow rates. The test set-up allowed both the swirl velocity of the leakage flow and the curtain and leakage channel mass flows to be

varied independently. This allowed the effect of varying both parameter *F* (Equation 6.2) and the leakage flow swirl velocity on the leakage reduction factor, *L*, to be investigated for fluid curtains operating over the same range of curtain pressure ratio values, *PR*.

The results validated the trends observed in the CFD results in Chapter 6. The results showed that as parameter *F* increases, leakage reduction factor decreases. They also show that for a given seal geometry and working fluid, there is a strong correlation between the leakage reduction factor, *L*, and the parameter *F* and not the absolute value of the inlet swirl velocity. This strongly suggests that the reduction in sealing capability due to inlet swirl is a direct result of the shearing forces in the mixing layer between the incoming leakage flow and the fluid curtain flow.

The trend of decreasing leakage reduction factor, *L*, as the value of parameter *F* increases, was similar to the results seen in Chapter 6 in terms of the characteristic shape of the trend. But, the curves do not collapse onto a single characteristic. The experimental results showed the leakage reduction drop from ~36 % to ~10 % between *F* = 0 and *F* = 0.00163 at *PR* ~6.5. This compares with the CFD results in Chapter 6 where the R134a case showed a decrease from ~27 % to ~0 % between *F* = 0 and *F* = 0.00180 at *PR* ~2.5 and for the superheated steam case, *L* decrease to ~0 % over roughly half of this range of values of *F* . The seal design in the experiment had a geometry where *A* = 19.5 and *C* = 3.12, whereas the seal modelled in the CFD study in Chapter 6 had a geometry where *A* = 13.4 and *C* = 6.3. The results show that the leakage reduction factor, *L*, is not a unique function of parameter *F*. This has been explored further at the end of the Chapter using Dimensional Analysis and, in addition to the seal geometry, parameters such as the Reynolds number of the fluid curtain flow may also be important in the relationship between *L* and *F*. This should be investigated in further work. For the time being, the design steps to account for the impact of leakage flow swirl on the fluid curtain flow should be to minimise the value of *F* when designing the seal and then to check the impact of swirl on the fluid curtain performance using CFD.

8. Conclusions and Recommendations for Further Work

This piece of research has expanded the current knowledge on fluid curtain sealing. Authors such as Auyer [**27**] in 1954 or Unsworth and Burton [**29**] in 1971 first considered how this type of technology could be applied to reducing turbomachinery leakage flows. The concept has received more attention since Curtis et al [**9**] demonstrated experimentally that a fluid curtain injected through a circumferential slot into a shrouded turbine tip seal could increase the efficiency of that turbine stage by ~0.5 %. Most recently, Hilfer [**38**] investigated how to incorporate a fluidic seal in a small waste heat recovery turboexpander to reduce turbine tip leakage. This thesis continues from these earlier studies, describing research to investigate how to better characterise the behaviour of fluid curtain seals in terms of their geometry and operating conditions. Consideration is given to how the technology might be applied to high pressure steam turbine tip seals, as a case study. This investigation is the first fully systematic study to understand the effect of seal geometry and operating conditions on the key performance characteristics of the technology. The research on the effect of swirl is the first time that this has been investigated in relation to fluid curtain seals and its impact on leakage performance demonstrated.

8.1. Summary of Thesis

First, generic fluid curtain seal geometry was defined consisting of a fluid curtain placed upstream of a single labyrinth restriction, using a block or step in the surface immediately upstream of the labyrinth fin clearance to prevent kinetic energy carry over from the curtain flow through the seal. A single fin labyrinth fin was used because its performance could be made to match any given labyrinth or brush seal by controlling the clearance. This geometry was parameterised using ratios of key dimensions. Non-dimensional parameters were created describing curtain width, labyrinth fin clearance, and axial spacing between the curtain and the labyrinth seal. These were varied over a range of values and the resulting seal performance was correlated against the seal geometry. This provided the design tool in Figure 33 which a designer can use to quickly assess the performance characteristics of a fluid curtain seal with a given geometry. The design tool was validated using an experiment in which a range of seal geometries were tested in a stationary annular channel simulating a shrouded turbine tip seal leakage path without rotation. Seal designs were proposed for application in a high pressure steam turbine stage based on the information is Figure 33 and their performance was optimised by controlling the flow structure in the region between the fluid curtain and downstream labyrinth fin. This led to the identification of further design rules for achieving the form of flow structure needed for good sealing performance. The optimised tip seal design was

considered for testing in a scale steam turbine test rig, but a more refined computational study which included swirl in the tip seal leakage inlet flow for the first time, revealed that the shear across the fluid curtain from the swirl in the inlet flow has a significant impact of diffusing the curtain flow greatly reducing the impact of the fluid curtain on reducing the leakage flow. This effect of swirl was investigated in more detail with another computational study and a non-dimensional measure of its effect on the fluid curtain was proposed. Finally, the effect of swirl was confirmed experimentally by modifying an existing turbine seal test rig. The results validated the computational findings and resulted in the development of further design guidelines for mitigating the impact of inlet flow swirl on fluid curtain seal performance. This body of research has been drawn together into the design process described in the Section 8.2.

8.2. Fluid Curtain Seal Design Process

The findings in this body of research can be brought together to produce a design process for fluid curtain seals. The first step is to generate an initial fluid curtain seal design using the results from Chapter 3 for the generic fluid curtain/labyrinth seal baseline design. Figure 33 can be used to produce an initial design which takes into account the constraints of physical space and the maximum fluid curtain supply pressure that are available for the application. This design can then be refined using the outputs from the work described in Chapter 5. The idea presented in Sections 5.1 can be adopted to achieve a manufactureable seal design with the appropriate local leakage channel height at the location where the fluid curtain is injected. CFD simulations can then be used to position the kinetic energy blocker in the design so that the flow structure between the fluid curtain injection and the downstream seal needed for good performance as described in Section 5.2 is achieved. Finally, the findings on the effect of inlet swirl on diffusion of the fluid curtain should be applied to ensure that any reduction in performance due to the effect of swirl is taken into account when optimising the seal design for the particular application. It is essential to design for a low value of parameter *F* and to use CFD to check the impact of inlet swirl on seal performance as part of the design cycle. If the performance is found to be unacceptable at any point, the design process can be iterated by making adjustments to a fluid curtain seal design with an acceptable performance has been achieved for the particular application being considered.

This process is summarised in the flow chart in Figure 102.

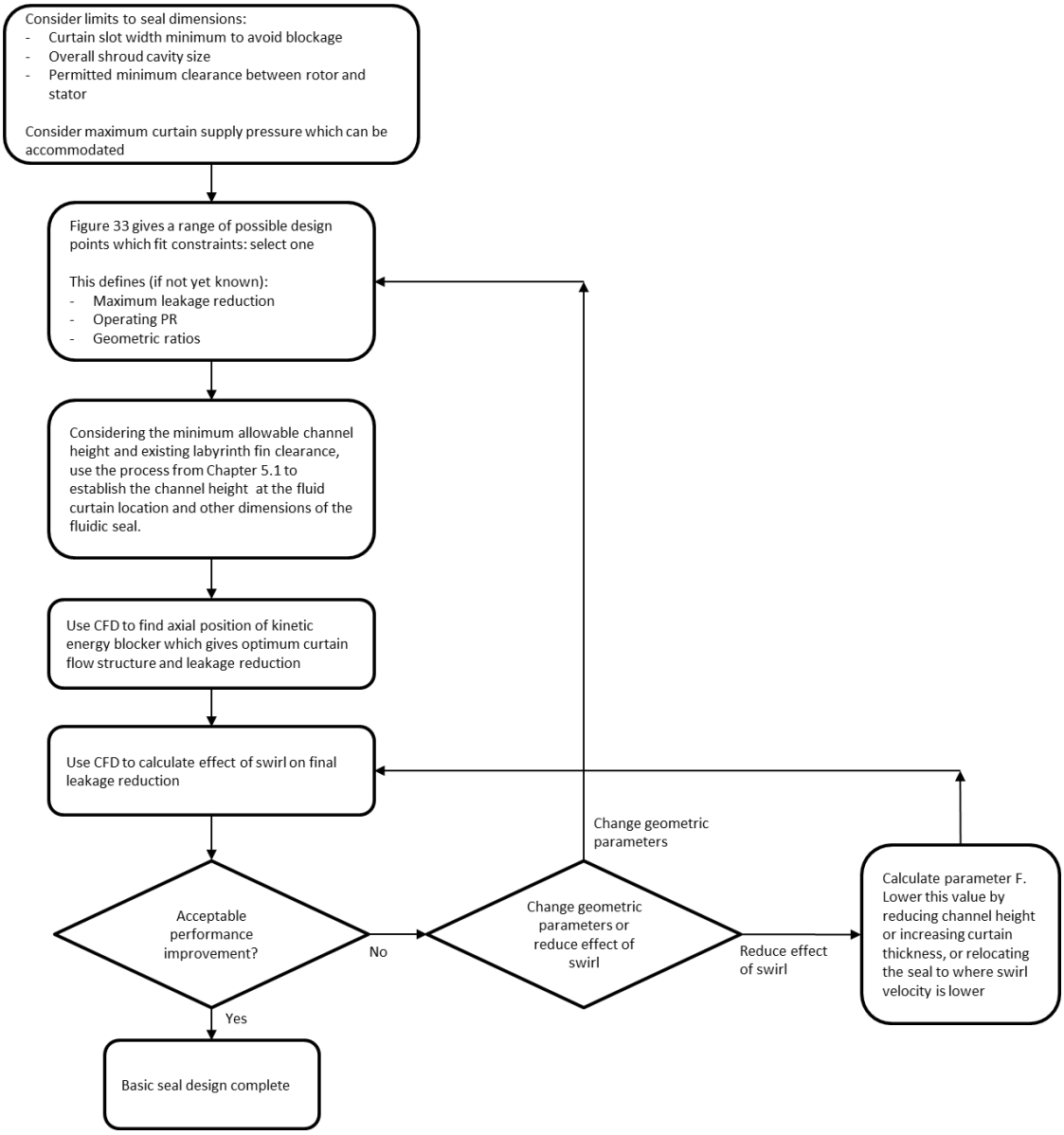

Figure 102: Flowchart showing possible fluid curtain seal design process

8.3.Summary of Research Outcomes

The objectives at the outset of the research described in this thesis were defined in Section 1.4. Research objectives 1 and 2 were well satisfied; the performance of a fluidic curtain seal was characterised in terms of its dimensions and basic design rules were created. A set of repeatable test campaigns were carried out using well defined geometry to expand the existing set of data on fluidic curtain seals. Research objective 3 was not met as the focus of research changed after the effect of swirl was discovered in Chapter 5. This resulted in a new research outcome. The three final outcomes of the project are described below. Collectively these outcomes result in the new design methodology shown in Figure 102.

1. A systematic characterisation of how fluidic curtain seal performance is affected by its geometric design was carried out. A wide range of seal geometries were trialled by computational and experimental means, and seal performance was mapped in terms of ratios between key dimensions in the geometry. Figure 33 shows this characterisation for a wide range of possible fluidic seal layouts.
2. Design rules were established for implementing a fluidic seal based on the dimensions of an existing seal, and flow conditions at the inlet and outlet to this leakage pathway. This information can be used by engineers to quickly estimate the optimum geometry, the potential increase in sealing performance, and the required supply pressure of the new fluidic curtain seal design. Sections 3.5 and 5.1 describe basic design rules for the key dimensions and geometric ratios. Section 5.2.5 describes how to optimise the vortex structure of the fluidic curtain to maximise performance by adjusting the relative axial positions of the curtain, kinetic energy blocker, and downstream restriction.
3. During the course of designing a fluidic curtain seal for a scale steam turbine test rig the effect of swirl on fluidic curtain behaviour was first discovered. The level of swirl expected in the test turbine was seen to make the seal ineffective in simulations. This resulted in a change of research objective to instead investigate and quantify the effect of inlet swirl on fluidic curtain seal performance. Research into fluidic curtain seals has not previously investigated how the curtain is sheared by the tangential velocity of the incoming leakage flow; therefore this research objective still represents a new contribution to the subject of fluidic curtain sealing. A new non-dimensional parameter was created (see equation 6.2) to describe the tangential shearing force on a fluidic curtain. The effect of varying this parameter was investigated using CFD which was validated experimentally using an existing generic turbine seal test rig.

8.4.Recommendations for Future Research

If fluid curtain seals are considered by other researchers in the future, some particularly interesting areas of investigation have been identified:

Better understanding the effect of swirl on leakage reduction for different fluid conditions

The effect of swirl on leakage reduction was demonstrated using CFD for R134a at 3.7 bara, using CFD for steam at 92.4 bara, and using an experiment for air at ~2 bara. As seen in Figure 83, the effect on performance of non-dimensional swirl shear (*F*) on leakage reduction is

different for different working fluids. In section 7.4 it is speculated that other non-dimensional parameters such as curtain Reynolds number must be considered as well as *F*.

As discussed in Section 1.3, the fluid curtain introduces a drop in static pressure in the channel, lowering the pressure difference downstream and therefore reducing the mass flow rate. The pressure drop caused by the curtain is a function of the variables given in Equation 7.2.

$$\Delta P = f(W_{swirl}, \dot{m}_{curtain}, v_{curtain}, v_{channel}, t, \mu, A_c) \tag{7.2}$$

Where:

ΔP = Pressure difference across curtain (kg.m^3/s^2)

W_{swirl} = Upstream swirl velocity (m/s)

$\dot{m}_{curtain}$ = Curtain mass flow rate (kg/s)

$v_{curtain}$ = Curtain core velocity (m/s)

$v_{channel}$ = Channel velocity (m/s)

t = Curtain thickness (m)

μ = Dynamic viscosity (kg/m.s)

A_c = Annular area of fluidic curtain (m^2)

According to the Buckingham Pi theorem, one dependent variable as a function of seven independent variables in three different dimensions results in five dimensionless groups [**51**].

The effectiveness of the curtain could be defined non-dimensionally as the force applied by the curtain to reduce leakage per unit of momentum flux in the curtain. This is expressed on the left hand side of Equation 7.3. The Buckingham pi theorem shows that this is a function of four other non-dimensional groups, shown on the right hand side of Equation 7.3. One of these groups is *F* which is defined in Equation 6.2. The others are the Reynolds number in the fluid curtain, the velocity ratio between the curtain flow and leakage channel flow, and an aspect ratio type expression giving a ratio between leakage channel height and annular area. For the low Mach number flows seen in fluid curtain seals the velocity ratio is approximately the simple ratio between curtain velocity and channel velocity [**52**].

$$\frac{\Delta P \cdot A_c}{\dot{m}_{curtain} \cdot v_{curtain}} = f\left(F,\ Re_{curtain}\ , R_v\ , \frac{t^2}{A_c}\right) \tag{7.3}$$

Where:

ΔP *= Pressure difference across curtain (kg.m^3/s^2)*

A_c *= Annular area of fluidic curtain (m^2)*

$\dot{m}_{curtain}$ *= Curtain mass flow rate (kg/s)*

$v_{curtain}$ *= Curtain core velocity (m/s)*

$Re_{curtain} = \frac{\rho_{curtain} \cdot v_{curtain} \cdot t}{\mu}$ *= Curtain Reynolds number (-)*

$R_v = \sqrt{\frac{\rho_{curtain} \cdot v_{curtain}^2}{\rho_{channel} \cdot v_{channel}^2}} \approx \frac{v_{curtain}}{v_{channel}}$ *= Velocity ratio (-)*

t *= Curtain thickness (m)*

F = Non dimensional circumferential shearing force (-)

The same value of *F* does not give the same leakage reduction for all three cases shown. This means that calculating *F* does not allow *L* to be calculated without an experiment or CFD being performed. By considering the other non-dimensional groups it may be possible to create an equation which allows the effect of swirl on leakage reduction to be calculated analytically for different geometries or working fluids. The sets of results were considered, and the data points where leakage reduction is 10 % were compared in terms of the non-dimensional parameters given in Equation 7.3.

Table 25: Comparison of non-dimensional parameters for three data sets where *L* = 10 %

	F	$Re_{curtain}$	R_v	$\frac{t^2}{A_c}$
Air (experiment)	0.00120	157	31	6.44E-06
R134a (CFD)	0.00100	522	11	7.56E-06
Steam (CFD)	0.00018	3592	14	7.56E-06

Both *F* and Reynolds number see a much larger change when switching between cases than the other two non-dimensional parameters. This suggests that *F* and Reynolds number have a stronger effect than velocity ratio or geometry on the mechanism which causes the loss in performance due to swirl.

With the findings obtained in this research, the loss in leakage reduction due to swirl compared to the value predicted by Figure 33 must be obtained using CFD. If the effect of swirl could be fully predicted only using parameters which can be calculated from basic seal dimensions and fluid properties, then the need to evaluate each design iteration using CFD would be

eliminated. This means the design process in **Figure 102** would be simplified and a seal design could be obtained by a shorter design process.

The Effect of Pre swirl in the Fluid Curtain

Swirling leakage flow was found to shear the fluid curtain and reduce its leakage reduction capability. If the curtain were to swirl in the same direction as the incoming leakage flow then the shearing effect could be reduced or even eliminated. This would require higher curtain supply pressure to account for the additional dynamic pressure in the fluid curtain flow; however there may be a specific application in which this is the best means of mitigating the effect of inlet swirl on fluid curtain seal performance.

Lowering the Inlet Swirl Encountered by the Curtain

The Curtis design showed that by placing the fluid curtain further downstream in the leakage channel, the level of swirl in the leakage flow can reduce to levels which do not cause a loss in seal performance by the time it reaches the curtain. This reduction in swirl velocity happens due to a combination of the conservation of angular momentum as the flow moves radially outward, and passes through restrictions upstream of the curtain. By locating the curtain closer to the leakage channel outlet or adding restrictions upstream, the swirl velocity could be reduced. This would reduce the shearing effect on the curtain and therefore improve seal performance.

Model turbine test validation

One of the original research objectives was to build a fluidic curtain seal into a model test turbine. This objective was not met as the project objectives changed. It therefore remains a worthwhile objective to validate the findings obtained so far by designing a fluidic curtain seal to be tested in some leakage path in a model turbine test rig and demonstrate an overall change in turbine performance.

First prototype

Currently, the fluidic curtain seal has reached a technology readiness level (TRL) of 4. This means the design has been successfully validated in a laboratory environment [**53**]. If the seal can be successfully tested in a model test turbine it would be considered to have a TRL of 5, meaning the basic elements of the design have been integrated with “reasonably realistic supporting elements,” and the design has been validated in a “somewhat realistic environment” [**53**]. Once this has been achieved the design should be raised to a TRL of 6 by testing a full prototype of the design in a “relevant environment,” that is, in an operational turbine application.

References

[1] Earl Logan and Ramendra Roy, *Handbook of Turbomachinery*.: ISBN 0824709950 , 2003, p. 631.

[2] Ural Turbine Works, *Ural Turbine Works Catalog 2019*. Ekaterinburg, 2019.

[3] ESDU, *Labyrinth seal flow - ESDU 09004*., 2009.

[4] J. W. Chew, F. Gao, and D. M. Palermo, "Flow mechanisms in axial turbine rim sealing," *Journal of Mechanical Engineering Science*, vol. 233, 2018.

[5] M. Hilfer, "Fluidic Sealing - Fundamental Physics and Development for Turbomachinery Implementation," Durham University, PhD Thesis 2015.

[6] A. Messenger, "The Aerostatic Seal: Analysis and Development of a New Dynamic Seal Concept for Steam Turbine Application," Durham University, PhD Thesis 2018.

[7] J. G. Ferguson, "Brushes as High Performance Gas Turbine Seals," in *International Gas Turbine and Aeroengine Congress and Exposition, (88-GT-182)*, Amsterdam, 1988.

[8] Dover Precision Components, "Brush Seals: A Proven Enhancer to Labyrinth Seal Performance - Information Sheet," 2019.

[9] E. M. Curtis, J. D. Denton, J. P. Longley, and B. Rosic, "Controlling Tip Leakage Flow Over A Shrouded Turbine Rotor Using An Air-Curtain," in *ASME Turbo Expo 2009, (GT2009-59411)*, Orlando, 2009.

[10] A. Auld, M. Hilfer, S. Hogg, G. Ingram, and A. Messenger, "Application Of An Air Curtain Fluidic Jet Type Seal To Reduce Turbine Shroud Leakage," in *ASME Turbo Expo, (GT2013-94198)*, San Antonio, 2013.

[11] I. G. Ruiz, "Fluidic Seals for Applications in Turbomachinery," Durham University, MEng Research Project 2010.

[12] J. MacCalman, S. Hogg, G. Ingram, R. Williams, and S. Tibos, "Using Fluidic Curtains to Reduce Turbine Leakage," in *23rd ISABE Conference, (ISABE-2017-22588)*, Manchester, 2017.

[13] J. MacCalman, S. Hogg, and G. Ingram, "Application of Fluidic Curtains to Turbine Rotor Tip Seal Geometries," in *ASME Turbo Expo, (GT2018-75835)*, Lillestrøm, 2018.

[14] D. Eser and J. Y. Kazakia, "Air Flow In Cavities Of Labyrinth Seals," *International Journal of Engineering Science*, vol. 33, no. 15, 1995.

[15] G. Vermes, "A Fluid Mechanics Approach to the Labyrinth Seal Leakage Problem," in *ASME 1960 Gas Turbine Power and Hydraulic Divisions Conference and Exhibition, (60-GTP-12)*, Houston, Texas, 1960.

[16] B. Hodkinson, "Estimation of the Leakage through a Labyrinth Gland," *Proceedings of the Institute of Mechanical Engineers*, vol. 141, no. 1, pp. 283-288, 1939.

[17] R. C. Hendricks and T. T. Stetz, "Flow Rate and Pressure Profiles for One to Four Axially Alined Orifice Inlets," NASA, Technical Paper 2460 1985.

[18] H. Zimmermann and K. H. Wolff, "Air System Correlations: Part 1 — Labyrinth Seals," in *ASME International Gas Turbine and Aeroengine Congress and Exhibition, (98-GT206)*, Stockholm, 1998.

[19] H. M. Martin, "Labyrinth Packings," *Engineer*, vol. 85, pp. 35-36, 1908.

[20] P. F. Crudgington, "Brush Seal Perormance Evaluation," in *34th AIAA/ASME/SAE/ASEE Joint Propulsion Conference and Exhibit, (AIAA-98-3172)*, Cleveland, 1998.

[21] Waukesha Bearings, "Brush Seals: A Proven Enhancer to Labyrinth Seal Performance - Information Sheet," 2019.

[22] F. E. Aslan-zada, V. A. Mammadov, and F. Dohnal, "Brush seals and labyrinth seals in gas turbine applications," *Proceedings of the Institution of Mechanical Engineers, Part A*, vol. 227, no. 2, 2012.

[23] S. Beichl, A. Gail, and T. Huppertz, "The MTU Brush Seal Design," Patent No.US7644928B2, 2012.

[24] M. Hoebel, N. A. Rhodes, and I. J. Summerside, "Leaf Seal, In Particular For A Gas Turbine," Patent No. US7828297B2, 2010.

[25] T. Kirk et al., "Film Riding Pressure Activated Leaf Seal Proof of Concept," in *52nd AIAA/SAE/ASEE Joint Propulsion Conference, (AIAA 2016-4920)*, Salt Lake City, 2016.

[26] K. Clark et al., "Effects of Purge Jet Momentum on Sealing Effectiveness," in *ASME Turbo Expo, (GT2016-58099)*, Seoul, 2016.

[27] E. L. Auyer, "Dynamic Sealing Arrangements for Turbomachines," Patent No. US2685429, August 1954.

[28] H. J. Smile and E. E. Paulson, "Pressurized Seal," Patent No. 2963268, December 1960.

[29] R. G. Unsworth and R. K. Burton, "Turbines," Patent No. 3597102, August 1971.

[30] N. Turnquist, K. Bruce, C. Cerretelli, and J. Tourigny, "Fluidic sealing for turbomachinery," Patent No. US20090297341A1, December 2009.

[31] S. Hogg and I. G. Ruiz, "Fluidic Jet Barriers For Sealing Applications," in *ASME Turbo Expo, (GT2011-45353)*, Vancouver, 2011.

[32] M. R. Payne and S. I. Hogg, "Development of a fluidic seal design for turbomachinery applications," Durham University, MEng Research Project 2011.

[33] M. N. Dimova and S. I. Hogg, "Sealing device for reducing fluid leakage in turbine apparatus," Durham University, MEng Research Project 2012.

[34] M. Hilfer, S. Hogg, and G. Ingram, "Experimental Validation of a Curtain type Fluidic Jet Seal on a Turbine Rotor Shroud," in *Proceedings of ASME Turbo Expo, (GT2015-42624)*, Montreal, 2015.

[35] B. Rosic and J. D. Denton, "Control of Shroud Leakage Loss by Reducing Circumferential Mixing," *ASME Journal of Turbomachinery*, vol. 130, no. 2, 2008.

[36] P. Ghaffari and R. Willinger, "On the Impact of Passive Tip Injection on the Downstream Flow Field of a Shrouded LP Turbine: CFD and Experimental Results," in *ASME Turbo Expo, (GT2016-56196)*, Seoul, 2016.

[37] A. C. Rai, D. Prabhudharwadkar, S. Murthy, A. Giametta, and D. Johns, "Effect of Air Curtains on Labyrinth Seal Performance," in *ASME Turbo Expo, (GT2016-57188)*, Seoul,

2016.

[38] M. Hilfer, S. Hogg, and G. Ingram, "Design and Testing of an Improved Rotor Tip Seal Design for the Cummins WHRS Turbo-Expander," Durham University, Internal Report 2015.

[39] A. Messenger, "Design of a Fluidic Seal Test Facility," Durham University, MEng Research Project 2013.

[40] G. Nautiyal, "Fluidic Jet Barriers for the Reduction of Leakage Loss in Shrouded Turbines," Durham University, MEng Research Project 2014.

[41] ANSYS. Fluent 15.0 User's Guide - Chapter 12: Modelling Turbulence.

[42] "Pipe threads where pressure tight joints are made on the threads," Committee, ISO Standards Policy and Strategy, London, BS EN 10226:2005, 2005.

[43] "Measurement of fluid flow by means of pressure differential devices inserted in circular cross section conduits running full - Part 1: General principals and requirements," Committee, ISO Standards Policy and Strategy, London, BS EN ISO 5167:2003, 2003.

[44] "Measurement of fluid flow by means of pressure differential devices inserted in circular cross-section conduits running full- Part 2: Orifice Plates," Committee, ISO Standards Policy and Strategy, London, BS EN ISO 5167-2:2003, 2003.

[45] S. Havakechian and R. Greim, "Aerodynamic Design of 50 Percent Reaction Steam Turbines," *Proceedings of the Institution of Mechanical Engineers*, vol. 213, 1999.

[46] "HAZE Version 1.6," GE Power, 1995.

[47] J. Cheon, P. Milčák, and M. Šťastný, "Numerical Study of Reynolds Number Effects on Steam Turbine Performance," in *ASME Turbo Expo, (GT2015-42052)*, Montreal, 2015.

[48] O. Haylock, "The Effect of Swirl on the Performance of Fluidic Curtain Seals in Shrouded Turbines," Durham, MEng Research Project 2019.

[49] R. Williams, Private communication on research findings, 2019.

[50] "Written Schemes of Examination: Pressure Systems Safety Regulations 2000," Health and

Safety Executive, ISBN: 9780717665198, 2012.

[51] Y. A. Cengel and J. M. Cimbala, *Fluid Mechanics - Fundamentals and Applications*, 2nd ed., 2010.

[52] J. Chang, X. Shao, and J. Li, "Flow characteristics of two dimensional classical and pulsating jet in crossflow at low Reynolds number," vol. 12, 2018.

[53] European Space Agency, "Technology Readiness Levels Handbook For Space Applications," Technical Report 2008.